

Syntheses of (pyridyl) pyrazine carboxamide palladium(II) complexes, their DNA/BSA interactions, and cytotoxicity studies

By

Sabathile Thandeka Mvelase

Submitted in fulfilment of the academic requirement for the degree

Master of Science

in

Chemistry

in the

College of Agriculture, Engineering and Science,

School of Chemistry and Physics,

University of KwaZulu-Natal

Supervisor: Professor Stephen O. Ojwach



**UNIVERSITY OFTM
KWAZULU-NATAL**

**INYUVESI
YAKWAZULU-NATALI**

DECLARATION

I, Sabathile Thandeka Mvelase declare that the work presented in the thesis titled Syntheses of (pyridyl) pyrazine carboxamide palladium(II) complexes, their DNA/BSA interactions, and cytotoxicity studies are the original research result of my own work. This thesis has never been submitted for the award of any degree at any other institution. All the contributions and work of others used in this thesis have been acknowledged and accredited in the references.


Signed:

Date: ...01/09/2023.....

Sabathile Thandeka Mvelase

As the supervisor of the candidate. I have approved the submission of this MSc thesis for examination.


Signed:

Date: 4th September, 2023

Prof Stephen Ojwach

DECLARATION: PLAGIARISM

I, Sabathile Thandeka Mvelase, declare that:

1. The research reported in this dissertation, is my original work, except where otherwise acknowledged or indicated, is my own original work.

2. This dissertation has never been submitted in part or full for any examination or degree to any other university.

3. This dissertation does not contain another person's writing unless specifically acknowledged as being sourced from the researcher. Where other written sources have been quoted, then:
 - a. Their words have been re-written and the general information ascribed to them has been referenced.

 - b. Where their exact words have been used, their writing has been placed inside quotation marks, and referenced.

4. This dissertation does not contain any other individual's data, graphs, pictures, or other information unless acknowledged.

5. This dissertation does not contain text, graphics, or tables copied and pasted from the internet unless acknowledged, and the sources are indicated in the dissertation and the references sections.

This dissertation is a collection of data and material, prepared by myself, presented orally or as posters at conferences, or published as journal articles whereas, in some instances, additional material has been included.

Student Name: Sabathile Thandeka Mvelase



Signature:

Date: ...06/06/2023.....

DEDICATION

This thesis is dedicated to my mother, Ntombizonke Florence Dlamini.

ABSTRACT

Reaction of pyrazine-2,3-dicarboxylic acid with a respective amine in the presence of triphenyl phosphite afforded the corresponding carboxamide ligands: [N^2 , N^3 -bis(pyridin-2-yl)pyrazine-2,3-dicarboxamide] (**L1**), [N^2 , N^3 -bis(6-methylpyridin-2-yl)pyrazine-2,3-dicarboxamide] (**L2**), [N^2 , N^3 -bis(4-methylpyridin-2-yl)pyrazine-2,3-dicarboxamide] (**L3**), and [N^2 , N^3 -bis(quinoline-8-yl)pyrazine-2,3-dicarboxamide] (**L4**). Treatments of the corresponding (pyridyl)pyrazine carboxamide ligands with $[\text{PdCl}_2(\text{NCCH}_3)_2]$ afforded new mononuclear and dinuclear palladium(II) complexes with a general formula, $[\text{Pd}_2(\text{L1})_2\text{Cl}_2]$ (**Pd1**), $[\text{Pd}_2(\text{L2})_2\text{Cl}_2]$ (**Pd2**), $[\text{Pd}_2(\text{L3})_2\text{Cl}_2]$ (**Pd3**) and $[\text{Pd}(\text{L4})\text{Cl}]$ (**Pd4**). The identities and coordination nature of the palladium(II) complexes were established through a combination of characterization techniques such as NMR, FT-IR spectroscopy, mass spectrometry, elemental analysis, and single X-ray crystallography. The molecular structures of the dinuclear **Pd1** and **Pd3** complexes reveal that the two (pyridyl) pyrazine carboxamide ligands coordinate with the palladium atom *via* one arm, while the other arm remains non-coordinating. The ligands are bridged by two palladium atoms to form dinuclear palladium(II) complexes. While one ligand coordinates to the palladium in a bidentate fashion *via* the nitrogen atoms of the pyrazine and amide groups, the other ligand unit coordinates to the palladium through the pyridine nitrogen atom to give two ligand units and two palladium atoms in the complex coordination sphere. On the other hand, ligand **L4** binds to palladium atom in a tridentate fashion *via* the pyrazine, amide, and pyridine nitrogen atoms to give complex **Pd4** as a mononuclear species. The interaction of the palladium complexes (**Pd1-Pd4**) with calf thymus DNA (CT-DNA) was monitored using UV-Vis, and fluorescence spectroscopy. Absorption spectroscopic studies revealed that complexes **Pd1-Pd4** interact with CT-DNA via intercalative mode, and the computed intrinsic binding constant (K_b) values range from $(4.28-13.12) \times 10^6 \text{ M}^{-1}$. In addition,

K_{sv} values of $(1.82-28.41) \times 10^6 \text{ M}^{-1}$ and K_F values of $(1.01-53.44) \times 10^4 \text{ M}^{-1}$ determined in competitive binding studies confirmed the intercalative binding mode. The interaction of the complexes with CT-DNA decrease in the order of **Pd3** > **Pd2** > **Pd1** > **Pd4**. Furthermore, bovine serum albumin (BSA) interaction was evaluated using fluorescence studies and the results revealed the existence of a static quenching mechanism with bimolecular constant, k_q range of $(0.66-13.99) \times 10^{14} \text{ M}^{-1} \text{ s}^{-1}$. The K_{sv} values of $(1.48-29.67) \times 10^6 \text{ M}^{-1}$ and K_F values of $(0.10-16.10) \times 10^5 \text{ M}^{-1}$ confirmed the interaction between BSA and palladium complexes. The interaction follows this order **Pd2** > **Pd1** > **Pd3** > **Pd4**, which is inconsistent with the CT-DNA trend. In general, ligands bearing electron-donating methyl groups (**L2** and **L3**) contributed to higher binding constants in their respective complexes **Pd2** and **Pd3** compared to the unsubstituted complex **Pd1**. In addition, the mononuclear complex **Pd4** showed the weakest interactions with both the DNA and BSA, pointing to some beneficial effects of increased metal atoms in the complexes. The cytotoxic effect of the ligands **L1-L3** and complexes **Pd1-Pd4** were examined against a human breast cancer cell line (MCF-7) using 3-(4,5-Dimethyl-2thiazolyl)-2,5-diphenyl-2H-tetrazolium bromide (MTT) assay. In general, the ligands displayed poor cytotoxicity **L1** ($IC_{50} > 400 \mu\text{M}$), **L2** ($IC_{50} = 182.4 \mu\text{M}$), **L3** ($IC_{50} = 80.2 \mu\text{M}$), when compared to their respective palladium(II) complexes **Pd2** ($IC_{50} = 154.9 \mu\text{M}$), **Pd3** ($IC_{50} = 230.1 \mu\text{M}$). Complexes **Pd1** ($IC_{50} = 11.4 \mu\text{M}$), and **Pd4** ($IC_{50} = 61.5 \mu\text{M}$) displayed high and moderate cytotoxic activity which was attributed to the planarity of the complexes.

TABLE OF CONTENTS

DECLARATION	ii
DECLARATION: PLAGIARISM.....	iii
DEDICATION.....	iv
ABSTRACT.....	v
ACKNOWLEDGEMENTS.....	xii
LIST OF FIGURES	xiii
LIST OF SCHEMES.....	xvii
LIST OF TABLES	xviii
LIST OF ABBREVIATIONS AND SYMBOLS	xix
Chapter 1	1
General background, the introduction of DNA/BSA interactions with metal complexes and spectroscopic and physical techniques	1
1.1 General background.....	1
1.2 Significance of deoxyribonucleic acid (DNA) in anticancer drug	2
1.2.1 Modes of interactions in DNA.....	3
1.2.1.1 Covalent interactions	4
1.2.1.2 Minor and major groove	4
1.2.1.3 Intercalation binding mode	5
1.2.1.4 Electrostatic interaction.....	6
1.3 The role of bovine serum albumin (BSA) in the development of anticancer drug	7
1.4 Techniques employed in the study of DNA/BSA interactions.....	9

1.4.1 Fluorescence spectroscopic methods	9
1.4.1.1 <i>Competitive studies with ethidium bromide</i>	9
1.4.1.2 <i>Hoechst experiment</i>	11
1.4.1.3 <i>Rhodamine B experiment</i>	11
1.4.1.4 <i>Tryptophan fluorescence studies</i>	12
1.4.1.5 <i>Synchronous fluorescence studies of BSA</i>	13
1.4.2 UV-Vis absorption spectroscopy studies	13
1.4.3 Circular dichroic spectral studies	14
1.4.4 Viscosity measurements.....	16
1.4.5 Salt concentration-dependent assays.....	16
1.4.6 Gel electrophoresis.....	16
1.4.7 Electrochemical technique	17
1.4.8 Thermodynamic parameters.....	18
1.4.9 Molecular modelling and simulations.....	19
1.5 <i>In vitro</i> cytotoxicity assays	19
1.6 References	22
Chapter 2	28
A review of palladium(II) complexes as anticancer agents and their interactions with	28
DNA/BSA interactions.....	28
2.1 General background.....	28
2.2. Studies of DNA/BSA interactions and cytotoxicity of metallodrugs.....	31

2.2.1 Mononuclear palladium complexes	32
2.2.2. Dinuclear palladium complexes	38
2.3. Summary.....	42
2.4. Statement of the problem.....	45
2.5. Justification and rationale of the study	45
2.6. Aim and objectives of the study	46
2.7. References	47
Chapter 3	51
Synthesis and structural characterization of carboxamide (pyridyl)pyrazine palladium(II) complexes.....	51
3.1 Introduction	51
3.2. Experimental section	52
3.2.1 General materials	52
3.2.2. Instrumentation	53
3.2.2.1 NMR, FT-IR spectroscopy, mass spectrometry, and elemental analysis	53
3.2.2.2. Single crystal X-ray crystallography analyses.....	53
3.2.3. Syntheses of (pyridyl)pyrazine carboxamide ligands and corresponding palladium(II) complexes	54
3.2.3.1. [<i>N</i> ² , <i>N</i> ³ -bis(pyridin-2-yl)pyrazine-2,3-dicarboxamide] (L1)	54
3.2.3.2. [<i>N</i> ² , <i>N</i> ³ -bis(6-methylpyridin-2-yl)pyrazine-2,3-dicarboxamide] (L2)	55
3.2.3.3. [<i>N</i> ² , <i>N</i> ³ -bis(4-methylpyridin-2-yl)pyrazine-2,3-dicarboxamide] (L3)	56
3.2.3.4. [<i>N</i> ² , <i>N</i> ³ -bis(quinoline-8-yl)pyrazine-2,3-dicarboxamide] (L4).....	56

3.2.3.5. $[Pd_2(L1)_2Cl_2]$ (Pd1).....	57
3.2.3.6. $[Pd_2(L2)_2Cl_2]$ (Pd2).....	58
3.2.3.7. $[Pd_2(L3)_2Cl_2]$ (Pd3).....	59
3.2.3.8. $[Pd(L4)Cl]$ (Pd4).....	60
3.3. Results and discussion	61
3.3.1. Synthesis of pyrazine-pyridyl-carboxamide ligands and palladium(II) complexes	61
3.3.2. Molecular structures of compounds L1 , Pd1 , and Pd3	72
3.4. Conclusions	78
3.5. References	79
Chapter 4	Error! Bookmark not defined.
Investigations of DNA/BSA binding interactions, and cytotoxicity of (pyridyl)pyrazine carboxamide palladium(II) complexes	Error! Bookmark not defined.
4.1. Introduction	Error! Bookmark not defined.
4.2. Experimental section	Error! Bookmark not defined.
4.2.1. General instrumentations and materials.....	Error! Bookmark not defined.
4.2.2. Experimental procedure of CT-DNA and BSA binding studies.....	Error!
Bookmark not defined.	
4.2.2.1. <i>CT-DNA absorption spectral studies</i>	Error! Bookmark not defined.
4.2.2.2. <i>CT-DNA ethidium displacement studies</i>	Error! Bookmark not defined.
4.2.2.3. <i>Bovine serum albumin quenching studies</i>	Error! Bookmark not defined.
4.2.3. <i>In vitro</i> cytotoxicity.....	Error! Bookmark not defined.

4.3. Result and discussion.....	Error! Bookmark not defined.
4.3.1 CT-DNA absorption spectral studies	Error! Bookmark not defined.
4.3.2. Competitive CT-DNA ethidium fluorescence quenching studies	Error! Bookmark not defined.
4.3.3. BSA fluorescence quenching.....	Error! Bookmark not defined.
4.3.4. In vitro cytotoxicity studies of ligands L1-L3 and palladium complexes Pd1- Pd4	Error! Bookmark not defined.
4.4. Conclusions	Error! Bookmark not defined.
4.5 References	Error! Bookmark not defined.
Chapter 5	108
General conclusions and proposed future work	108
5.1 General conclusions.....	108
5.2. Future work.....	110
5.3. References	112
5.4. Appendix	113

ACKNOWLEDGEMENTS

My earnest appreciation goes to all the people who contributed to the process of carrying out this research project. I am most grateful to the Almighty Lord for the strength and grace He has given me to execute this work. My sincere gratitude goes to Professor Stephen Ojwach for his supervision, profound dedication, informative and constructive advices. I would like to warmly acknowledge Dr Reinner Omondi for his valuable guidance, and suggestions in this project. I am deeply grateful to Dr Robert Kumah for contributing constructive comments to this project. I am very grateful to Leigh Hunter for his assistance with the DNA/BSA studies.

I would like to sincerely thank the University of KwaZulu-Natal, the School of Chemistry and Physics, of which all of this would not have been possible to achieve. To the academic, technical staff and my colleagues in the School of Chemistry and Physics, your support is acknowledged. The financial support from National Research Foundation is sincerely appreciated.

I would like to express my sincere gratitude to my family for providing moral, spiritual, and emotional support. Your encouragement and continual support cannot be measured.

LIST OF FIGURES

Figure 1.1: Illustration of the development of cancer disease. ⁶	1
Figure 1.2. Major and minor groove interaction of metal complexes to DNA. ²⁹	5
Figure 2: Intercalation binding mode of metal complexes to DNA. ³³	6
Figure 1.3: Electrostatic interaction of metal complexes to DNA. ³⁷	7
Figure 1.4: Structure of bovine serum albumin depicting the Trp-134 and Trp-212 residues. ⁴⁶	8
Figure 2.1: Platinum complexes used in the treatment of cancer. ⁷	28
Figure 2.2: Mechanism of cisplatin; intracellular hydrolysis and activation of cisplatin leading to apoptosis. ¹⁶	30
Figure 2.3: Chemical structure of trans-palladium (II) complex supported on diethyl- 2quinolylmethylphosphonate ligand. ²⁹	32
Figure 2.4: Chemical structures of palladium(II) complexes bearing bis-(pyrazolyl) ligands. ³⁰	33
Figure 2.5: Chemical structures of palladium(II) complexes supported on tridentate bis(benzazole) ligands. ³¹	34
Figure 2.6: Chemical structures of a series of palladium(II) complexes bearing π -conjugated carboxamide ligand. ³²	35
Figure 2.7: Chemical structure of (pyrazolyl)pyridine palladium(II) complexes. ³³	36
Figure 2.8: Chemical structures of (E)-2-[(anthracene-9-ylmethylene)amino] aniline palladium(II) complexes. ³⁴	37

Figure 2.9: Chemical structure of 2-(benzothiazol-2-yl)-6-(((2-	38
(ethylthio)phenyl)imino)methyl)phenol)benzothiazole palladium(II) complex. ³⁵	38
Figure 2.10: Chemical structure of dinuclear spermine palladium(II) complex. ³⁶	39
Figure 2.11: Chemical structure of platinum(II) complexes bearing (2- pyridylmethyl)benzene1,4-diamine ligand. ³⁷	39
Figure 2.12: Chemical structures of dinuclear bridged-pyrazine palladium(II) complexes. ³⁸	40
Figure 2.13: Chemical structures of dinuclear palladium(II) complexes bearing pyridine-based bridging ligands. ³⁹	41
Figure 3.1: ¹ H NMR spectra of ligand (L3) showing N-H singlet signal at 10.64 ppm wit I=2 and three pyridine signals; and the corresponding complex Pd3 showing singlet N-H signal at 11.02 ppm with I=1, and five pyridine signals upon coordination. The unsymmetrical nature of the complex Pd3 confirmed the formation of the complex.....	65
Figure 3.2: ¹ H NMR spectra of ligand L4 showing N-H signal at 11.45 ppm with I=2 and the corresponding complex Pd4 showing singlet N-H signal at 11.02 ppm with I=1 upon coordination. This confirms the formation of the unsymmetrical complex Pd4	65
Figure 3.3: ¹³ C NMR spectrum of ligand L3 showing carbonyl signal at 163.3 ppm and the ¹³ C NMR spectrum of complex Pd3 showing two carbonyl signals at 163.4 and 166.9 ppm. This confirms the unsymmetrical nature of the dinuclear complex Pd3 due to the non-coordination of one arm of ligand L3	67
Figure 3.4: ¹³ C NMR spectrum of ligand L4 showing carbonyl signal at 163.17 ppm and the ¹³ C NMR spectrum of complex Pd4 showing two carbonyl signals at 163.34 and 165.42 ppm. This confirms the unsymmetrical nature of the mononuclear complex Pd4 due to the non- coordination of one arm of ligand L4	67

Figure 3.5: FT-IR spectra of L3 showing single $\nu(\text{C}=\text{O})$ peak at 1682 cm^{-1} complex and Pd3 showing the appearance of two carbonyl carbon $\nu(\text{C}=\text{O})$ at 1632 and 1705 cm^{-1} confirming the unsymmetrical nature of the dinuclear complex Pd3 due the coordination of one arm of the ligand L3 to palladium(II).	69
Figure 3.6: FT-IR spectra of ligand L4 showing one $\nu(\text{C}=\text{O})$ peak at 1674 cm^{-1} and its corresponding complex Pd4 , showing the two $\nu(\text{C}=\text{O})$ signals at 1636 and 1686 cm^{-1} confirming the unsymmetrical nature of the mononuclear complex Pd4 due the coordination of one arm of the ligand L4 to palladium(II).	70
Figure 3.7: TOF-MS spectrum of complex Pd3 showing m/z at 979 $[\text{M}^+ + \text{H}]$. Inset: theoretical (a) and experimental (b) isotopic mass distribution spectra complex Pd3 with m/z at 979.	71
Figure 3.8: HR-MS spectrum of complex Pd4 showing m/z at 561 $[\text{M}^+ + \text{H}]$. Inset: theoretical (a) isotopic mass distribution spectra complex Pd4 with m/z at 560.	71
Figure 3.9: Solid state structure of L3 , drawn with 50% probability ellipsoids. Hydrogen atoms were omitted for clarity.	74
Figure 3.10: Solid state structure of complex Pd1 , drawn with 50 % probability ellipsoids. Hydrogen atoms were omitted for clarity.	74
Figure 3.11: Solid-state structure of Pd3 , drawn with 50% probability ellipsoids. Hydrogen atoms are omitted for clarity.	75
Figure 4.1: (Pyridyl)pyrazine carboxamide palladium(II) complexes used in the biological studies in this chapter.	Error! Bookmark not defined.
Figure 4.2: Electronic absorption spectra of Pd3 (25 μM) in 0.01 M PBS buffer at pH=7.4 upon addition of CT-DNA (0 - 16 μM). The arrow shows the decrease in absorbance upon the addition of increasing concentration of CT-DNA. Inserted is the linear plot of $[\text{CT-DNA}]$ vs $[\text{DNA}] / (\epsilon_a - \epsilon_f)$	Error! Bookmark not defined.

Figure 4.3: Fluorescence emission spectra depicting the quenching upon addition of an increasing amount of **Pd3** to CT-DNA-EB: [EB] = 10 μ M, [CT-DNA] = 10 μ M. The arrow shows the intensity changes upon increasing the **Pd3** complex concentration. Inserted is the Stern-Volmer plot of I_0/I vs [Q] and Scatchard plot of $\log[(I_0-I)/I]$ vs $\log[Q]$**Error!**
Bookmark not defined.

Figure 4.4: Quenching in fluorescence emission spectra of BSA in the presence of an increasing concentration of **Pd3** = 0-40 μ M and [BSA] = 14 μ M. The arrow shows the decrease in fluorescence intensity upon increasing the **Pd3** concentration. Inserted is the Stern-Volmer plot of I_0/I vs [Q] and Scatchard plot of $\log[(I_0-I)/I]$ vs $\log[Q]$.**Error!** **Bookmark not defined.**

Figure 4.5: Effect of ligands **L1-L3** and palladium (II) complexes **Pd1-Pd4** on the human breast cancer cell line (MCF-7) after 48 h treatment. Each bar represents the percentage cell viability value for the effect of the concentration of each compound.**Error!** **Bookmark not defined.**

LIST OF SCHEMES

Scheme 3.1. Synthesis of the carboxamide ligands L1-L4	62
Scheme 3.2: Synthesis of mononuclear and dinuclear (pyridyl)pyrazine carboxamide palladium(II) complexes Pd1-Pd4	63
Scheme 5.1: Role of electron-donating and electron-withdrawing groups of dicarboxamide ruthenium(II) <i>p</i> -cymene complexes in CT-DNA/BSA interactions, and cytotoxicity. ⁴	111

LIST OF TABLES

Table 1.1: Classification of half maximal inhibitory concentration (IC_{50}).....	21
Table 2.1: Summarized DNA, BSA binding constants, and cytotoxic activity of mononuclear palladium(II) complexes.....	43
Table 2.2: Summarized DNA, BSA binding constants and cytotoxic activity of dinuclear palladium(II) complexes.....	44
Table 3.1: Signature 1H NMR signals of the ligands and their palladium(II) complexes	66
Table 3.2: Selected FT-IR and ^{13}C NMR data of ligands and palladium(II) complexes.....	68
Table 3.3: Crystal data and structure refinement for compounds L3 , Pd1 and Pd3	73
Table 3.4: Selected bond lengths and bond angles for molecular structures of L3 , Pd1 , and Pd3	77
Table 4.1: CT-DNA binding constants, quenching constants, and Gibbs energy values for Pd1-Pd4	Error! Bookmark not defined.
Table 4.2: BSA binding constant, quenching constants, and number of binding sites for Pd1-Pd4	Error! Bookmark not defined.
Table 4.3: Cytotoxic activity of the ligands (L1-L3) and palladium(II) complexes (Pd1-Pd4) against the human breast cancer cell line (MCF-7) ^a	Error! Bookmark not defined.

Table 4.4: Summarized values of biological activity palladium(II) complexes**Error!**

Bookmark not defined.

LIST OF ABBREVIATIONS AND SYMBOLS

Å	Angstrom
δ	Chemical shift
<i>J</i>	Coupling constant
CT-DNA	Calf thymus deoxyribonucleic acid
°C	Degree Celsius
DNA	Deoxyribonucleic acid
DMSO	Dimethyl sulfoxide
d	Doublet
ESI	Electron spray ionization
FT-IR	Fourier-transform infrared spectroscopy
g	Gram(s)
LC-MS	Liquid chromatography-mass spectrometry
MS	Mass spectrometry

MHz	Megahertz
ml	millilitres
mmol	millimoles
m	Multiplet
NMR	Nuclear magnetic resonance
ppm	Parts per million
s	Singlet
t	Triplet
TOF	Turn over frequency

Chapter 1

General background, the introduction of DNA/BSA interactions with metal complexes and spectroscopic and physical techniques

1.1 General background

Cancer is among the disease that threaten public health worldwide.¹ The disease develops as a result of the transformation of normal cells to abnormal cancer cells that grow uncontrollably.²⁻
⁴ Additionally, unfixable mutations that occur during DNA replication promote the proliferation of cancer cells. Continuous division of these cancerous cells results in massive cells that spread throughout the body called malignant tumours.⁵

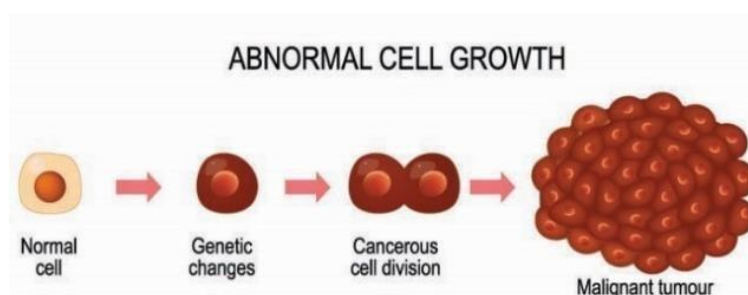


Figure 1.1: Illustration of the development of cancer disease.⁶

The disease has multiple causes including exposure to environmental carcinogens (such as air pollution), and toxic chemicals (such as tobacco, asbestos, arsenic, polychlorinated biphenyls, and metals).⁷ Excessive exposure to ionization radiation (such as ultraviolet lights, uranium, and radiations from alpha, beta, gamma, and X-ray emitting sources).⁸ Also, age has been reported as the cause for growth of cancerous cells. Other causes of cancers include internal factors such as inherited mutations, hormones, and the immune system.⁹ According to the world health organisation the mortality rate due to cancer is increasing yearly, nearly 10 million

deaths reported in 2020 were associated with cancer. These deaths were caused by lung (1.8 million deaths), colon and rectum (916 000 deaths), liver (830 000 deaths), stomach (769 000 deaths), and breast (685 000 deaths) cancers. Most common types of cancers reported are breast, lung, stomach, colon and rectum, prostate, and skin cancer.¹⁰ Cancer can be treated by a single treatment or a combination of treatments depending on the stage, type, location of the tumor, and response to medication by the patient.^{11,12} These methods of treating cancer include radiation therapy, immunotherapy, surgery, and chemotherapy.¹³⁻¹⁶ Even though these treatments are used to kill cancer cells, they are challenged by the resistance-sensitive tumours that develop after the initial response of the treatment.¹⁷ Despite this, cancer cells can spread uncontrollably to other places of the body and most chemotherapy treatments do not have a broader spectrum of activity towards cancer cells. Some cancer cells have shown resistance to drugs such as cisplatin. Thus, efforts are made to design and develop other metal-based drugs with no resistance and improved anticancer activity.

1.2 Significance of deoxyribonucleic acid (DNA) in anticancer drug

DNA is the fundamental source of genetic information and one of the primary cellular targets in the development of anticancer drugs, understanding how drugs interact with biological molecules like DNA is essential in biological research. Newly developed or discovered drugs have an impact on DNA.¹⁸ Significantly, DNA serves several important roles in living organisms, including transferring genetic information and directing the biological creation of proteins and cell division. Furthermore, it is important to comprehend the molecular process of the interaction between DNA and the small chemical since it offers a thorough comprehension of their structure and biological activity.¹⁹

DNA is a macromolecule composed of two complementary chains of nucleotides and it was discovered in 1953 by Watson and Crick. In their ground-breaking discovery, they concluded that DNA is made up of two strands that are duplex coiled helical-style around one another. It is composed of components known as nucleotides that are linked in polymeric form by a phosphodiester bond. Nucleotides also referred to as monomers are small compounds that consist of a pentose sugar, nitrogenous base, and phosphoric acid. The sugar component is known as 2'-deoxyribose and it is in a ring form. There are two kinds of nitrogenous bases, purines which is a double ring structure consisting of a six-membered ring linked to a five membered ring. These include adenine and guanine. Another nitrogenous base class is pyrimidine, a single-ring structure that is a six-membered ring and it includes cytosine and thymine. Normally, these nitrogenous bases are joined to the 1'-carbon of sugar to produce a nucleoside, which can then be changed into a nucleotide by joining the phosphoric acid group to the 5'-carbon of the sugar. These nucleotides are linked together.^{20, 21}

1.2.1 Modes of interactions in DNA

Metal complexes may either bind to DNA covalently whereby nitrogen of base pairs replaces an unstable ligand in a complex or non-covalently which is the interaction between stable metal complex and DNA.²² Metal complexes may interact non-covalently with DNA through different modes that include intercalation, groove binding, and electrostatic interaction.^{23,24} These interactions can be distinguished from one another based on the magnitude of their association constants, which varies according to the small molecules binding to DNA.

1.2.1.1 Covalent interactions

The majority of therapeutic drugs used to treat cancer interact covalently with DNA, resulting in the formation of adducts *via* alkylation or interstrand and intrastrand cross-linking. Several alkylating substances, including dacarbazine, chlorambucil, and nimustine, bind alkyl groups to DNA bases, changing the structure of the DNA. To overcome this, DNA has repair enzymes that displace the alkylated base. This type of binding mode is irreversible, completely inhibits DNA processes, and results in cell death. The most widely used covalent binder is cisplatin [cis-dichlorodiammineplatinum(II)], which determines intra/interstrand crosslink by forming covalent connections between Pt(II) and the nitrogen atoms in the nucleobase structures. However, due to its high toxicity and the fact that some tumor forms display treatment resistance, its efficacy is constrained.²⁵

1.2.1.2 Minor and major groove

Groove binding does not require any modification to the structure of the DNA strands, it merely functions as a lock and key mechanism.²⁶ Groove interaction can be differentiated in two ways, there is a major and minor groove interaction through hydrogen bonding or van de Waals interactions.²² Their distinction is based on the properties they encounter when recognizing molecules. For example, major groove interaction is observed when DNA interacts with large molecules, whereas minor groove interacts with small molecules. This type of interaction is normally indicated by the occurrence of a hypochromic shift with neither a blue shift nor a red shift.²⁷ Groove binders require no free energy for the formation of the binding site, this has made its association constants (about 10^{11} M^{-1}) to be higher than that of intercalators.²⁸

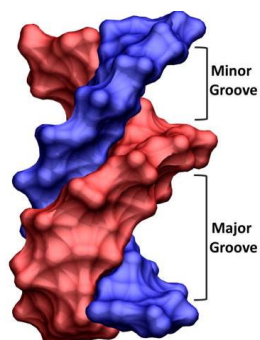


Figure 1.2. Major and minor groove interaction of metal complexes to DNA.²⁹

Small molecules that bind to DNA are stabilized by hydrogen bonding and van der Waals interactions of functionalities that are bound along the groove of the DNA helix.³⁰ Van der Waals interactions are formed due to stacked base pairs in the double helix. The formation of hydrogen bonds usually occurs through condensation, whereby the carbonyl groups of metal complexes interact with the H atoms in DNA base pairs. These hydrogen bonds are weaker at high temperatures, so they can easily be broken. The presence of other interactions such as electrostatic and external hydrogen bonding enables DNA molecules to compact. However, a decrease in temperature allows the broken hydrogen bonds to reform according to the principle of complementary base pairing in DNA. The external hydrogen bonds between the carbonyls and the base pairs disappear, and the charge neutralization could not maintain the compact conformation of condensed DNA, resulting in the release of the condensates.³¹

1.2.1.3 Intercalation binding mode

Generally, intercalation involves binding of the complex to DNA through π - π stacking within DNA base pairs leading to the alteration of DNA double helix base pairs. DNA uncoils to allow the planar heteroaromatic complex with π -backbone to bind within the DNA double helix. Importantly, the intercalation mode is demonstrated by the occurrence of hypochromic and bathochromic shift metal complexes interacting with DNA.³² In addition, a strong stacking

interaction between an aromatic chromophore and base pairs of DNA is observed. As mentioned above, the association constants vary depending on the compound that binds to DNA. However, intercalators association constants is about 10^5 M^{-1} for simple intercalators.²⁶

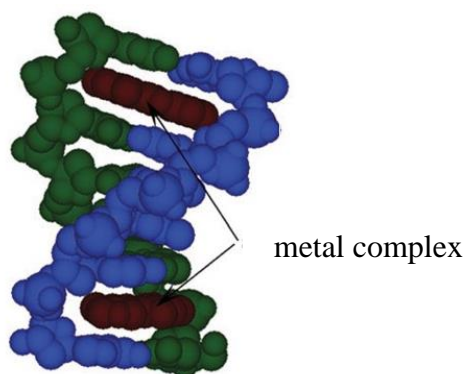


Figure 2: Intercalation binding mode of metal complexes to DNA.³³

1.2.1.4 Electrostatic interaction

Electrostatic interaction is another common interaction that arises when the metal complex binds to the external sugar-phosphate group of DNA strands using Coulombs forces.²² Generally, this interaction stabilizes the intercalation and groove binding in DNA.³⁴ Upon binding, the hyperchromic which also depict groove binding, and blue shift which also indicate groove binding results in damaging the DNA structure, and conformational changes to the DNA double helix become conspicuous.^{35, 36}

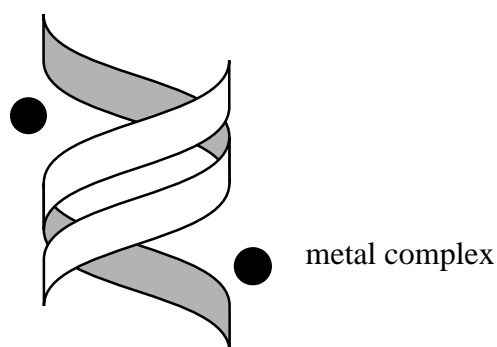


Figure 1.3: Electrostatic interaction of metal complexes to DNA.³⁷

1.3 The role of bovine serum albumin (BSA) in the development of anticancer drug

Serum albumins are generally minor non-glycosylated proteins produced by the liver. Serum albumins can be divided into four categories: human, bovine, horse, and leporine serum albumins.³⁸ However, this study will predominantly focus on the bovine serum albumin proteins. These are important circulatory dissoluble proteins that act as the main transport medium for a variety of drugs and physiologically important metal complexes.³⁹ In addition, they bind and distribute substances such as fatty acids, bilirubin, porphyrins, thyroxine, tryptophan, and steroids.⁴⁰ Blood plasma proteins can interact with drugs at specific binding sites which is of great importance since strong albumin reduce the active concentration of the drugs. This leads to the simultaneous distribution of other competitive drugs that may be bound to albumin.^{40, 41} Investigating protein-drug interactions may provide knowledge of the structural characteristics that govern the therapeutic efficacy of the drug. Therefore, it is crucial to investigate how BSA interacts with prospective molecules in the fields of life science, chemistry, and clinical medicine.⁴²

Bovine serum albumin is the most abundant protein in the plasma. These serum albumin proteins have been widely used as a substitute for human serum albumin in research due to their structural similarities, medicinal importance, low cost, ready availability, stability, and water solubility.⁴³ BSA is made up of a single polypeptide which consists of 583 amino acids. It comprises 17 disulfide bonds formed between the cysteine residues that stabilize the structure of BSA. The protein BSA is considered a macromolecule due to its high molecular weight of 66.8 kDa. The structure of BSA consists of three homologous domains I-III and each domain has two subdomains denoted A and B. In the subdomain IB and subdomain IIA, BSA contains two Tryptophan (Trp) amino acid residues Trp-134 and Trp-212 that possess intrinsic fluorescence, respectively.⁴⁴ Trp-134 is located in the first domain and Trp-212 is in the second domain. Trp is found within a hydrophobic pocket of the protein and Trp-134 located on the surface of a molecule.⁴⁵

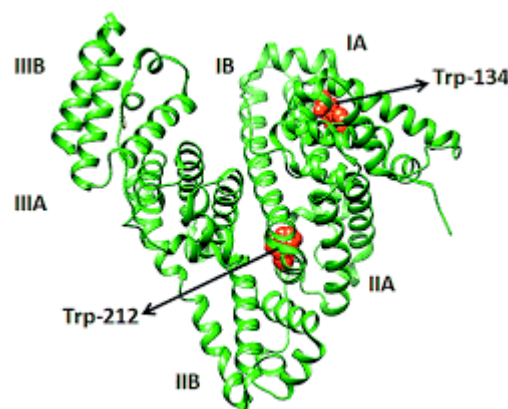


Figure 1.4: Structure of bovine serum albumin depicting the Trp-134 and Trp-212 residues.⁴⁶

Small molecules interact with bovine serum albumin through the quenching process which consists of two different mechanisms, static and dynamic. The formation of a complex between the fluorophore and the quencher at the ground state is referred as a static process, while dynamic quenching takes place at the transient excited state where the fluorophore and the quencher interact.⁴⁷ The efficiency of interaction between a small molecule and BSA is

described by a binding constant, whose values typically fall between 10^4 and 10^6 M^{-1} . In this ideal range, the binding is too low to allow the compound to be released once a specific target is reached yet sufficiently high to allow the molecule to be distributed and transported throughout the organism.⁴⁸

1.4 Techniques employed in the study of DNA/BSA interactions

1.4.1 Fluorescence spectroscopic methods

Fluorescence spectroscopy is one of the active common methods that is utilized in the examination of DNA interactions with metal complexes. This method provides information on the binding characteristics such as binding mechanism, binding sites as well as the mode of binding.^{49, 50} In DNA, the fluorescence method is performed to investigate the displacement of different stains such as ethidium bromide, Hoechst, and Rhodamine B that are bonded to DNA by metal complexes. Each stain follows a unique method in which a metal complex displaces it from DNA.

1.4.1.1 Competitive studies with ethidium bromide

This is also referred to as a quenching assay that measures the strength of DNA binding tendency by displacing intercalating ethidium bromide from DNA.⁵¹ Ethidium bromide typically has low fluorescence intensity. However, in the presence of DNA, the fluorescence intensity of EB is otherwise due to the strong intercalation of EB to the base pairs of DNA.⁵² In DNA fluorescence experiments, the metal complex is added to the EB-DNA solution, and the ethidium bromide emission intensity is then evaluated. Increasing the concentration of metal complexes that can bind to DNA quench the emission intensity of DNA-EB adduct by

accepting the excited-state electron of the EB through a photoelectron transfer mechanism⁵³ DNA-EB fluorescence intensity is expressed as a percentage. Furthermore, a high percentage is indicative of the intercalation binding mode, in which EB intercalates to DNA as previously discussed. However, a low percentage can suggest other alternatives to binding mode. The binding constant (K_b), which varies based on the kind of complex from 10^4 for low binding affinity to 10^6 for great binding affinity, is used to measure the binding affinity of complexes to DNA.⁵⁴ The binding affinity of a metal complex to DNA is quantified by Stern-Volmer equation.

$$I_0/I = 1 + K_{sv} [Q] = 1 + K_q \tau [Q] \quad (\text{Eq. 1.1})$$

where I_0 and I are the emission intensity in the absence and presence of a quencher. K_{sv} is the Stern-Volmer quenching constant which is the product of the bimolecular quenching constant and the fluorescence lifetime in the absence of added quencher in a purely dynamic quenching process. K_q is the bimolecular quenching rate constant of the fluorescence quenching process. The maximum scattering collision quenching constant of different quenchers in dynamic quenchers is (2.0×10^{10} L/mol s).⁵⁵ Thus, a high value of bimolecular quenching constant than that of dynamic fluorescence quenchers (10^{10} M⁻¹s⁻¹) demonstrates that complexes displace EB-DNA statistically rather than dynamically.⁵⁶ τ is the average DNA lifetime without quencher, which is equal to 10^{-8} s for bio-macromolecules. The quenching constant (K_{sv}) value is obtained as a slope from the plot of I_0/I vs. $[Q]$ and it is used to determine the bimolecular quenching constant. The K_b and n can be calculated from the Scatchard equation,

$$\log (I_0-I)/I = \log K_b + n \log [Q] \quad (\text{Eq.1.2})$$

where K_b is the binding constant, usually ranging from 10^4 for low binding affinity to 10^5 for strong binding affinity, varying depending on the type of a complex and n is the number of binding sites in DNA base pairs. For instance, if n is equal to one, that indicates that metal complexes bind at a single site in DNA.⁵⁴

1.4.1.2 Hoechst experiment

DNA binding affinity in fluorescence studies can also be studied using the Hoechst method. Hoechst 33258, 2-(4-hydroxyphenyl)-5-[5-(4-methylpiperazine-1-yl)benzimidazo-2-yl]-benzimidazole, is a synthetic N-methylpiperazine derivative that interacts with DNA in the minor groove at A: T-rich sequences in B-DNA at the edges of four to five contiguous base pairs with nanomolar affinity.⁴⁹ Hoechst emits a strong amount of fluorescence at 490 nm, which makes it possible to identify newly generated Hoechst-DNA adducts (upon excitation at 346 nm). It is possible to identify the mode of interaction between a transition metal ion complex and DNA by observing the variations in the fluorescence spectrum of the Hoechst-DNA adduct that occur when increasing amounts of added complexes. Reduced fluorescence intensity is a reflection of the displacement of bound Hoechst by complex.⁵⁷

1.4.1.3 Rhodamine B experiment

Rhodamine B is a luminescence that is utilized to study the interaction between the DNA molecule and the compound. This stain generally interacts with DNA through groove binding. Furthermore, it investigates the ability of a compound to replace Rhodamine B bonded to DNA through groove binders. The type of interaction in the stain is observed from a reduction of fluorescence intensity with no red shift or blue shift noticed, this indicate that a certain compound displaces Rhodamine B from DNA through groove binding.⁵⁸

1.4.1.4 Tryptophan fluorescence studies

BSA has been reported to consist of three intrinsic fluorescence characteristics that impact the fluorescence of protein, these include tryptophan, tyrosine, and phenylalanine residues.⁵⁹ However, tryptophan is the only residue that has intrinsic fluorescence, since tyrosine can be quenched if it is located near the tryptophan, amino group, and carbonyl group or if it is ionized. Phenylalanine has a very low quantum yield.⁴⁹ When metal complexes interact with bovine serum albumin the fluorescence emission intensity released depends on the amount or level of the tryptophan chains 212 and 134 open to the polar solvent.⁵⁹ For instance, the addition of the transition metal complexes to the BSA solution results in the reduction of intensity in the fluorescence spectra through different interactions on a certain fluorophore.⁴⁹ The extent of BSA binding in the fluorescence of tryptophan is also measured using the binding constant,⁶⁰ and the range of values is similar to that of DNA-Ethidium bromide binding studies. Below is a Stern-Volmer quenching equation.⁶¹

$$F_0/F = 1 + K_{sv} [Q] = 1 + k_q \tau [Q] \quad (\text{Eq. 1.3})$$

where F_0 and F are the fluorescence intensities in the absence and presence of a quencher, K_{sv} is the dynamic Stern–Volmer quenching constant [M^{-1}], k_q is the quenching rate constant [$M^{-1} s^{-1}$], τ_0 is the average lifetime of BSA in the absence of any quencher and is generally equal to 2×10^{-8} [s] and $[Q]$ is the concentration of quencher [M]. The binding constant as well as the number of binding sites are obtained from Scatchard double logarithm regression curve equation, with fluorescence intensity data, as it displays the equilibrium between free and bound molecules which is a result of small molecules that independently bind to a set of equivalent sites on BSA. Below is Scatchard equation for determining the binding constant and the number of binding site.⁶²

$$\log (F_0-F/F)= \log K_b + n \log [Q] \quad (\text{Eq. 1.4})$$

where K_b is the binding constant for drug–BSA interaction, which indicates the extent of the reaction of BSA with the drug, and n is the number of binding sites to which drug molecules are bound in the BSA macromolecule. For example, if n is equal to one, that denotes that the drug molecule binds at a single site in BSA.⁶⁰

1.4.1.5 Synchronous fluorescence studies of BSA

Synchronous fluorescence spectroscopy is another efficient method that is used to examine the binding affinity in BSA. It enables one to perceive the changes of fluorophore in the interaction of the metal complex with BSA. Also, this technique offers information on the molecular environment in regions close to the fluorophore functional groups and characteristic information of two protein residues tyrosine and tryptophan. Additionally, these modifications can be seen at wavelengths of up to 60 nm for tryptophan residue or 15 nm for tyrosine residue.⁵²

1.4.2 UV-Vis absorption spectroscopy studies

Electronic absorption spectroscopy is one of the most efficient techniques employed in the examination of DNA binding studies of metal complexes. Absorption spectral titrations are performed by monitoring the constant concentration of the metal complex upon the addition of DNA concentration.⁶³ Variation observed in the UV-Vis spectrum during titrations is indicative of the existing interaction mode. For example, a hypochromic shift due to $\pi \rightarrow \pi^*$ stacking interactions indicate the presence of intercalative binding mode, and a red shift or bathochromic

shift represents the stable double-stranded DNA.⁶⁴ The binding constant is determined from the plot of $[DNA] / (\epsilon_f - \epsilon_a)$ vs $[DNA]$, obtained from the following equation.

$$[DNA] / (\epsilon_f - \epsilon_a) = [DNA] / (\epsilon_f - \epsilon_b) + 1 / K_b (\epsilon_f - \epsilon_b) \quad (\text{Eq. 1.5})$$

where $[DNA]$ is the concentration of DNA, and ϵ_f , ϵ_a , and ϵ_b are the extinction coefficient for free complexes, the apparent extinction coefficients $A_{\text{obs}}/[\text{complex}]$, and the extinction coefficient for the complexes in the fully bound form respectively.⁶⁵

This technique can also be used to investigate any structural changes in the protein that are affected by the binding of metal complexes through different interaction modes.⁶⁶ This method also discloses the type of quenching mechanism mentioned above that metal complexes adhere to when binding to BSA.^{66, 67} With the rising temperature, the rate of movement of molecules in the solution increases. Dynamic quenching occurs when quenching efficiency increases. If the quenching is not increased static quenching must be assumed.³⁴ As a result static mechanism may be observed in the increased intensity of absorption that occurs when a complex is added to the BSA solution.⁶⁷ Any shifts in the electronic spectral bands depict the type of interactions a metal complex bound to the BSA chromophore.³⁹

1.4.3 Circular dichroic spectral studies

In biological chemistry and structural biology, circular dichroism (CD) spectroscopy is used to assess any change in macromolecule morphology when DNA interacts with metal complexes. This technique is useful for DNA binding because it can accurately identify minor conformational changes in DNA double strands that may result from the binding of metal complexes. CD spectra of DNA illustrate a positive band which is a result of base stacking

interactions and a negative band caused by the right-handed helicity of DNA. Groove binding and electrostatic interactions with metal complexes indicate less of a perturbation or no perturbation on the helicity and base stacking bands. Intercalation binding mode is demonstrated by a decrease in the intensities of both positive and negative CD bands upon the addition of metal complex concentration to the DNA solution.^{24, 50, 68}

CD studies are performed in BSA to understand conformational features in BSA molecules upon environmental perturbation due to the interaction with the metal complex. In the CD spectrum of BSA, two negative peaks that are located at 208 and 222 nm may be observed. These are mainly characteristic of the α -helix structure of the protein. As the metal complex binds to BSA, the intensities are decreased due to the unfolding of the peptide strand in the protein secondary structure. The interaction of BSA with metal complexes using circular dichroism (CD) spectroscopy is summarized by the following equation. The α -helix content of BSA before and after the addition of the metal complex can be assessed by MRE value at 208 nm according to the following equation.

$$\alpha\text{-helix}(\%) = \frac{-MRE_{208} - 4000}{33000 - 4000} \times 100 \quad (\text{Eq. 1.6})$$

where MRE₂₀₈ is the experimental MRE value at 208 nm. The MRE value for pure helix is 33,000 and its value for b-form and random coil conformation is 4000 at 208 nm. The MRE₂₀₈ used to express variations in the secondary structure of the BSA molecule is calculated by the following equation.²⁴

$$MRE_{208} = \frac{\text{observedCD}(mdeg)_{208}}{C_p \times n \times l \times 10} \quad (\text{Eq. 1.7})$$

Where n is the number of amino acid residues that is equal to 583 for BSA, C_p is the molar concentration of BSA, l is the cell path length (1mm).²⁴

1.4.4 Viscosity measurements

Viscometry is one of the tools used to support the intercalative binding mode of small molecules in DNA. As it has been previously reported that viscosity is quite sensitive to changes that affect the length of DNA double strands.⁵³ Classical intercalation model can elongate DNA double helix as they require the space between base pairs to be large enough to accommodate the attachment of small molecules resulting in viscosity enhancement. Conversely, such changes (positive or negative) are minor when small molecules are binding in the DNA grooves.⁵⁰

1.4.5 Salt concentration-dependent assays

Salt concentration-dependence assay is a method that is used to inspect the presence of electrostatic interaction. The salt cations compete with small molecules to bind to DNA as they are mutually attracted to the negative charge of the phosphate backbone group of DNA and consequently making the DNA-compound interaction weak. Moreover, increasing the ionic strength is a solution that decreases the fluorescence quenching efficiency.³⁴

1.4.6 Gel electrophoresis

The above-mentioned technique is employed in the separation of charged species that migrate to DNA in the presence of electric potential.⁵⁸ Agarose gel electrophoresis is commonly used to study the interaction between DNA and complexes through DNA cleavage. Plasmid DNA

and solution of the complex are incubated at a certain temperature, upon incubation variation of the intensity is observed. Decreased intensity after gel electrophoresis displays the existence of interaction between DNA and complex. Furthermore, the presence of interaction indicates that complexes have the propensity of reducing the pathogenic organism by interacting with the genome.⁶⁹

1.4.7 Electrochemical technique

Numerous electrochemical techniques have been reported to examine how metal-based drugs interact with DNA. The redox species have been investigated using electrochemical techniques such differential pulse voltammetry, polarography, amperometry, chronoamperometry, and cyclic voltammetry. High selectivity and sensitivity have allowed these to demonstrate their adaptability.⁷⁰ When nucleic acids interact with an electrode, they get highly adsorbed, undergo through a charge transfer reaction, and produce signals that reveal information about their concentration, structural changes, and interactions with different techniques.^{71,72} DNA binding potentials are analysed using the redox behaviour of electrochemically active molecules in absence and present of DNA.⁷⁰ Cyclic voltammetry is the most effective electrochemical method because of weak absorption bands. It provides an in-depth understanding of the DNA interaction of molecules that undergoes redox reaction active as well as information about the interaction mode of metal ions that are oxidized and reduced.⁷³ Redox active species in various oxidation states as well as combinations of various species are detectable by CV. Shift peak potentials can be used to determine the equilibrium constants for the interaction of metal complexes with DNA, and the number of base pair sites involved in binding through intercalative, electrostatic, or hydrophobic interactions can be determined by the reliance of the current(I) passed during oxidation or reduction of the bound species on the addition of DNA.⁷⁰

Given that the redox states of metal-based drugs are accessible, CV is helpful for determining the mode of action and binding strength of drug-DNA interactions.⁷⁴ The binding constant is quantified by equation.⁷⁵

$$\log (1/[DNA]) = \log K + \log (I/I_0 - I) \quad \text{Equation (1.8)}$$

where K is the binding constant, and I_0 and I are, respectively, the peak currents of the drug in the absence and presence of the DNA. The binding constant, K is determined from the intercept of the plot of $\log (1/[DNA])$ vs $\log (I/I_0 - I)$.

1.4.8 Thermodynamic parameters

The analysis of thermodynamic characteristics is essential for understanding how drugs interact with proteins. On the other hand, they enable for the assessment of whether the interaction will occur spontaneously; on the other hand, they can support the further identification of the different types of binding forces involved. The strength of the binding affinity is directly determined by the latter, whereas drug-protein interactions primarily rely on noncovalent forces.⁷⁶ The interaction forces or different forms of complex-protein bonds are characterized by changes in thermodynamic characteristics with temperature. The main values for determining the bond strength are ΔH and ΔS since ΔG is associated with spontaneous reaction process. Negative values of ΔH and ΔS demonstrate the presence of hydrogen bonds or van de Waals bonds forces. The existence of electrostatic interactions is shown by negative ΔH and positive ΔS . Positive ΔH and ΔS values confirm the presence of hydrophobic interactions.^{77,78}

$$\ln K_b = - (\Delta H^\circ / RT) + (\Delta S^\circ / R) \quad \text{(Eq. 1.9)}$$

$$\Delta G^\circ = \Delta H^\circ - T \Delta S^\circ = -RT \ln K \quad \text{(Eq. 1.10)}$$

1.4.9 Molecular modelling and simulations

Molecular docking was introduced in the mid-1970s. Docking has established itself as a crucial method for drug research and drug design over the years, because it offers insight into how chemical compounds interact with biological molecular targets. Additionally, the primary objective for the development of this tool was to understand the interaction between small and large.⁷⁹ Molecular docking is a computational method for examining the interaction between metal complexes and biological molecules.⁶⁵ Small and large molecules such as DNA and BSA are predicted in terms of their conformation and orientation. Furthermore, the outcomes of molecular docking provide useful information on the ligand-bio macromolecule systems that engage in docking. Included in this are the binding free energy (G) value, appropriate binding locations in the DNA/BSA structure, and several interaction modes that can be compared to experimentally established interactions.⁸⁰ Molecular docking calculations are performed using different software such as AutoDock 4.2 program suite, MOE version 2016.08, Gaussian 09 software.

1.5 *In vitro* cytotoxicity assays

Researchers have employed cytotoxicity as one method for studying biological molecules *in vitro*. Drugs and other chemical substances have been shown to affect cell health and metabolism. Additionally, these substances toxify cells in a variety of ways, including destroying cell membranes, preventing protein synthesis, irreversibly attaching to receptors, etc. The advantages of cytotoxicity and cell viability assays which include affordable, reliable, and reproducible have facilitated the determination of these damaged cells. *In vitro* cell viability and cytotoxicity assays with cultured cells are frequently used for cytotoxicity tests of chemicals and drug screening. Oncological researchers also employ these assays to assess the

toxicity of compounds and the prevention of tumor cell growth during treatment development. because they are quick, affordable, and do not involve using animals. These tests can be divided into four categories: dye exclusion assays, colorimetric assays, fluorometric assays, and luminometric assays. The most often employed tests are colorimetric assays, which measure biochemical markers to study the metabolic activity of the cells.⁸¹ MTS assay, (3-(4,5-dimethylthiazol-2-yl)-5-(3-carboxymethoxyphenyl)-2-(4-sulfophenyl)2Htetrazolium), is one of the calorimetric assays that practical yields formazan products that are instantly soluble in cell culture medium.⁸² Whereas MTT assay[3-(4,5-dimethylthiazol2-yl)-2,5-diphenyltetrazolium bromide], determine cell viability through mitochondrial function cells by measuring the activity of mitochondrial enzymes. NADH reduce MTT to a purple formazan.⁸¹ This method is more advantageous in comparison to the dye exclusion methods due to high reproducibility, safety, and applicable to both cell viability and cytotoxicity.⁸¹ The half inhibition concentration, which is defined as a molar concentration of a given inhibitor(I) that reduces the response rate of the uninhibited to one-half, expresses the degree of cytotoxicity of cancer cell lines produced by complexes. It is believed that substances with extremely low IC₅₀ values are highly active against cancer cell lines, whereas substances with large IC₅₀ values are ineffective.⁸³ Below is the activity criteria of half maximal inhibitory concentration.⁸⁴

Table 1.1: Classification of half maximal inhibitory concentration (IC_{50})

IC_{50} Values	Activity criteria
$< 1\mu\text{M}$	Excellent activity
1-20 μM	Good activity
20-100 μM	Moderate activity
100-200 μM	Low activity
$>200\mu\text{M}$	Inactive

The following Chapter 2 provides a detailed literature review of palladium(II) complexes that have been previously designed and developed as anticancer drugs. It also reviews the interactions of these palladium(II) complexes with DNA and bovine serum albumin.

1.6 References

1. Siegel, R. L.; Miller, K. D.; Fuchs, H. E.; Jemal, A., *CA Cancer J. Clin.*, **2022**, 72 (1), 7-33.
2. Seyfried, T. N.; Shelton, L. M., *Nutr. Metab.*, **2010**, 7, 1-22.
3. Pan, M.-H.; Ho, C.-T., *Chem. Soc. Rev.*, **2008**, 37 (11), 2558-2574.
4. Baskar, R.; Dai, J.; Wenlong, N.; Yeo, R.; Yeoh, K.-W., *Front. Mol. Biosci.*, **2014**, 1, 24.
5. Robertson, D., *J. Cell. Physiol.*, **2014**, 229 (6), 705-710.
6. Dreamstime Cancer cell. Illustration showing cancer disease development. <https://www.dreamstime.com/cancer-cell-illustration-showing-cancer-disease-development-cancer-cells-illustration-showing-cancer-disease-development-healthy-image136635080> (accessed 17 March 2023).
7. Vineis, P.; Wild, C. P., *Lancet.*, **2014**, 383 (9916), 549-557.
8. Saini, A.; Kumar, M.; Bhatt, S.; Saini, V.; Malik, A., *Int. J. Pharm. Sci.*, **2020**, 11 (7), 3121-3134.
9. Anand, P.; Kunnumakkara A.B.; Sundaram, C; Harikumar, K.B.; Tharakan, S.T.; Lai, O.S.; Sung, B.; Aggarwal, B.B.; *Pharm. Res.*, **2008**, 25 (9), 2097-116.
10. World Health Organisation Cancer. <https://www.who.int/news-room/fact-sheets/detail/cancer> (accessed 17 March 2023).
11. Omura, K., *Int. Clin. Oncol.*, **2014**, 19, 423-430.
12. Waks, A. G.; Winer, E. P., *JAMA.*, **2019**, 321 (3), 316-316.
13. Abbas, Z.; Rehman, S., *Neoplasms.*, **2018**, 1, 139-157.
14. Nikolaou, M.; Pavlopoulou, A.; Georgakilas, A. G.; Kyrodimos, E., *Clin. Exp. Metastasis.*, **2018**, 35, 309-318.

15. Litwin, M. S.; Tan, H.-J., *JAMA.*, **2017**, *317* (24), 2532-2542.
16. Price, P.; Sikora, K., *Treatment of cancer*. 7th Edition, CRC Press: **2020**.
17. Panda, V.; Khambat, P.; Patil, S., *Int. J. Clin. Med.*, **2011**, *2* (04), 515-529.
18. Mohammadlou, F.; Mansouri-Torshizi, H.; Abdi, K., *J. Biomol. Struct. Dyn.*, **2020**, 1-19.
19. Aramesh-Boroujeni, Z.; Aramesh, N.; Jahani, S.; Khorasani-Motlagh, M.; Kerman, K.; Noroozifar, M., *J. Biomol. Struct. Dyn.*, **2020**, 1-12.
20. Snustad, D. P.; Simmons, M. J., *Principles of genetics*. 7th Edition, John Wiley & Sons: **2015**.
21. Hoy, M. A., *Insect molecular genetics: an introduction to principles and applications*. 2nd Edition, Academic Press: **2003**.
22. Zianna, A.; Geromichalos, G. D.; Hatzidimitriou, A. G.; Coutouli-Argyropoulou, E.; Lalia-Kantouri, M.; Psomas, G., *J. Inorg. Biochem.*, **2019**, *194*, 85-96.
23. Dash, S. P.; Panda, A. K.; Dhaka, S.; Pasayat, S.; Biswas, A.; Maurya, M. R.; Majhi, P. K.; Crochet, A.; Dinda, R., *Dalton Trans.*, **2016**, *45* (45), 18292-18307.
24. Sorinezami, Z.; Mansouri-Torshizi, H.; Aminzadeh, M.; Ghahghaei, A.; Jamgohari, N.; Heidari Majd, M., *J. Biomol. Struct. Dyn.*, **2019**, *37* (16), 4238-4250.
25. Topală, T.; Bodoki, A.; Oprean, L.; Oprean, R., *Exp. Tech.*, **2014**, *62* (6), 1.
26. Chaires, J. B., *Curr. Opin. Struct. Biol.*, **1998**, *8* (3), 314-320.
27. Bhimaneni, S. P.; Bhati, V.; Bhosale, S.; Kumar, A., *J. Mol. Struct.*, **2021**, *1224*, 129018.
28. Erxleben, A., *CHIMIA.*, **2017**, *71* (3), 102-102.
29. Nanjunda, R.; Wilson, W. D., *Curr. Protoc. Nucleic acid Chem.*, **2012**, *51* (1), 8.8. 1-8.8. 20.
30. Zhou, C.-Y.; Xi, X.-L.; Yang, P., *Biochem. (Mosc.)*, **2007**, *72*, 37-43.

31. Li, G.-Y.; Guan, R.-L.; Ji, L.-N.; Chao, H., *Coord. Chem. Rev.*, **2014**, *281*, 100-113.
32. Kondori, T.; Shahraki, O.; Akbarzadeh-T, N.; Aramesh-Boroujeni, Z., *J. Biomol. Struct. Dyn.*, **2021**, *39* (2), 595-609.
33. Liu, X.; Diao, H.; Nishi, N., *Chem. Soc. Rev.*, **2008**, *37* (12), 2745-2757.
34. Sha, Y.; Chen, X.; Niu, B.; Chen, Q., *Chem. Biodivers.*, **2017**, *14* (10), e1700133.
35. Hayat, F.; Zia-ur-Rehman; Khan, M. H., *J. Coord. Chem.*, **2017**, *70* (2), 279-295.
36. Vieira, A. P.; Wegermann, C. A.; Ferreira, A. M. D. C., *New J. Chem.*, **2018**, *42* (15), 13169-13179.
37. Chen, Z.; Wang, Z.; Chen, J.; Chen, X.; Wu, J.; Wu, Y.; Liang, J., *Eur. J. Med. Chem.*, **2013**, *66*, 380-387.
38. Bujacz, A., *Acta Crystallogr. D: Biolog. Crystallogr.*, **2012**, *68* (10), 1278-1289.
39. Maikoo, S.; Chakraborty, A.; Vukea, N.; Dingle, L. M. K.; Samson, W. J.; de la Mare, J.-A.; Edkins, A. L.; Booyesen, I. N., *J. Biomol. Struct. Dyn.*, **2020**, 1-12.
40. Roy, S.; Nandi, R. K.; Ganai, S.; Majumdar, K.; Das, T. K., *J. Pharm. Anal.*, **2017**, *7* (1), 19-26.
41. Carter, D. C.; Ho, J. X., *Adv. Protein Chem.*, **1994**, *45*, 153-203.
42. Bourassa, P.; Kanakis, C.; Tarantilis, P.; Pollissiou, M.; Tajmir-Riahi, H., *J. Phys. Chem. B.*, **2010**, *114* (9), 3348-3354.
43. Hsieh, S.-R.; Reddy, P. M.; Chang, C.-J.; Kumar, A.; Wu, W.-C.; Lin, H.-Y., *Polymers.*, **2016**, *8* (6), 238.
44. Jahanban-Esfahlan, A.; Ostadrahimi, A.; Jahanban-Esfahlan, R.; Roufegarinejad, L.; Tabibiazar, M.; Amarowicz, R., *Int. J. Biol. Macromol.*, **2019**, *138*, 602-617.
45. Belatik, A.; Hotchandani, S.; Carpentier, R.; Tajmir-Riahi, H.-A., *PLoS One.*, **2012**, *7* (5), e36723.

46. Prasanth, S.; Raj, D. R.; Vineeshkumar, T.; Thomas, R. K.; Sudarsanakumar, C., *RSC Adv.*, **2016**, 6 (63), 58288-58295.
47. Mishra, M.; Tiwari, K.; Shukla, S.; Mishra, R.; Singh, V. P., *Spectrochim. Acta A: Mol. Biomol. Spectrosc.*, **2014**, 132, 452-464.
48. Protas, A. V.; Popova, E. A.; Mikolaichuk, O. V.; Porozov, Y. B.; Mehtiev, A. R.; Ott, I.; Alekseev, G. V.; Kasyanenko, N. A.; Trifonov, R. E., *Inorg. Chim. Acta.*, **2018**, 473, 133-144.
49. Ćočić, D.; Jovanović-Stević, S.; Jelić, R.; Matic, S.; Popović, S.; Djurdjević, P.; Baskić, D.; Petrović, B., *Dalton Trans.*, **2020**, 49 (41), 14411-14431.
50. Aramesh-Boroujeni, Z.; Jahani, S.; Khorasani-Motlagh, M.; Kerman, K.; Noroozifar, M., *J. Biomol. Struct. Dyn.*, **2019**.
51. Arjmand, F.; Muddassir, M.; Yousuf, I., *J. Photochem. Photobiol. B: Biol.*, **2014**, 136, 62-71.
52. Zhang, Y. P.; Li, Y.; Xu, G. C.; Li, J. Y.; Luo, H. Y.; Li, J. Y.; Zhang, L.; Jia, D. Z., *Appl. Organomet. Chem.*, **2019**, 33 (3), e4668.
53. Neelakantan, M.; Balamurugan, K.; Balakrishnan, C.; Subha, L., *Appl. Organomet. Chem.*, **2018**, 32 (4), e4259.
54. Tabrizi, L.; Chiniforoshan, H.; Tavakol, H., *Spectrochim. Acta A: Mol. Biomol. Spectrosc.*, **2015**, 141, 16-26.
55. Suryawanshi, V. D.; Walekar, L. S.; Gore, A. H.; Anbhule, P. V.; Kolekar, G. B., *J. Pharm. Anal.*, **2016**, 6 (1), 56-63.
56. Omondi, R. O.; Bellam, R.; Ojwach, S. O.; Jaganyi, D.; Fatokun, A. A., *J. Inorg. Biochem.*, **2020**, 210, 111156.
57. Medjedović, M.; Simović, A. R.; Ćočić, D.; Milutinović, M.; Senft, L.; Blagojević, S.; Milivojević, N.; Petrović, B., *Polyhedron.*, **2020**, 178, 114334.

58. Aramesh-Boroujeni, Z.; Jahani, S.; Khorasani-Motlagh, M.; Kerman, K.; Aramesh, N.; Asadpour, S.; Noroozifar, M., *J. Biomol. Struct. Dyn.*, **2020**, *38* (16), 4746-4763.
59. Karami, K.; Hosseini-Kharat, M.; Sadeghi-Aliabadi, H.; Lipkowski, J.; Mirian, M., *Eur. J. Med. Chem.*, **2014**, *73*, 8-17.
60. Karami, K.; Jamshidian, N.; Zakariazadeh, M., *Appl. Organomet. Chem.*, **2019**, *33* (3), e4728.
61. Karami, K.; Hashemi, S.; Lipkowski, J.; Mardani, F.; Momtazi-boroujeni, A. A.; Lighvan, Z. M., *Appl. Organomet. Chem.*, **2017**, *31* (10), e3740.
62. Ayyannan, G.; Mohanraj, M.; Gopiraman, M.; Uthayamalar, R.; Raja, G.; Bhuvanesh, N.; Nandhakumar, R.; Jayabalakrishnan, C., *Inorg. Chim. Acta.*, **2020**, *512*, 119868.
63. Kosiha, A.; Parthiban, C.; Ciattini, S.; Chelazzi, L.; Elango, K. P., *J. Biomol. Struct. Dyn.*, **2018**, *36* (16), 4170-4181.
64. Franich, A. A.; Živković, M. D.; Čočić, D.; Petrović, B.; Milovanović, M.; Arsenijević, A.; Milovanović, J.; Arsenijević, D.; Stojanović, B.; Djuran, M. I., *J. Biol. Inorg. Chem.*, **2019**, *24* (7), 1009-1022.
65. Abdel-Rahman, L. H.; Adam, M. S. S.; Abu-Dief, A. M.; Moustafa, H.; Basha, M. T.; Aboraia, A. S.; Al-Farhan, B. S.; Ahmed, H. E. S., *Appl. Organomet. Chem.*, **2018**, *32* (12), e4527.
66. Bhimaneni, S. P.; Bhati, V.; Bhosale, S.; Kumar, A., *J. Mol. Struct.*, **2021**, *1224*, 129018.
67. Thirunavukkarasu, T.; Sparkes, H. A.; Natarajan, K., *Inorg. Chim. Acta.* **2018**, *482*, 229-239.
68. Zhao, Z.; Zhang, J.; Zhi, S.; Song, W., *J. Inorg. Biochem.*, **2019**, *197*, 110696.

69. Abdel-Rahman, L. H.; Abu-Dief, A. M.; Shehata, M. R.; Atlam, F. M.; Abdel-Mawgoud, A. A. H., *Appl. Organomet. Chem.*, **2019**, *33* (4), p.e4699.
70. Ajmal, M., *J. Coord. Chem.*, **2017**, *70* (15), 2551-2588.
71. Armistead, P. M.; Thorp, H. H., *Anal. Chem.*, **2000**, *72* (16), 3764-3770.
72. Hvastkovs, E. G.; Buttry, D. A. *Langmuir*, **2009**, *25* (6), 3839-3844.
73. Li, Y.; Zhao, J.; He, C.-C.; Zhang, L.; Sun, S.-R.; Xu, G.-C., *J. Inorg. Biochem.*, **2015**, *150*, 28-37.
74. Feng, Q.; Li, N.-Q.; Jiang, Y.-Y., *Anal. Chim. Acta.*, **1997**, *344* (1-2), 97-104.
75. Ramotowska, S.; Ciesielska, A.; Makowski, M., *Molecules*, **2021**, *26* (11), 3478.
76. Wang, L.; Zhang, W.; Shao, Y.; Zhang, D.; Guo, G.; Wang, X., *Anal. Chim. Acta.*, **2022**, *1219*, 340012.
77. Galkina, P. A.; Proskurnin, M. A., *Appl. Organomet. Chem.*, **2018**, *32* (4), e4150.
78. Lima, E. C.; Gomes, A. A.; Tran, H. N., *J. Mol. Liq.*, **2020**, *311*, 113315.
79. Pinzi, L.; Rastelli, G., *Int. J. Mol. Sci.*, **2019**, *20* (18), 4331.
80. Karami, K.; Jamshidian, N.; Zakariazadeh, M.; Momtazi-Borojeni, A. A.; Abdollahi, E.; Amirghofran, Z.; Shahpiri, A.; Nasab, A. K., *Comput. Biol. Chem.*, **2021**, *91*, 107435.
81. Aslantürk, Ö. S., *Genotoxicity: A Predictable Risk to Our Actual World.*, Larramendy, M. and Soloneski, S. eds, IntechOpen, **2018**, *2*, 64-80.
82. Arab-Bafrani, Z.; Shahbazi-Gahrouei, D.; Abbasian, M.; Fesharaki, M., *J. Mol. Struct.*, **2016**, *6* (2), 112.
83. Kaya, B.; Yılmaz, Z. K.; Şahin, O.; Aslim, B.; Tükenmez, Ü.; Ülküseven, B., *J. Biol. Inorg. Chem.*, **2019**, *24* (3), 365-376.
84. Indrayanto, G.; Putra, G. S.; Suhud, F., *Profiles of Drug Subst. Excip. Relat. Methodol.*, **2020**, *46*, 273-307.

Chapter 2

A review of palladium(II) complexes as anticancer agents and their interactions with DNA/BSA interactions

2.1 General background

Metal complexes have been utilized as therapeutic agents against a wide range of diseases.¹ The serendipitous discovery of *cisplatin* as an anticancer drug has unfolded transition metals to be explored in chemotherapy.² To date, cisplatin has been applied to numerous cancer cells such as the cervix, breast, ovary, testis, lung, bladder, and colon cancer.³ The modification of cisplatin structure led to the design and development of other clinically approved platinum-based drugs which include, *heptaplatin*, *lobaplatin*, *nedaplatin*, *oxaliplatin*, and *carboplatin*, which have been extensively used in the treatment of cancer.⁴ However, the use of therapeutic cisplatin and its analogues is associated with shortcomings such as toxicity to normal cells, limited solubility in aqueous media, and acquire or intrinsic resistance.^{2,5,6} These limitations introduced the search for other metal-based drugs that are non-resistant to some cancer cells, selective, and have a broad spectrum of activity.⁴

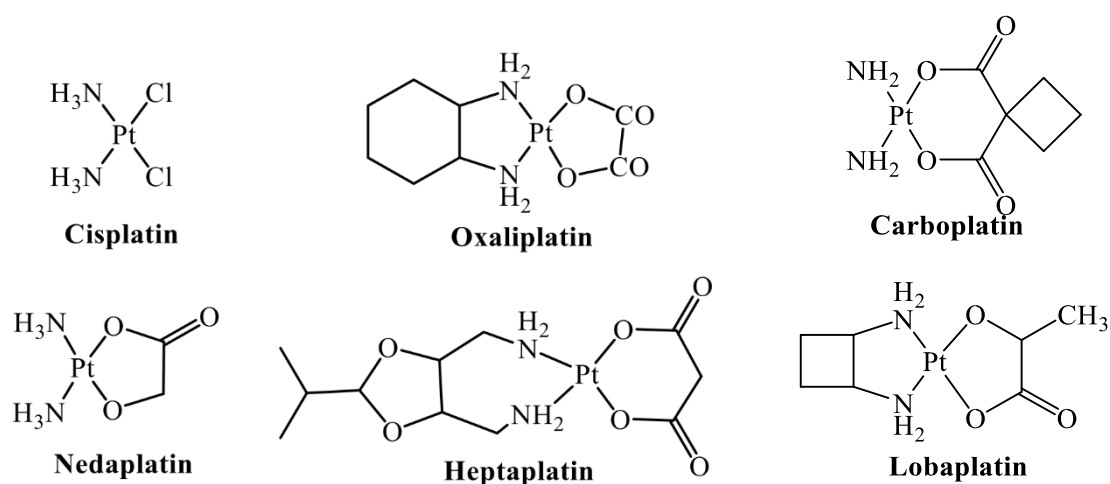


Figure 2.1: Platinum complexes used in the treatment of cancer.⁷

The mechanism of action of cisplatin against cancer cells involves the interaction of platinum-based drugs with DNA. Initially, cisplatin is introduced into the bloodstream and interacts with blood plasma protein which transports the drug to the cell membrane by passive diffusion.⁸ In the extracellular matrix and blood, the presence of a high concentration of chloride ions (104 mM) prevents the activation of cisplatin. Thus, inside the membrane, cisplatin is activated by hydrolysis in which the chloride ions are kinetically displaced with water molecules due to a high concentration of water molecules and low concentration of chloride ions (4-20 mM) resulting in the formation of an intermediate hydrolyzed platinum product cis-[Pt(NH₃)₂(H₂O)Cl]⁺.⁹ Further displacement of chloride ions produces cis-[Pt(NH₃)₂(H₂O)₂.

The diaqua species cis-[Pt(NH₃)₂(H₂O)₂] is highly reactive due to its electron deficiency. Hence, it interacts with nucleophilic biological molecules such as glutathione, methionine, metallothionein, and protein other than DNA, reducing the amount of cisplatin that coordinates with DNA. These compounds are associated with cisplatin resistance and toxicity. The preferred site for the coordination of cisplatin to DNA nucleobases is nitrogen 7 of guanine due to the high nucleophilicity of N7. Consequently, the mechanism involves two binding modes to the DNA, the mono aqua species binds to the purine base or the di aqua species binds through intra or interstrand bifunctional binding.¹⁰⁻¹³ Cellular processing which is the last step involved repairing the damaged cell by allowing a DNA single strand to form a DNA template to prevent the progression of the cancer cell.^{14, 15} Thus, palladium(II) complexes adopt a similar mechanism of action toward cell death.

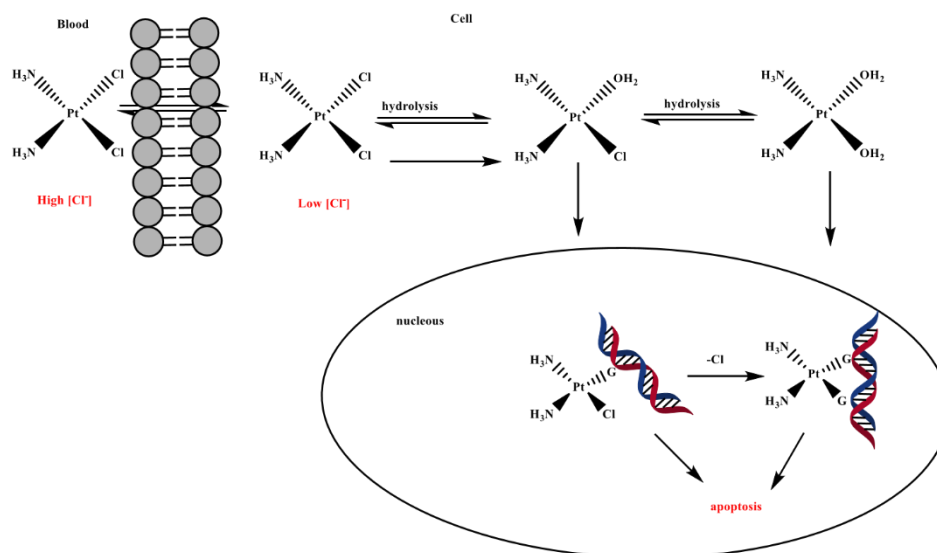


Figure 2.2: Mechanism of cisplatin; intracellular hydrolysis and activation of cisplatin leading to apoptosis.¹⁶

As mentioned above, the drawbacks of platinum-based drugs have caused researchers to study other metal-based drugs with low toxicity and better efficacy.¹⁷ The research is directed to the manipulation of the metal ion, variable oxidation states, coordination numbers, and ligands. This can provide unique characteristics resulting in numerous metal-based drugs with improved anticancer activity being developed. In addition, varied oxidation states and coordination geometry of numerous transition metals, influence thermodynamics and kinetic properties during biochemical reactions.^{1, 18} Other metal-based drugs including ruthenium complexes have shown promising anticancer activity and have reached clinical trials (KP1019 and NAMI-A).¹⁹ The significant similarities of coordination chemistry between palladium(II) and platinum(II) complexes, improved solubility as well as better cytotoxicity which allow palladium complexes to be investigated further in the development of new potent anticancer drugs.²⁰ Thus, this section highlights the relation of the DNA, a protein used for transportation and distribution in the blood plasma such as bovine serum albumin as well as cytotoxicity of palladium(II) complexes.

The electronic and steric influence of chelating ligands consisting of two or more donor atoms may determine the nature of coordination complexes formed, ranging from mononuclear, and dinuclear to multinuclear species.^{21,22} The cationic character of the metal-ion in complexes consequently increases their membrane permeability and facilitates the electrostatic interactions between the metal complex and the negatively charged phosphate backbone of the DNA molecule.²³ The propensity of these complexes to treat human disease has been evaluated, and the most commonly evaluated in cancer cells are polynuclear palladium(II) complexes with polyamines.^{24,25} In Addition, the derivatives of palladium complexes bearing nitrogen donor atoms exhibit promising biological activity and reduced toxicity.^{26, 27}

2.2. Studies of DNA/BSA interactions and cytotoxicity of metallodrugs

Cis-palladium, *cis*-[Pd(NH₃)₂Cl₂] was the first palladium(II) complex to be investigated for anticancer activity.²⁸ Cis-palladium, in contrast to cisplatin, does not exhibit anticancer activity. Although cis palladium undergoes an inactive trans-conformation and hydrolyses very quickly, when it interacts *in vivo* with biological molecules, especially proteins, it does not reach its pharmacological target, DNA. Enhanced activity of the above-mentioned complexes advocates the development of palladium-based drugs stabilized by the coordination of nitrogen ligated compound and a non-labile leaving group which contributes to maintaining the structural identity of the complex long enough *in vivo*.

Tusek-Bozic and his group improved the anticancer activity of one of the early palladium(II) complexes by introducing monoethylphosphonate and diethylphosphonate species on the quinolmethyl substructure that facilitated increased solubility. This compound has a general

formula *trans*-[PdCl₂(2-dqmp)] (2-dqmp = diethyl-2-quinolmethylphosphonate, **1**), as shown in **Figure 2.3**.²⁹

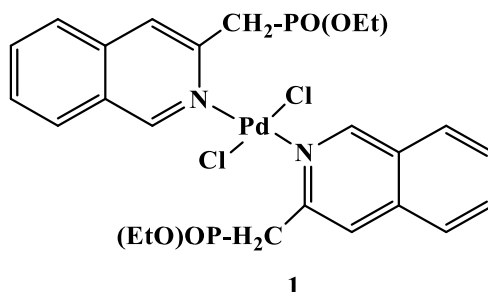


Figure 2.3: Chemical structure of *trans*-palladium (II) complex supported on diethyl-2-quinolylmethylphosphonate ligand.²⁹

2.2.1 Mononuclear palladium complexes

Several mononuclear palladium(II) complexes have been studied and exhibit promising anticancer activity and DNA/BSA interactions. In one such report, Ojwach and co-workers reported the role of *trans*-heteroatoms carrier ligands of palladium(II) pincer complexes with the general formula [Pd(**L1**)Cl]BF₄ (**2**), [Pd(**L2**)Cl]BF₄ (**3**), [Pd(**L3**)Cl]BF₄ (**4**), [Pd(**L4**)Cl]BF₄ (**5**) where 2,6-bis[(1H-pyrazol-1-yl)methyl]pyridine (**L1**), bis[2-(1H-pyrazol-1-yl)ethyl]amine (**L2**), bis[2-(1H-pyrazol-1-yl)ethyl]ether (**L3**), and bis[2-(1H-pyrazol-1-yl)ethyl]sulphide (**L4**) to cytotoxicity and DNA/BSA interactions, see **Figure 2.4**.³⁰ The complexes were found to intercalate to CT-DNA and follow the trend **5** > **2** > **3** > **4**. This trend is consistent with the binding affinity of BSA. The higher binding strength of **5** is assigned to both the electronic and steric effects. The *in vitro* studies against HeLa and MRC-5 SV2 showed a half inhibitory concentration effect that is greater than 100 μM indicating a negative correlation to the CT-DNA/BSA trend. Additionally, this shows that high binding constants of

the complexes in DNA/BSA interactions do not guarantee the efficacy of the complexes in cytotoxicity. Moreover, low cytotoxic activity is ascribed to the lack of aromaticity and planarity of the spectator ligands.

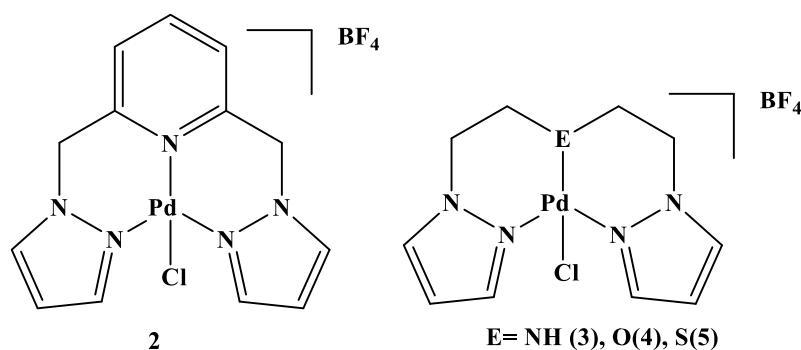


Figure 2.4: Chemical structures of palladium(II) complexes bearing bis-(pyrazolyl) ligands.³⁰

Omondi *et al* investigated the anticancer activity and CT-DNA interaction of palladium(II) complexes supported on tridentate bis(benzazole) ligands with a general formula $[\text{Pd}(\text{L } 1)\text{Cl}]\text{BF}_4$ (**6**); $[\text{Pd}(\text{L } 2)\text{Cl}]\text{BF}_4$ (**7**); $[\text{Pd}(\text{L } 3)\text{Cl}]\text{BF}_4$ (**8**), where 2,6-bis(benzimidazol-2-yl)pyridine (**L 1**), 2,6-bis(benzoxazol-2-yl)pyridine (**L 2**), and 2,6-bis(benzothiazol-2-yl)pyridine (**L 3**) with $[\text{Pd}(\text{NCMe})_2\text{Cl}_2]$ and $[\text{Pd}(\text{L } 4)\text{Cl}]\text{Cl}$ (**9**) where bis[(1H-benzimidazol-2-yl)methyl]amine is **L4**, see **Figure 2.5**.³¹ Interaction of palladium (II) complexes with CTDNA is influenced by the steric bulk of the ligands, therefore the complexes follows the sequence **6** > **7** > **8** > **9**. The antiproliferative effect of the complexes against two cancer cell lines (HeLa, MRC5-SV2) and in a healthy cell line (MRC5) was examined. The potency against cancer cell lines, HeLa and MRC5-SV2 follow this order **6** > **7** > **8** > **9**, IC_{50} values, **6**($16.3 \pm 4.9 \mu\text{M}$) > **7**($70.3 \pm 16.6 \mu\text{M}$)> **8**($73.6 \pm 7.0 \mu\text{M}$)> **9**($88.4 \pm 21.5 \mu\text{M}$) and **8**($18.5 \pm 2.6 \mu\text{M}$)> **7**($21.1 \pm 4.0 \mu\text{M}$)> **6**($25.0 \pm 0.3 \mu\text{M}$)> **9**($39.8 \pm 3.4 \mu\text{M}$). Complex **9** demonstrated low cytotoxic effects on the cancer cell lines, this is attributed to the reduced number of

aromaticity and planarity in the complex as well as the steric hindrance caused by methylene moiety.

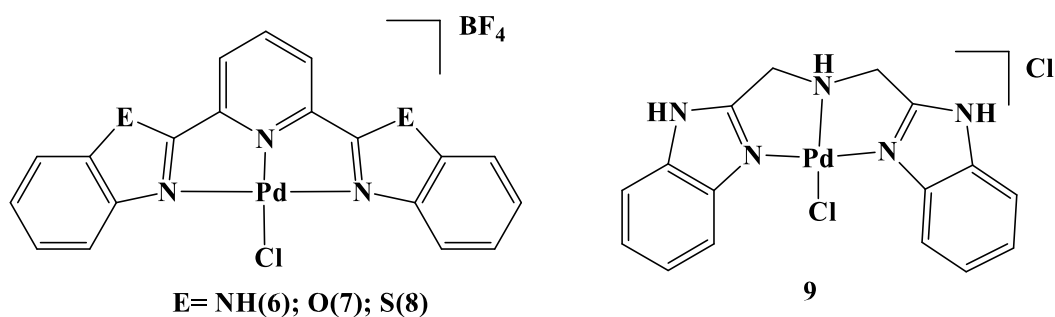


Figure 2.5: Chemical structures of palladium(II) complexes supported on tridentate bis(benzazole) ligands.³¹

In a follow-up work, Omondi *et al* reported the cytotoxicity and DNA/BSA interaction of palladium(II) complexes bearing π -conjugated carboxamide ligand. These complexes consist of general formula of [Pd(L1)Cl] (**10**); [Pd(L2)Cl] (**11**); [Pd(L3)Cl] (**12**); and [Pd(L4)Cl] (**13**) where N-(pyridin-2-ylmethyl)pyrazine-2-carboxamide (**L1**), N-(quinolin-8-yl)pyrazine-2-carboxamide (**L2**), N-(quinolin-8-yl)picolinamide (**L3**) and N-(quinolin-8-yl)quinoline-2-carboxamide (**L4**), as shown in **Figure 2.6**.³² The relative binding affinities of the complexes with DNA and BSA follows the order **10** > **11** > **12** > **13**. This trend is attributed to the electronic properties of the spectator ligand. Half inhibitory concentration (IC₅₀) of the complexes obtained during the evaluation of the complexes **10-13**, against A549, PC-3, HT29, Caco-2, HeLa, and a normal cell (KMST-6) demonstrated that complexes **11** and **13** have minimal cytotoxic activity in all cancer lines. Cytotoxic effect against A549 cells follows a slightly different trend compared to the DNA interaction, **10**(3.9 μ M) > **12**(30.8 μ M) > **11**

(57.7 μM) > **13**(90.8 μM). This trend is explained by the nature of the inert spectator ligand which determines the biological activities of the corresponding complexes, the higher the cytotoxic activity of the complex the smaller the inert chelating ligand that promotes facile and strong binding to the molecular target DNA.

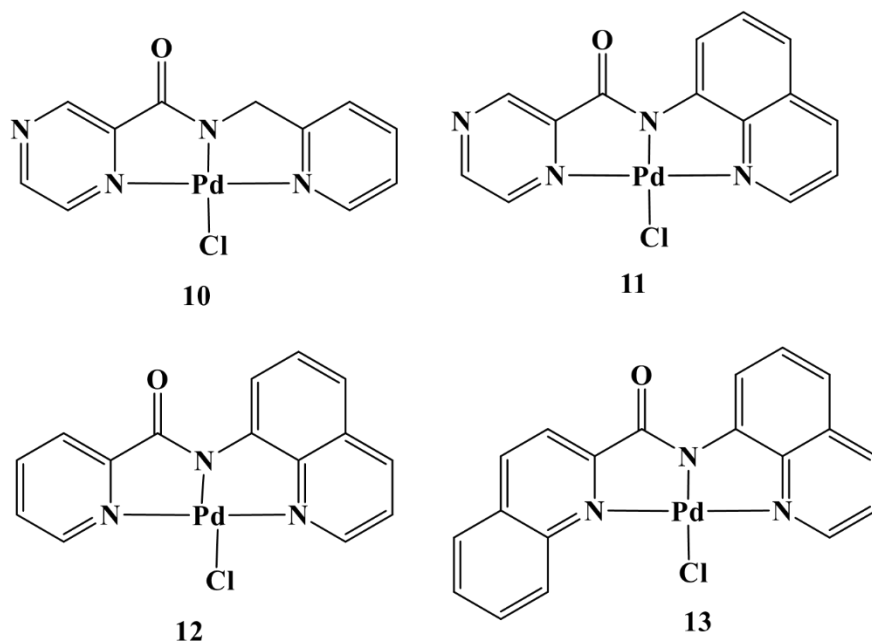


Figure 2.6: Chemical structures of a series of palladium(II) complexes bearing π -conjugated carboxamide ligand. ³²

Petrović *et al* investigated DNA/BSA interactions and cytotoxicity of the palladium(II) complexes of the type; $[\text{Pd}(\text{H}_2\text{LtBu})\text{Cl}]\text{Cl}$ (**14**) and $[\text{Pd}(\text{Me}_2\text{LtBu})\text{Cl}]\text{Cl}$ (**15**) (where H_2LtBu = 2,6-bis(5-(tert-butyl)-1H-pyrazol-3-yl)pyridine and Me_2LtBu is 2,6-bis(5-(tert-butyl)-1-methyl-1Hpyrazol-3-yl)pyridine), as shown in **Figure 2.7**. ³³ DNA/BSA interaction of the complexes was found to follow the **14** > **15**. The cytotoxic effects of the complexes against the studied HeLa and PANC-1 cell lines, indicate that complex **14** is more active than **15**, due to

the less steric effect of complex **14**. Therefore, in this study, there is a positive correlation between DNA/BSA binding propensities and antiproliferative properties.

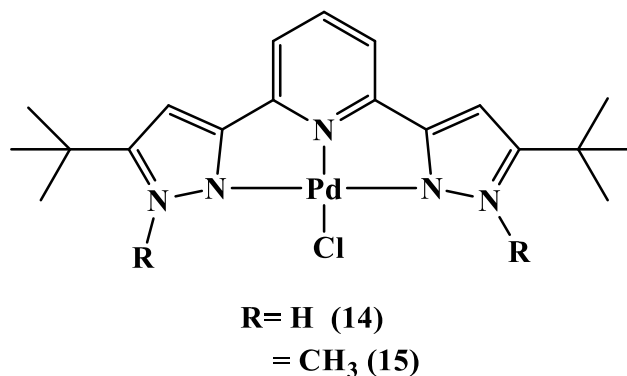


Figure 2.7: Chemical structure of (pyrazolyl)pyridine palladium(II) complexes.³³

The work of Karami *et al* reported the effect of electron-donating and electron-withdrawing groups in DNA, bovine serum albumin as well as cytotoxicity. The palladium(II) complexes with the general formula [Pd(L1)Cl] (**16**) and [Pd(L2)Cl₂] (**17**) where [(E)-2-[(anthracene-9-ylmethylene)amino]-5-nitroaniline] **L1** and (E)-2-[(anthracene-9-ylmethylene)amino]-5methyl aniline (**L2**) see **Figure 2.8**.³⁴ The interaction of the complexes with DNA follow this increasing sequence **16** ($0.027 \times 10^6 \text{ M}^{-1}$) < **17** ($0.297 \times 10^6 \text{ M}^{-1}$), indicating that electron donating group control the binding propensity of the complexes to the DNA. The interaction of the complexes with bovine serum albumin is in agreement with the DNA trend. Complex **17** demonstrated a higher cytotoxic effect against MCF-7 cancer cell lines in comparison to complex **16**, this is attributed to the presence of an electron-donating group. These findings are consistent with the DNA/BSA binding constants, showing that DNA is the main target in the mechanism of cell death.

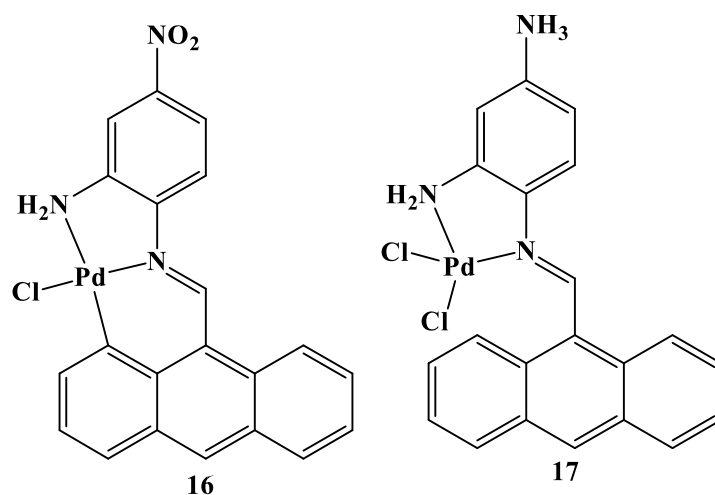


Figure 2.8: Chemical structures of (E)-2-[(anthracene-9-ylmethylene)amino] aniline palladium(II) complexes.³⁴

In another related development, Naskar and co-workers evaluated the cytotoxicity as well as DNA/BSA interactions of palladium(II) complexes supported on benzothiazole ligands with general formula [Pd(2-(benzothiazol-2-yl)-6-((2(ethylthio)phenyl)imino)methyl)phenol)Cl], see **Figure 2.9**.³⁵ The complex displays a higher half inhibitory concentration ($IC_{50} = 9.55 \pm 1.23 \mu\text{M}$) against human gastric cancer cell lines which is lower than the common cisplatin drug ($IC_{50} = 23.13 \pm 1.03 \mu\text{M}$). The complex also exhibited no toxicity towards normal cell lines (200 μM). In addition, the complex binds to the DNA through groove binding with a reported binding constant of $4.019 \times 10^5 \text{ M}^{-1}$ and $2.929 \times 10^4 \text{ M}^{-1}$ for BSA. Therefore, the complex exhibits a positive correlation between cytotoxicity and DNA/BSA interaction.

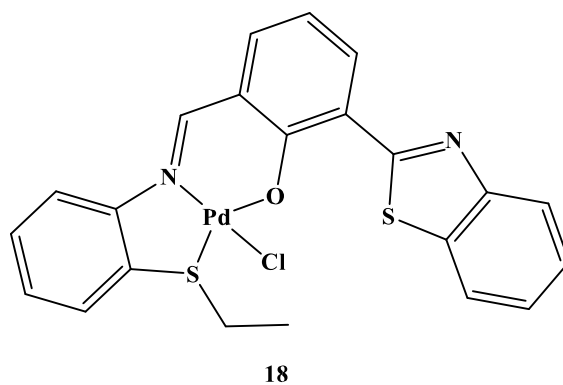


Figure 2.9: Chemical structure of 2-(benzothiazol-2-yl)-6-(((2-(ethylthio)phenyl)imino)methyl)phenol)benzothiazole palladium(II) complex.³⁵

2.2.2. Dinuclear palladium complexes

Investigation of anticancer activity of metal complexes is being explored in multinuclear complexes. Additionally, some dinuclear complexes exhibit enhanced anticancer activity. For instance, Vijtek and the group reported the cytotoxicity of dinuclear spermine palladium complex against triple-negative breast cancer, as shown in **Figure 2.10**.³⁶ This breast carcinoma was reported to have a low prognosis and restricted when treated with platinum drugs. Dinuclear palladium(II) spermine complex exhibited anticancer activity *in vivo* and *in vitro* and lower toxicity in comparison to platinum drugs which is an indication of the used palladium complex to TNBC.

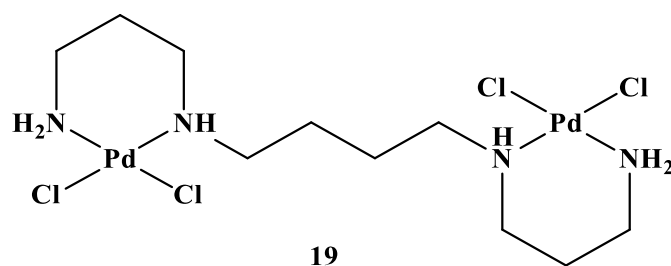


Figure 2.10: Chemical structure of dinuclear spermine palladium(II) complex.³⁶

In another work, the influence of homometallic palladium(II) complex supported on bridging ligand in DNA/BSA interaction, and cytotoxicity was reported by Ćocić *et al.*³⁷ The evaluated palladium(II) complex with type $[\text{Pd}_2(\text{tpbd})\text{Cl}_2]\text{Cl}_2$ (**20**) where (tpbd = N,N,N',N'-tetrakis(2pyridylmethyl)benzene-1,4-diamine), as shown in **Figure 2.11**. Complex **20** interacts with DNA through intercalation and groove binding mode with a binding constant of $K_b = 5.75 \pm 0.01 \times 10^4 \text{ M}^{-1}$. In addition, the complex interacts with bovine serum albumin, and the binding constant $(5.95 \pm 0.05) \times 10^4 \text{ M}^{-1}$. Complex **20** displayed low inhibitory effects ($139 \pm 7 \mu\text{M}$) towards human melanoma cancer cell line HTB150 indicating that the complexes are inactive.

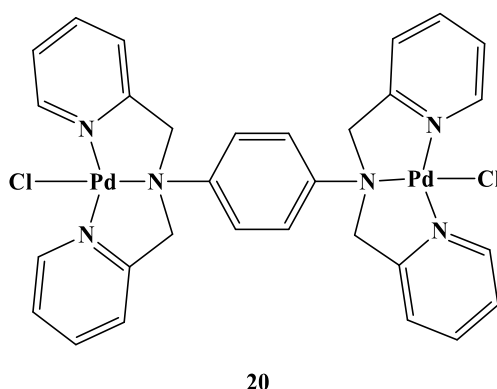


Figure 2.11: Chemical structure of platinum(II) complexes bearing (2-pyridylmethyl)benzene-1,4-diamine ligand.³⁷

Ćoćić *et al*, investigated the cytotoxicity and DNA/BSA interactions of the dinuclear palladium complexes. They studied palladium complexes with a general formula, $[\{Pd(2,2'$ -bipy)Cl $\}_2(\mu\text{pz})](ClO_4)_2$ (**21**), $[\{Pd(dach)Cl\}_2(\mu\text{-pz})](ClO_4)_2$ (**22**), $[\{Pd(en)Cl\}_2(\mu\text{-pz})](ClO_4)_2$ (**23**), (where pz = pyrazine, 2,2'-bipy = 2,2'-bipyridyl, dach = trans-(±)-1,2-diaminocyclohexane, and en = ethylenediamine), see **Figure 2.12**.³⁸ Complex **21** exhibits a high binding strength toward DNA molecule compared to other complexes and the binding constants of the complexes follow the trend **21** > **22** > **23**. The order of BSA binding constants is consistent with that of the DNA and thus demonstrating a positive relationship between the two parameters. Interestingly, the cytotoxic effects of the complexes against the HeLa cell line follow the same order recorded for the DNA interactions, **21** > **22** > **23**.

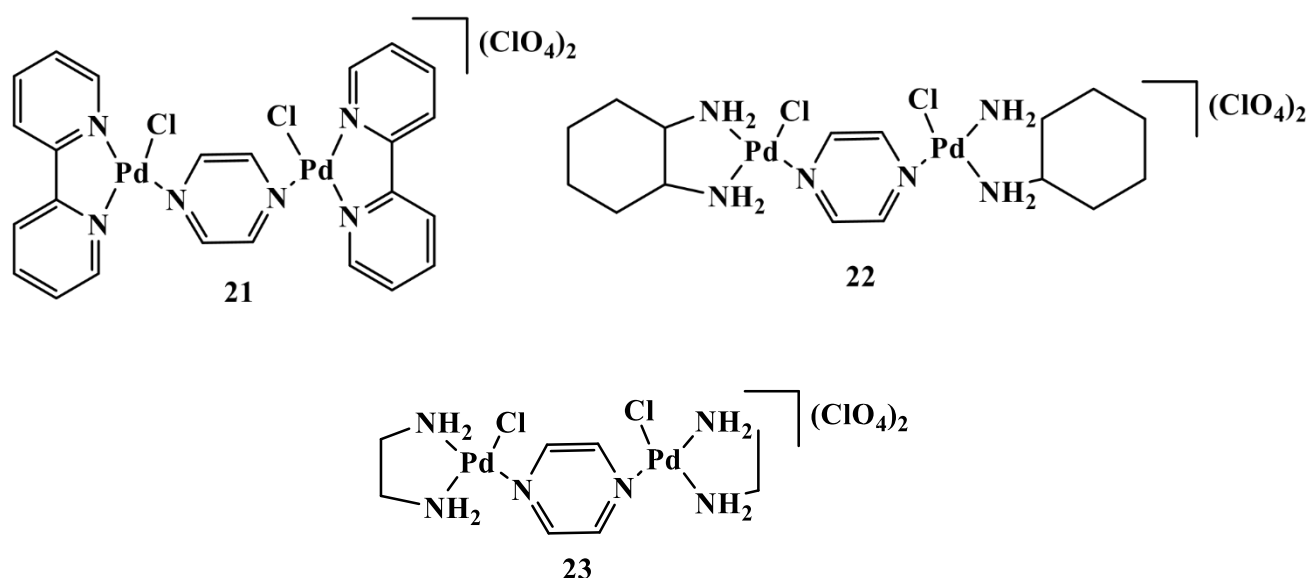


Figure 2.12: Chemical structures of dinuclear bridged-pyrazine palladium(II) complexes.³⁸

In another study done by Franich *et al* evaluated *in vitro* cytotoxic activities and DNA/BSA binding in dinuclear palladium(II) complexes with a series of pyridine-based bridging ligands that have a formula, $[\{Pd(en)Cl\}_2(\mu\text{-L})_2]$ (L is pyridine-based bridging ligand 4,4'-bipyridine

(4,4'-bipy, **24**), 1,2-bis(4-pyridyl)ethane (bpa, **25**), 1,2-bis(4-pyridyl)ethylene (bpe, **26**) and en is bidentate coordinated ethylenediamine), see **Figure 2.13**.³⁹ The cytotoxicity effect of palladium(II) complexes towards both A549 and LLC1 cells indicated that complex **26** is more active than the other complexes following the order **26** > **25** > **24**. However, the interaction of the complexes with DNA / BSA follows a different order **26** > **25** > **24**, complex **26** and **25** bind more strongly to these biological molecules than complex **24**. Positive correspondence between the cytotoxic effectiveness sequence followed by these complexes and that of DNA and BSA interaction is demonstrated.

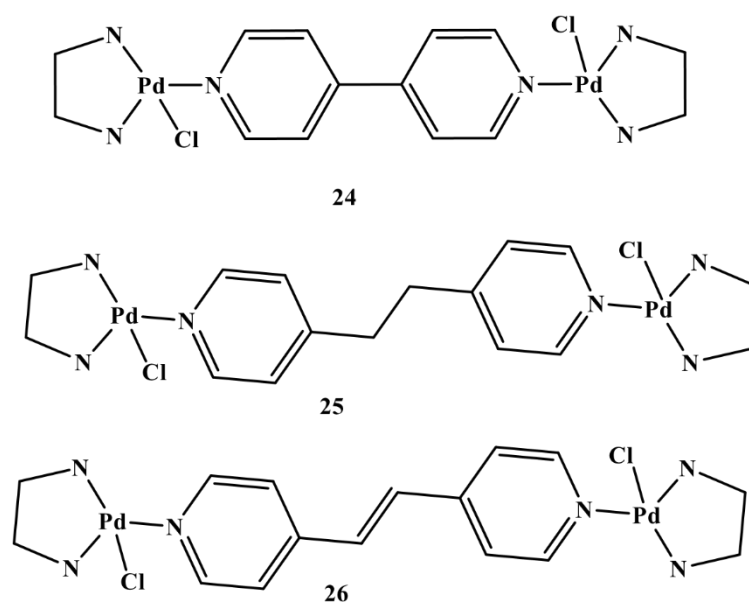


Figure 2.13: Chemical structures of dinuclear palladium(II) complexes bearing pyridine-based bridging ligands.³⁹

2.3. Summary

Despite the efficiency of the common platinum-based drug in chemotherapy, its application against a variety of cancer cells is restricted due to resistance to some cancer cells and toxicity to normal cells. This catastrophe could be resolved by developing new metallodrugs with suitable ligands in terms of biological properties. With palladium showing a chemical resemblance to platinum complexes, a variety of palladium complexes have been prepared and investigated for their biological activity. Recent studies have shown that palladium complexes exhibit higher cytotoxicity and lower toxicity compared to some clinically used platinum drugs.⁴⁰ However, it should be noted that due to the quick ligand-exchange rates, palladium(II) derivatives cannot maintain their structural integrity in the cytoplasm for long enough to reach the DNA target.⁴¹ This challenge can be overcome by coordinating chelating ligands to palladium. Hence, in this review, both mononuclear and dinuclear palladium(II) complexes consisting of chelating ligands have shown good anticancer activity with less toxicity to normal cells. Additionally, most palladium(II) complexes interact with DNA through intercalative mode and it has been demonstrated that the complexes are transported to the target cells using bovine serum albumin. The data of this review showing the correlation between the DNA/BSA and cytotoxicity of mononuclear and dinuclear palladium(II) complexes is summarized in **Table 2.1** and **Table 2.2**.

Table 2.1: Summarized DNA, BSA binding constants, and cytotoxic activity of mononuclear palladium(II) complexes.

Complex	DNA binding, K_b (M^{-1})	BSA Binding, K (M^{-1})	Cytotoxicity (IC_{50} , μM)			Ref
			HeLa	MRC-5 SV2		
2	$(4.99 \pm 0.50) \times 10^5$	$(6.70 \pm 0.11) \times 10^6$	>100	>100		30
3	$(3.66 \pm 0.41) \times 10^5$	$(3.42 \pm 0.22) \times 10^6$	>100	>100		
4	$(1.38 \pm 0.32) \times 10^5$	$(1.00 \pm 0.12) \times 10^6$	>100	>100		
5	$(5.54 \pm 0.51) \times 10^5$	$(40.16 \pm 0.66) \times 10^6$	>100	>100		
			HeLa	MRC5-SV2	MRC5	
6	5.53×10^6	n.d	16.3 ± 4.9	25.0 ± 0.3	37.3 ± 0.2	31
7	2.20×10^6	n.d	70.3 ± 16.6	21.1 ± 4.0	26.1 ± 3.3	
8	1.01×10^6	n.d	88.4 ± 21.5	18.5 ± 2.6	20.5 ± 1.9	
9	0.53×10^6	n.d	73.6 ± 7.0	39.8 ± 3.4	96.8 ± 0.7	
			A549	PC-3	HT-29	
10	$(11.01 \pm 0.52) \times 10^4$	$(12.25 \pm 0.14) \times 10^5$	3.9	9.8	0.1	32
11	$(1.67 \pm 0.44) \times 10^4$	$(9.14 \pm 0.21) \times 10^5$	57.7	>100	>100	
12	$(0.71 \pm 0.01) \times 10^4$	$(0.422 \pm 0.03) \times 10^5$	30.8	5.4	1.9	
13	$(0.35 \pm 0.02) \times 10^4$	$(0.13 \pm 0.01) \times 10^5$	90.8	>100	>100	
			HeLa	PANC-1	MRC-5	
14	$(1.9 \pm 0.1) \times 10^4$	$(1.9 \pm 0.1) \times 10^4$	13.7 ± 3.4	38 ± 5	33 ± 6	33
15	$(2.4 \pm 0.2) \times 10^4$	$3.2 \pm 0.2) \times 10^4$	83 ± 4	372 ± 9	180 ± 50	
			MCF-7			
16	0.027×10^6		288 ± 0.1			
17	0.297×10^6		31 ± 4.2			
			AGS			35
18	4.019×10^5	2.929×10^4	9.55 ± 1.23			

K_b = DNA-binding constant; K = BSA association binding constant; IC_{50} = Half maximal inhibitory concentration and n.d = not determined

Table 2.2: Summarized DNA, BSA binding constants and cytotoxic activity of dinuclear palladium(II) complexes.

Complex	DNA binding, K_b (M^{-1})	BSA Binding, K (M^{-1})	Cytotoxicity (IC_{50}, μM)			Ref
			MDA-MB-231			36
19	nd	nd	7.3			
			HTB140	H460	MRC-5	37
20	$(5.75 \pm 0.01) \times 10^4$	$(5.95 \pm 0.05) \times 10^4$	139 ± 7	144 ± 9	n.d	
			HeLa	MDA-MB-231	MRC-5	38
21	$4.8 \pm 0.2) \times 10^4$	$(1.24 \pm 0.05) \times 10^5$	6 ± 3	17 ± 4	> 100	
22	$1.6 \pm 0.1) \times 10^5$	$1.03 \pm 0.03) \times 10^5$	80 ± 10	26 ± 3	>100	
23	$1.1 \pm 0.1) \times 10^5$	$1.13 \pm 0.06) \times 10^5$	90 ± 30	25 ± 4	>100	
			A546	LLC1	SW480	39
24	1.2×10^5	5.9×10^4	90.57 ± 12.32	113.92 ± 9.87	173.16 ± 20.14	
25	7.4×10^4	3.7×10^3	74.94 ± 10.47	83.63 ± 7.47	231.21 ± 32.14	
26	1.5×10^5	9.1×10^4	63.89 ± 10.11	69.89 ± 8.52	117.73 ± 13.47	

K_b = DNA-binding constant; K = BSA association binding constant; IC_{50} = Half maximal inhibitory concentration and n.d = not determined

2.4. Statement of the problem

The mortality rate due to cancer disease is increasing yearly, with an estimated 19.3 million new cancer cases and 9.9 million deaths in 2020 were reported.⁴² Despite the curative properties of cisplatin and other clinically approved platinum drugs against cancerous tumours, they still demonstrate a wide range of side effects including (neuromuscular complication, renal tubular injury, abdominal pain, vomiting, nausea, and diarrhea).⁴³ While it is believed DNA conformation may be altered upon the interaction of newly developed palladium(II) complexes with DNA to prevent cell division of cancer cells.⁴⁴ The exact mechanism of action of the drug on the DNA and the nature of interactions is not fully understood.

2.5. Justification and rationale of the study

Shortcomings associated with the application of platinum-based drugs in cancer cells have attracted a search for alternative metal-based drugs with reduced limitations.⁴⁵ Thus, the design and development of non-platinum-based drugs that may increase the spectrum activity of metal-based drugs, improve solubility, and reduce toxicity are indeed required.²⁰ Due to structural and coordination resemblance analogy of palladium(II) complexes with those containing platinum(II) complexes.^{4, 46} The aquation and ligand-exchange kinetic rates of palladium(II) complexes are about 10^5 times faster than the corresponding platinum(II) analogous,⁴⁷ It is thus important to expand the investigation of metal complexes beyond cisplatin to design alternative metal-based anti-cancer agents, which have minimal side effects and resistance to cancerous tumours. To understand the mechanisms and nature of actions of these complexes, it is significant to examine the cytotoxic activity of palladium(II) complexes and their binding affinity to biological molecules such as DNA and BSA. Thus, understanding the interaction of palladium(II) complexes with DNA and protein as well as the in vitro

cytotoxicity could lead to the development of clinical effective anticancer drug. Herein, we aim to examine DNA/BSA interactions, and cytotoxic activities of dinuclear palladium(II) complexes of (pyridyl)pyrazine carboxamide-based ligands.

2.6. Aim and objectives of the study

The general aim of this thesis is to synthesize mononuclear and dinuclear palladium(II) complexes bearing multidentate (pyridyl) pyrazine carboxamide-based ligands and study their DNA/BSA interactions and anticancer activity. To achieve the stated aim, the specific objectives are formulated as follows:

1. To synthesize and characterize palladium(II) complexes bearing (pyridyl) pyrazine carboxamide ligands.
2. To study the DNA/BSA binding affinities of palladium(II) complexes bearing (pyridyl) pyrazine carboxamide ligands.
3. To examine *in vitro* cytotoxicity of palladium(II) complexes bearing (pyridyl) pyrazine carboxamide ligands.

2.7. References

1. Yousuf, I.; Bashir, M.; Arjmand, F.; Tabassum, S., *Cood. Chem. Rev.*, **2021**, *445*, 214104.
2. Rosenberg, B.; Vancamp, L.; Trosko, J. E.; Mansour, V. H., *Nature.*, **1969**, *222* (5191), 385-386.
3. Kar, K.; Ghosh, D.; Kabi, B.; Chandra, A., *Polyhendron.*, **2022**, 115890.
4. Alam, M. N.; Huq, F., *Coord. Chem. Rev.*, **2016**, *316*, 36-67.
5. Rosenberg, B.; Van Camp, L.; Krigas, T., *Nature.*, **1965**, *205* (4972), 698-699.
6. Lavanya, M.; Jagadeesh, M.; Haribabu, J.; Karvembu, R.; Rashmi, H.; Devi, P. U. M.; Reddy, A. V., *Inorg. Chim. Acta.*, **2018**, *469*, 76-86.
7. Alassadi, S.; Pisani, M. J.; Wheate, N. J., *Dalton Trans.*, **2022**, *51* (29), 10835-10846.
8. Ghosh, S., *Bioorg Chem.*, **2019**, *88*, 102925.
9. Eljack, N. D.; Ma, H.-Y. M.; Drucker, J.; Shen, C.; Hambley, T. W.; New, E. J.; Friedrich, T.; Clarke, R. J., *Metallomics.*, **2014**, *6* (11), 2126-2133.
10. Hanif, M.; Hartinger, C. G., *Future Med. Chem.*, **2018**, *10* (6), 615-617.
11. Aldossary, S. A., *Biomed. Pharmacol. J.*, **2019**, *12* (1), 7-15.
12. Riddell, I. A.; Lippard, S. J., *Met. Ions Life Sci.*, **2018**, *18*, 1-42.
13. Makovec, T., *Radiol. Oncol.*, **2019**, *53* (2), 148-158.
14. Johnstone, T. C.; Suntharalingam, K.; Lippard, S., *Philos. Trans. Royal Soc. A.*, **2015**, *373* (2037), 20140185.
15. Ahmad, S., *Chem. Biodivers.*, **2010**, *7* (3), 543-566.
16. Omondi, R. O.; Ojwach, S. O.; Jaganyi, D., *Inorg. Chim. Acta.*, **2020**, *512*, 119883.
17. Mukherjee, S.; Mitra, I.; Das, P.; Misini, B.; Linert, W.; Moi, S., *ChemistrySelect.*, **2018**, *3* (13), 3871-3885.

18. Alfonso-Herrera, L. A.; Rosete-Luna, S.; Hernández-Romero, D.; Rivera-Villanueva, J. M.; Olivares-Romero, J. L.; Cruz-Navarro, J. A.; Soto-Contreras, A.; Arenaza-Corona, A.; Morales-Morales, D.; Colorado-Peralta, R., *ChemMedChem.*, **2022**, *17* (20), e202200367.
19. Singh, N. K.; Kumar, Y.; Paitandi, R. P.; Tiwari, R. K.; Kumar, A.; Pandey, D. S., *Inorg. Chim. Acta.*, **2023**, *545*, 121241.
20. Bhaduri, R.; Pan, A.; Tarai, S. K.; Mandal, S.; Bagchi, A.; Biswas, A.; Moi, S. C., *J. Mol. Liq.*, **2022**, *367*, 120540.
21. Albéniz, A. C.; Espinet, P., *Encyclopedia of Inorganic Chemistry.*, 2nd Edition, R. Bruce King. ed., John Wiley & Sons, Ltd, **2006**, DOI: 10.1002/0470862106.ia178.
22. Singh, S. K., *Int. J. Res. Anal. Rev.*, **2019**, *6* (1)
23. Zegers, J.; Peters, M.; Albada, B., *J. Biol. Inorg. Chem.*, **2022**, 1-22.
24. Magalhães, J.; Franko, N.; Raboni, S.; Annunziato, G.; Tammela, P.; Bruno, A.; Bettati, S.; Armao, S.; Spadini, C.; Cabassi, C. S., *Pharmaceuticals.*, **2021**, *14* (2), 174.
25. Medici, S.; Peana, M.; Nurchi, V. M.; Lachowicz, J. I.; Crisponi, G.; Zoroddu, M. A., *Coord. Chem. Rev.*, **2015**, *284*, 329-350.
26. Faihan, A. S.; Hatshan, M. R.; Kadhim, M. M.; Alqahtani, A. S.; Nasr, F. A.; Saleh, A. M.; Al-Jibori, S. A.; Al-Janabi, A. S., *J. Mol. Struct.*, **2022**, *1252*, 132198.
27. Paca, A. M.; Ajibade, P. A.; Andrew, F. P.; Nundkumar, N.; Singh, M., *Arab. J. Chem.*, **2021**, *14* (9), 103326.
28. Graham, R. D.; Williams, D. R., *J. Inorg. Nucl. Chem.*, **1979**, *41* (8), 1245-1249.
29. Tušek-Božić, L.; Matijašić, I.; Bocelli, G.; Calestani, G.; Furlani, A.; Scarcia, V.; Papaioannou, A., *J. Chem. Soc., Dalton Trans.*, **1991**, (2), 195-201.
30. Omondi, R. O.; Fadaka, A. O.; Fatokun, A. A.; Jaganyi, D.; Ojwach, S. O., *J. Biol.*

Inorg. Chem., **2022**, 27 (7), 653-664.

31. Omondi, R. O.; Bellam, R.; Ojwach, S. O.; Jaganyi, D.; Fatokun, A. A., *J. Inorg. Biochem.*, **2020**, 210, 111156.
32. Omondi, R. O.; Sibuyi, N. R.; Fadaka, A. O.; Meyer, M.; Jaganyi, D.; Ojwach, S. O., *Dalton Trans.*, **2021**, 50 (23), 8127-8143.
33. Ćočić, D.; Jovanović, S.; Radisavljević, S.; Korzekwa, J.; Scheurer, A.; Puchta, R.; Baskić, D.; Todorović, D.; Popović, S.; Matić, S., *J. Inorg. Biochem.*, **2018**, 189, 91-102.
34. Karami, K.; Mehvari, F.; Ramezanzade, V.; Zakariazadeh, M.; Kharaziha, M.; Ramezanpour, A., *J. Mol. Liq.*, **2022**, 362, 119493.
35. Naskar, R.; Ghosh, P.; Mandal, S.; Jana, S.; Murmu, N.; Mondal, T. K., *J. Chem. Sci.*, **2022**, 134 (4), 103.
36. Vojtek, M.; Gonçalves-Monteiro, S.; Šeminská, P.; Valová, K.; Bellón, L.; DiasPereira, P.; Marques, F.; Marques, M. P.; Batista de Carvalho, A. L.; Mota-Filipe, H. J. B., *Biomedicines.*, **2022**, 10 (2), 210.
37. Ćočić, D.; Jovanović-Stević, S.; Jelić, R.; Matić, S.; Popović, S.; Djurdjević, P.; Baskić, D.; Petrović, B., *Dalton's Trans.*, **2020**, 49 (41), 14411-14431.
38. Ćočić, D.; Jovanović, S.; Nišavić, M.; Baskić, D.; Todorović, D.; Popović, S.; Bugarčić, Ž. D.; Petrović, B., *J. Inorg. Biochem.*, **2017**, 175, 67-79.
39. Franich, A. A.; Živković, M. D.; Milovanović, J.; Arsenijević, D.; Arsenijević, A.; Milovanović, M.; Djuran, M. I.; Rajković, S., *J. Inorg. Biochem.*, **2020**, 210, 111158.
40. Fanelli, M.; Formica, M.; Fusi, V.; Giorgi, L.; Micheloni, M.; Paoli, P., *Coord. Chem. Rev.*, **2016**, 310, 41-79.
41. Pooyan, M.; Shariatinia, Z.; Mohammadpanah, F.; Gholivand, K.; Junk, P. C.; Guo, Z.; Satari, M., *Inorg. Chim. Acta.*, **2022**, 121368.

42. De Silva, F.; Alcorn, J., *Cancers.*, **2022**, *14* (12), 2954.
43. Agudo-López, A.; Prieto-García, E.; Alemán, J.; Pérez, C.; Díaz-García, C. V.; Parrilla-Rubio, L.; Cabrera, S.; Navarro-Ranninger, C.; Cortés-Funes, H.; López-Martín, J. A., *Mol. Cancer.*, **2017**, *16* (1), 1-11.
44. Dorafshan Tabatabai, A. S.; Dehghanian, E.; Mansouri-Torshizi, H., *Biometals.*, **2022**, *35* (2), 245-266.
45. Hidalgo, T.; Escribano, D. F.; Montalban, R. A.; Matesanz, A. I.; Horcajada, P.; Biver, T.; Quiroga, A. G., *Inorg. Chem. Front.*, **2023**. DOI.org/10.1039/D2QI02424A 46.
- Mandal, S.; Tarai, S. K.; Pan, A.; Bhaduri, R.; Biswas, P.; Moi, S. C., *Bioorg. Chem.*, **2022**, *128*, 106093.
47. Zianna, A.; Geromichalos, G.; Fiotaki, A.-M.; Hatzidimitriou, A. G.; Kalogiannis, S.; Psomas, G., *Pharmaceuticals.*, **2022**, *15* (7), 886.

Chapter 3

Synthesis and structural characterization of carboxamide (pyridyl)pyrazine palladium(II) complexes.

3.1 Introduction

Amide groups are found in most biological molecules including peptides and proteins as well as synthetic polymers.¹ Deprotonated and neutral amides coordinate exceptionally to transition metals forming a wide range of metal complexes.² Anionic amide ligands coordinate to the metal center with N⁻N whereas neutral amides coordinate *via* N⁻O.^{3, 4} It is worth noting that anionic ligands are strong σ -donors capable of stabilizing metal ions in high oxidation states.⁵ Coordination of the ligand backbone to the metal center with amidato nitrogen exhibit cytotoxic efficiency in some cancer cells such as colon, ovarian, and cisplatin-resistant ovarian human cancer cell lines whereas complexes with N⁻O coordination are inactive.⁶ In addition, bulky heterocyclic and chelating ligands such as N-heterocyclic, and N⁻N chelating ligands including derivatives of pyridine, quinoline, and pyrazole exhibit anticancer activity.⁷⁻⁹

Among the metal-based drugs being investigated for anticancer activity, palladium(II) complexes are the preferred metal complexes as antineoplastic agents. They can replace clinically approved platinum-based drugs due to their structural resemblance and coordination chemistry.¹⁰⁻¹⁷ In addition, palladium(II) complexes display better solubility compared to platinum(II) complexes.¹⁸ The first palladium complex that was examined for anticancer activity exhibited low stability in biomolecules, however, this was overcome by the use of chelating ligands.¹⁹ Thus, the selection of ligands that enhance the stability, solubility as well

as cytotoxicity of palladium(II) complexes is significant. Free ligands consisting of N^N-chelating aromatic substituents interact with DNA through groove binding or intercalation which stabilizes π - π interactions.²⁰ Pyrazine is known to be a biochemical ligand and it is reported that pyrazine metal complexes of Pd, Rh, W, and Ru exhibit anticancer activity.²¹ Quinoline scaffold has been reported to exhibit cytotoxicity by inhibiting topoisomerase II.^{22,23}

A series of N^N aromatic chelating carboxamide ligands of palladium(II) complexes have been reported in the literature. The reported palladium(II) complexes are inclusive of monocarboxamide and dicarboxamide chelating ligands. For instance, Mjwara *et al.*²⁴ recently reported the synthesis of bis[N-(4-bromophenyl)-pyridine-2-carboxamidato]Palladium and N^N dicarboxamide palladium(II) complexes with a general formula [bis(pyridine-2-carboxamide)benzene dianion]Pd was reported by Mukherjee *et al.*²⁵ This chapter reports the synthesis, spectroscopic characterization, and molecular structures of (pyridyl)pyrazine carboxamide-based ligands and their corresponding palladium(II) complexes.

3.2. Experimental section

3.2.1 General materials

Air and water-sensitive compounds were synthesized under a nitrogen atmosphere using the standard Schlenk techniques. The solvents; diethyl ether was dried over distillation using calcium hydride and dichloromethane was purified by distillation using P₂O₅. The solvents were stored in molecular sieves. Acetonitrile, chloroform, and ethanol obtained from Merck were of analytical grade. Chemical reagents include pyrazine-2,3-dicarboxylic acid (>97%), 2-amino-4-methylpyridine (>99%), 2-amino-6-methylpyridine (>98%), 2-aminopyridine

(>99%), and triphenyl phosphite (>97%), 8-aminoquinoline (>98%) were purchased from Merck and used without further purification. The starting material, $[\text{PdCl}_2(\text{NCMe})_2]$, was prefabricated by adopting a literature procedure.²⁶

3.2.2. Instrumentation

3.2.2.1 NMR, FT-IR spectroscopy, mass spectrometry, and elemental analysis

^1H and $^{13}\text{C}\{^1\text{H}\}$ NMR spectra were recorded on a Bruker 400 MHz spectrometer in DMSO-d_6 at room temperature, and chemical shifts were reported in ppm with reference to tetramethyl silane $(\text{CH}_3)_4\text{Si}$. FT-IR spectra of all ligands and complexes were determined on Bruker apex 2.0 using OPUS programme in $4000\text{-}500\text{ cm}^{-1}$ range. Mass spectral analyses were acquired on a Shimadzu LC-MS Spectrometer and Waters LCT Premier Spectrometer TOF micro-mass. Elemental analyses were carried out on Thermal Scientific Flash 2000.

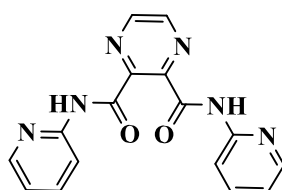
3.2.2.2. Single crystal X-ray crystallography analyses

Single crystal X-ray crystallography analyses of compounds **L3**, **Pd1**, and **Pd3** were measured on Bruker Apex Duo diffractometer made up of an Oxford Instruments Cryojet operating at 100(22) K and a Incoatec microsource operating at 30W. Data for molecular structures **L3**, **Pd1**, and **Pd3** was obtained by recording the measurements under the following conditions: Mo $\text{K}\alpha$ ($\lambda = 0.71073\text{ \AA}$) radiation at crystal-to-detector distance of 50 mm at omega and phi scans with exposures taken at 30 W-X-ray power and 0.50° frame widths using APEX-II conditions. Using SHELX-2014,²⁷ and OLEX2²⁸ direct methods, the molecular structures of **Pd1** and **Pd3** were solved and further refined with SHELX-2014 least squares approach.²⁹ All hydrogen atoms were incorporated as idealised contributors. In addition, standard riding model

was utilised in calculating the position of all hydrogen, with C-H_{aromatic} distances of 0.93 Å and $U_{\text{iso}} = 1.2U_{\text{eq}}$, C-H_{methylene} distances of 0.99 Å and $U_{\text{iso}} = 1.2U_{\text{eq}}$ and C-H_{methyl} distances of 0.98 Å and $U_{\text{iso}} = 1.5U_{\text{eq}}$. All non-hydrogen atoms were refined anisotropically with SHELX-2014.

3.2.3. Syntheses of (pyridyl)pyrazine carboxamide ligands and corresponding palladium(II) complexes

3.2.3.1. [*N*², *N*³-bis(pyridin-2-yl)pyrazine-2,3-dicarboxamide] (**L1**)

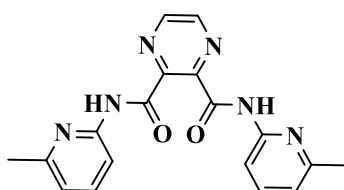


A solution of pyrazine-2,3- dicarboxylic acid (0.62 g, 5.00 mmol) in pyridine (10.00 ml) was heated for 15 min at 100 °C and a solution of 2-aminopyridine (0.94 g, 10.00 mmol) in pyridine (10.00 ml) was added. The mixture was refluxed for 20 min and triphenyl phosphite (1.55 g, 5.00 mmol) solution was added dropwise and refluxed for 24 h at 100 °C to form a brown-red solution. The resulting solution was cooled to room temperature and poured into 50.00 ml distilled water and 20.00 ml diethyl ether was added to form a white precipitate. The precipitate was collected by suction filtration, washed with diethyl ether, and dried under vacuum to give compound **L1** as a white solid. Yield: 0.59 g, (38%). ¹H NMR (400 MHz, CDCl₃): δ_H (ppm): 7.07 (dd, ³J_{HH} = 5.4, 2H, H_{pyridine}); 7.74 (m, ³J_{HH} = 7.2, 2H, H_{pyridine}); 8.25 (d, ³J_{HH} = 4.2, 2H, H_{pyridine}); 8.40 (d, ³J_{HH}=7.9, 2H, H_{pyrazine}); 8.73 (s, 2H, H_{pyrazine}); 9.76 (s, 2H, NH_{amide}). ¹³C{¹H} NMR (100 MHz, CDCl₃): δ_C (ppm): 114.6 (C_{pyridine}), 120.3 (C_{pyridine}), 138.5 (C_{pyridine}), 144.5

(C_{pyrazine}), 146.2 (C_{pyridine}), 147.9 (C_{pyridine}), 150.9 (C_{pyridine}), 162.1 (C=O). FT-IR (cm⁻¹): $\nu(\text{NH})_{\text{amide}} = 3331$, $\nu(\text{C}=\text{O}) = 1680$. LC-MS: m/z , calc for C₁₆H₁₂N₆O₂: 320.10; Found 343.09 [M⁺+Na].

A similar protocol was adopted in the synthesis of ligands **L2-L4**.

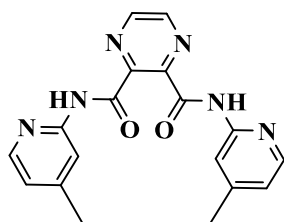
3.2.3.2. [*N*², *N*³-bis(6-methylpyridin-2-yl)pyrazine-2,3-dicarboxamide] (**L2**)



Pyrazine-2,3- dicarboxylic acid (1.00 g, 5.95 mmol), and 2-amino-6-methylpyridine (1.29 g, 11.90 mmol) and triphenyl phosphite (3.71 g, 11.90 mmol) were refluxed for 12 h to give a brown-red solution. The solution was cooled to room temperature and poured into 50 ml of icecold water to precipitate. The resulting brown precipitate was formed and washed with ice-cold water followed by ethanol, and then dried under vacuum. A white solid was obtained. Yield: 1.02g, (49%). ¹H NMR (400MHz, DMSO-d₆): δ_{H} (ppm): 2.43(s, 6H, H_{methyl}) 7.07(d, ³J_{HH} = 7.5, 2H, H_{pyridine}); 7.75(t, 2H, H_{pyridine}); 8.00 (m, 2H, H_{pyridine}); 8.93(s, 2H, H_{pyrazine}); 10.61(s, 2H, NH_{amide}). ¹³C{¹H} NMR (100MHz, CDCl₃): δ_{C} (ppm): 23.0 (C_{methyl}), 112.0 (C_{pyridine}), 119.9 (C_{pyridine}), 140.4 (C_{pyrazine}), 144.8 (C_{pyrazine}) 145.8 C_{pyridine} 149.6 (C_{pyridine}), 155.6 (C_{pyridine}), 162.0 (C_{carbonyl}). FT-IR (cm⁻¹): $\nu(\text{N-H})_{\text{amide}} = 3322$, $\nu(\text{C}=\text{O}) = 1701$. HR-MS: m/z , calc for C₁₈H₁₆N₆O₂: 348.13; Found: 349.1404 [M⁺ + H].

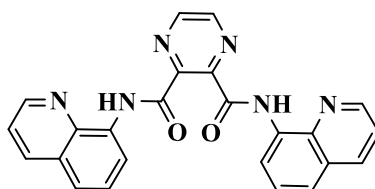
Ligands **L3** and **L4** were synthesized following a similar procedure described for **L2**

3.2.3.3. [*N*²,*N*³-bis(4-methylpyridin-2-yl)pyrazine-2,3-dicarboxamide] (**L3**)



Pyrazine-2,3- dicarboxylic acid (1.00 g, 5.95 mmol), 2-amino-4-methylpyridine (1.29 g, 11.90 mmol), and triphenyl phosphite (3.71 g, 11.90 mmol) in pyridine. A white solid was obtained. Yield: 1.30 g, (63%). ¹H NMR (400MHz, DMSO-d₆): δ_H (ppm): 2.36(s, 6H, H_{methyl}) 7.04 (d, ³J_{HH} = 4.5, 2H, CH); 8.05(s, 2H, C_{pyridine}); 8.22(d, ³J_{HH}=4.8, 2H, C_{pyridine}); 8.93(s, 2H, C_{pyrazine}); 10.63(s, 2H, NH_{amide}). ¹³C{¹H} NMR (100MHz, CDCl₃): δ_C (ppm): 21.3 (C_{methyl}), 114.5 (C_{pyridine}), 121.7 (C_{pyridine}), 145.7 (C_{pyrazine/pyridine}), 148.4 (C_{pyridine}), 149.8 (C_{pyridine}), 151.6 (C_{pyridine}), 163.3 (C_{carbonyl}). FT-IR (cm⁻¹): ν(N-H)_{amide}= 3347, ν(C=O)= 1682. HR-MS: m/z, calc for C₁₈H₁₆N₆O₂: 348.13; Found: 349.1400 [M⁺ + H].

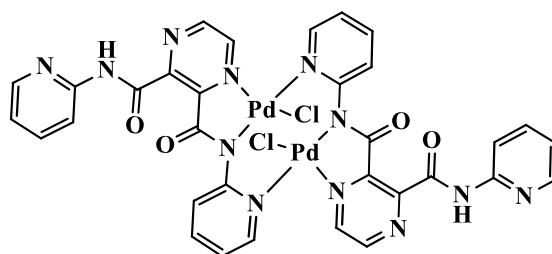
3.2.3.4. [*N*², *N*³-bis(quinoline-8-yl)pyrazine-2,3-dicarboxamide] (**L4**)



Pyrazine-2,3- dicarboxylic acid (1.00 g, 5.95 mmol), 8-amino quinoline (1.72 g, 11.90 mmol), and triphenyl phosphite (3.71 g, 11.90 mmol) in pyridine. The cream-white solid was obtained. Yield: 1.85 g (74%). ¹H NMR (400MHz, DMSO-d₆): δ_H (ppm): 7.77 (m, ³J_{HH} = 8.0, 2H,

H_{quinoline}); 7.77 (m, 2H, H_{quinoline}); 8.47 (m, 2H, H_{quinoline}); 8.83 (m, 2H, H_{quinoline}); 8.95 (m, 2H, H_{quinoline}); 9.04 (s, 2H, H_{pyrazine}); 11.45 (s, 2H, NH_{amide}). ¹³C{¹H} NMR (100MHz, DMSO-d₆): δ_C (ppm): 117.2 (C_{aromatic}), 122.7 (C_{aromatic}), 123.1 (C_{aromatic}) 127.5 (C_{aromatic}) 128.4 (C_{aromatic}) 134.6 (C_{aromatic}), 137.1 (C_{aromatic}), 138.7 (C_{aromatic}), 145.6 and 146.4 (C_{aromatic}), 149.6 (C_{aromatic}), 150.0 (C_{aromatic}), 163.1 (C_{C=O}). FT-IR (cm⁻¹): ν(N-H)_{amide} = 3349, ν(C=O) = 1674. (HR-MS): m/z, calc for C₂₄H₁₆N₆O₂: 420.13; Found: 421.1403 [M⁺ + H].

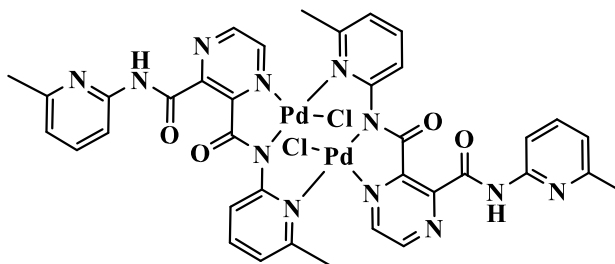
3.2.3.5. [Pd₂(L1)₂Cl₂] (Pd1)



A solution of N², N³-bis(4-methylpyridin-2-yl)pyrazine-2,3-dicarboxamide (**L1**) (0.12 g, 0.17 mmol) in acetonitrile was added to a stirring solution of [PdCl₂(NCMe)₂] (0.10 g, 0.37 mmol) in acetonitrile. The mixture was refluxed under nitrogen for 24 h resulting in a yellow precipitate. The precipitate was filtered and washed with chloroform followed by diethyl ether to give a yellow solid. Yield: 0.20 g (57%). ¹H NMR (400MHz, DMSO-d₆): δ_H(ppm): 7.02(m, 2H, H_{pyridine}); 7.72(m, 2H, H_{pyridine}); 7.44 (d, ³J_{HH} = 8.1, 2H, H_{pyridine}); 7.75 (m, 2H, H_{pyridine}); 7.88 (m, 2H, H_{pyridine}); 8.22 (d, ³J_{HH} = 8.5, 2H, H_{pyridine}); 8.37 (m, 2H, H_{pyridine}); 8.44 (m, 2H, H_{pyridine}); 9.12 (m, 4H, H_{pyrazine}); 11.09 (s, H, NH_{amide}) FT-IR spec (cm⁻¹): ν(N-H) = 3271, ν(C=O) = 1705, 1642. (TOF-MS): m/z, calc for C₃₂H₂₂Cl₂N₁₂O₄Pd₂: 921.93; Found: 922.96 [M⁺]. Anal. Calc (%) for C₃₂H₂₂N₁₂O₄Cl₂Pd₂.CHCl₃: C, 38.05; H, 2.23; N, 16.13. Found (%): C, 37.54; H, 2.76; N, 14.20.

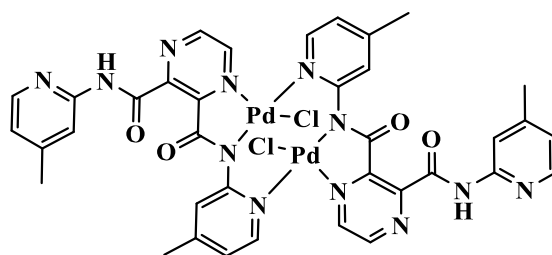
Complexes **Pd2** and **Pd3** were synthesized following a similar procedure described for **Pd1**

3.2.3.6. $[Pd_2(L2)_2Cl_2]$ (**Pd2**)



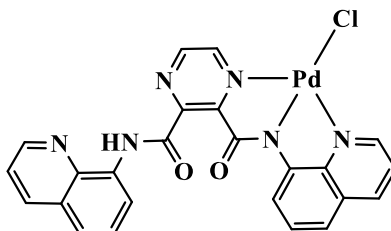
N^2, N^3 -bis(4-methylpyridin-2-yl)pyrazine-2,3-dicarboxamide (**L2**) (0.13 g, 0.37 mmol) and $[PdCl_2(NCMe)_2]$ (0.10 g, 0.37 mmol) in acetonitrile. The yellow solid was obtained. Yield: 0.14 g (37%). 1H NMR (400MHz, DMSO- d_6): δ_H (ppm): 2.43(s, 3H, H_{methyl}); 2.99(s, 3H, H_{methyl}); 6.98 (d, $^3J_{HH} = 7.5$, 2H, $H_{pyridine}$); 7.06 (d, $^3J_{HH} = 7.6$ 2H, $H_{pyridine}$); 7.30 (d, $^3J_{HH} = 7.9$, 2H, $H_{pyridine}$); 7.66-7.70 (t, $^3J_{HH} = 7.8$, 2H, $H_{pyridine}$); 7.73-7.77 (t, $^3J_{HH} = 7.9$, 2H, $H_{pyridine}$); 8.04 (d, $^3J_{HH} = 8.2$, 2H, $H_{pyridine}$); 9.07 (s, 4H, $H_{pyrazine}$); 10.97 (s, 2H, NH_{amide}). $^{13}C\{^1H\}$ NMR (100MHz, DMSO- d_6): 23.9 (C_{methyl}); 25.5 (C_{methyl}); 111.3 ($C_{aromatic}$); 119.6 ($C_{aromatic}$); 119.9 ($C_{aromatic}$); 139.2 ($C_{aromatic}$); 139.5 ($C_{aromatic}$); 145.8 ($C_{aromatic}$); 150.8 ($C_{aromatic}$); 151.4 ($C_{aromatic}$); 157.1 ($C_{aromatic}$); 157.3 ($C_{aromatic}$); 159.3 ($C_{aromatic}$); 163.2 ($C_{carbonyl}$); 166.9 ($C_{carbonyl}$) FT-IR spec (cm $^{-1}$): $\nu(N-H) = 3444$ $\nu(C=O)_{amide} = 1635$. (TOF-MS): m/z, calc for $C_{36}H_{30}Cl_2N_{12}O_4Pd_2.Na$: 1000.99; Found: 1000.2 [$M^+ + Na$]. Anal. Calc (%) for $C_{36}H_{30}N_{12}O_4Cl_2Pd_2 \cdot 1.5CHCl_3$: C, 38.91; H, 2.74; N, 14.52. Found (%): C, 38.53; H, 2.97; N, 14.35.

3.2.3.7. $[Pd_2(L3)_2Cl_2]$ (**Pd3**)



N^2,N^3 -bis(4-methylpyridin-2-yl)pyrazine-2,3-dicarboxamide (**L3**) (0.13 g, 0.37 mmol) and $[PdCl_2(NCMe)_2]$ (0.10 g, 0.37 mmol) in acetonitrile. The yellow solid was isolated. Yield: 0.11 g (30%). 1H NMR (400MHz, DMSO- d_6): δ_H (ppm): 2.27(s, 3H, H_{methyl}); 2.38(s, 3H, H_{methyl}); 6.88 (m, H, $H_{pyridine}$); 7.04(m, H, $H_{pyridine}$); 7.27(s, H, $H_{pyridine}$); 8.08(s, H, $H_{pyridine}$); 8.22-8.26 (m, 2H, $H_{pyridine}$); 9.09-9.12 (m, 4H, $H_{pyrazine}$); 11.02 (s, 2H, NH_{amide}). $^{13}C\{^1H\}$ NMR (100MHz, DMSO- d_6): 20.6 (C_{methyl}); 21.3 (C_{methyl}); 114.8 ($C_{aromatic}$); 122.8 ($C_{aromatic}$); 124.6 ($C_{aromatic}$); 144.0 ($C_{aromatic}$); 149.5 ($C_{aromatic}$); 150.2 ($C_{aromatic}$); 151.8 ($C_{aromatic}$); 152.3($C_{aromatic}$); 153.1 ($C_{aromatic}$); 159.3 ($C_{aromatic}$); 163.4 ($C_{carbonyl}$); 166.9 ($C_{carbonyl}$) FT-IR spec (cm^{-1}): $\nu(N-H)$ = 3495, $\nu(C=O)_{amide}$ = 1705, $\nu(O=C-N)$ = 1632. (TOF-MS): m/z , calc for $C_{36}H_{30}Cl_2N_{12}O_4Pd_2$: 978.00; Found: 979.10 [$M^+ + H$]. Anal. Calc (%) for $C_{36}H_{30}N_{12}O_4Cl_2Pd_2 \cdot 1.5CHCl_3$: C, 38.91; H, 2.74; N, 14.52. Found (%): C, 38.32; H, 2.89; N, 14.36.

3.2.3.8. [Pd(L4)Cl] (Pd4)

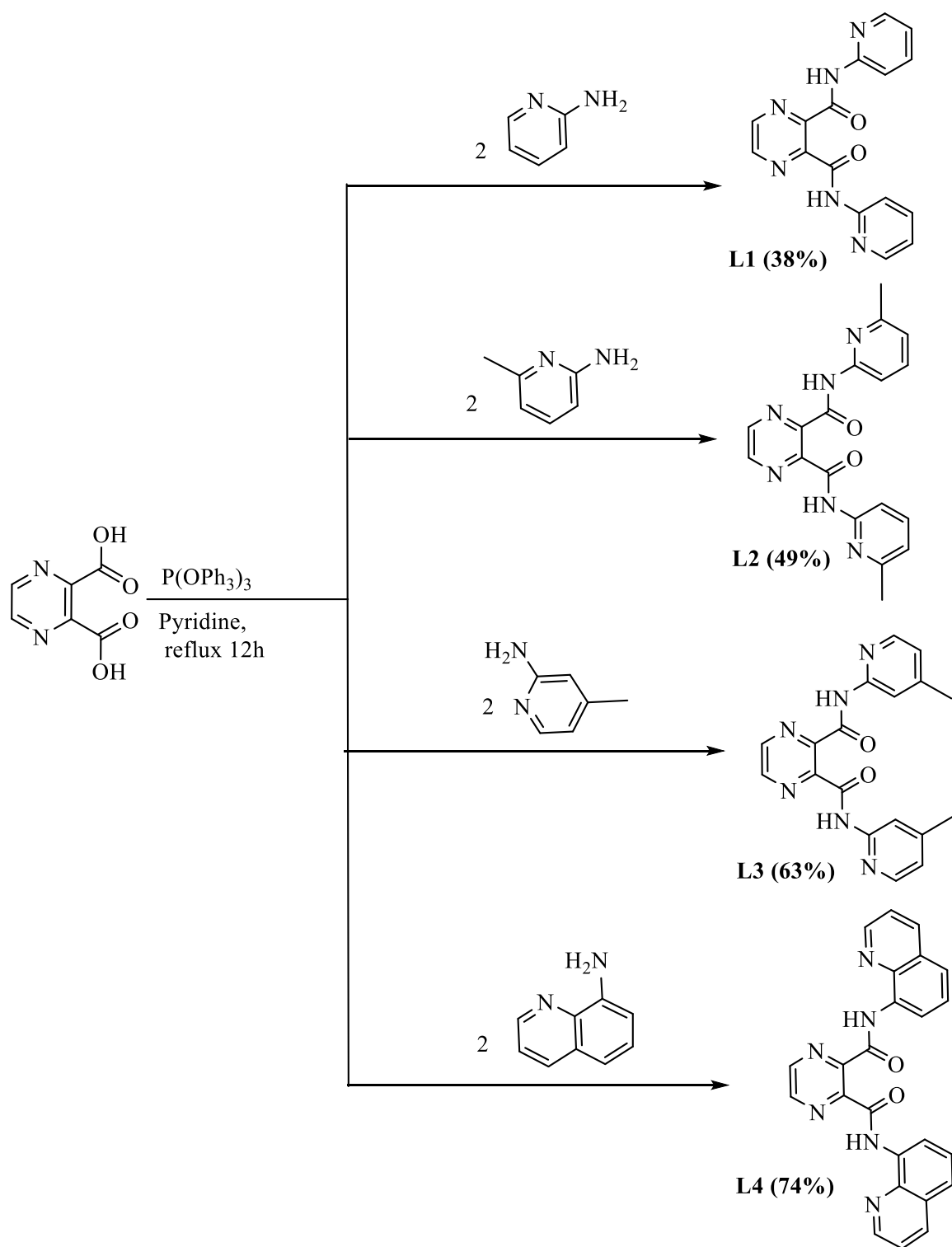


To a stirring solution of [PdCl₂(NCMe)₂] (0.11 g, 0.39 mmol) in CH₂Cl₂ (10 ml) a solution of *N*², *N*³-bis(quinoline-8-yl)pyrazine-2,3-dicarboxamide (**L4**) (0.16 g, 0.39 mmol) in CH₂Cl₂ (10 ml) was slowly added and the mixture was stirred for 12 h at room temperature. Dark red solid was obtained, filtered, and washed thoroughly with dichloromethane. Yield: 0.11 g, (85%). ¹H NMR (400MHz, DMSO-d₆): δ_H(ppm): 7.59(m, H, H_{quinoline}) 7.66(m, H, H_{quinoline}) 7.70(m, H, H_{quinoline}) 7.75 (t, ³J_{HH} = 8.0, H, H_{quinoline}), 7.77 (m, H, H_{quinoline}), 7.81 (m, H, H_{quinoline}), 8.47 (, H, H_{quinoline}), 8.54 (d, ³J_{HH} = 7.7, H, H_{quinoline}) 8.72 (d, ³J_{HH} = 8.5, H, H_{quinoline}), 8.85 (m, H, H_{quinoline}), 8.87 (m, H, H_{quinoline}), 8.89 (m, 3H, H_{quinoline}); 8.91 (m, H, H_{pyrazine}), 9.08 (d, ³J_{HH} = 2.8 H, H_{pyrazine}), 11.02 (s, 2H, NH_{amide}). ¹³C{¹H} NMR (100MHz, DMSO-d₆): 118.1 (C_{aromatic}); 120.5 (C_{aromatic}); 122.4 (C_{aromatic}); 122.5 (C_{aromatic}); 123.1 (C_{aromatic}); 123.2 (C_{aromatic}); 127.8 (C_{aromatic}); 128.4 (C_{aromatic}); 129.8 (C_{aromatic}); 130.7 (C_{aromatic}); 135.2(C_{aromatic}); 137.1 (C_{aromatic}); 138.8 (C_{aromatic}); 140.9 (C_{aromatic}); 143.3 (C_{aromatic}); 144.5 (C_{aromatic}); 147.4 (C_{aromatic}); 147.8 (C_{aromatic}); 149.3 (C_{aromatic}); 149.5 (C_{aromatic}); 151.5 (C_{aromatic}); 153.1 (C_{aromatic}); 163.3 (C_{carbonyl}); 165.4 (C_{carbonyl}). FT-IR spec (cm⁻¹): ν(N-H) = 3390, ν(C=O)_{amide}=1686, 1636. HR-MS: m/z, calc for C₁₈H₁₁N₆O₂ClPd: 560.14; Found: 561.0045 [M⁺ +H]. Anal. Calc. (%) for C₁₈H₁₁N₆O₂ClPd.0.2CH₂Cl₂: C, 50.35; H, 2.51; N, 14.56. Found (%): C, 50.15; H, 2.13; N, 14.25.

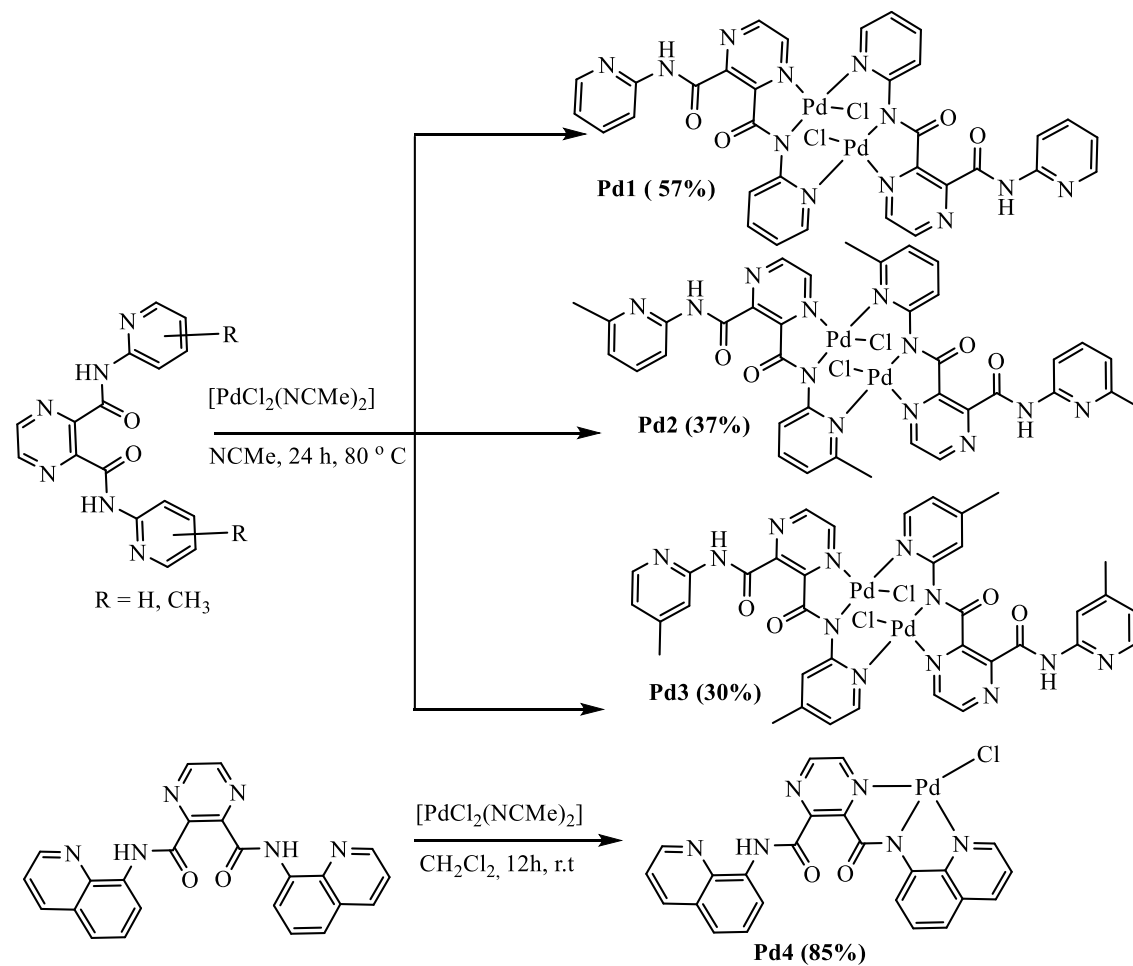
3.3. Results and discussion

3.3.1. Synthesis of pyrazine-pyridyl-carboxamide ligands and palladium(II) complexes

Pyrazine-2,3-dicarboxamide ligands, [N^2 , N^3 -bis(pyridin-2-yl)pyrazine-2,3-dicarboxamide] (**L1**), [N^2 , N^3 -bis(6-methylpyridin-2-yl)pyrazine-2,3-dicarboxamide], (**L2**) [N^2 , N^3 -bis(4-methylpyridin-2-yl)pyrazine-2,3-dicarboxamide](**L3**), and [N^2 , N^3 -bis(quinoline-8-yl)pyrazine-2,3-dicarboxamide] (**L4**) were prepared by following modified literature procedures.^{30, 31} Treatment of pyrazine-2,3-dicarboxylic acid with respective amines in the presence of triphenyl phosphite in pyridine resulted in the formation of compounds **L1-L4** in low to good yields (38-74%) as depicted in **Scheme 3.1**. The respective dinuclear palladium(II) complexes **Pd1-Pd3** were prepared in low to moderate yields (30-63%) from the reaction of respective dicarboxamide ligands with $\text{PdCl}_2(\text{NCMe})_2$ in a 1:1 ratio in acetonitrile, (**Scheme 3.2**). Similar complexes have been isolated in low to moderate yields by other researchers.^{24, 32} On the other hand, the mononuclear palladium(II) complex **Pd4** was prepared from the reactions of **L4** with equimolar amounts of $\text{PdCl}_2(\text{NCMe})_2$ in dichloromethane in good yields (74%). The reaction of **L4** with $\text{PdCl}_2(\text{NCMe})_2$ in a 1:2 mole ratio also resulted in the formation of a mononuclear complex. The formation of the mononuclear **Pd4** complex could be due to ligand **L4** adopting a tridentate binding mode ($N^{\wedge}N^{\wedge}N$) using the amide, pyrazine, and pyridine nitrogen atoms as shown in **Scheme 3.2**.



Scheme 3.1. Synthesis of the carboxamide ligands **L1-L4**.



Scheme 3.2: Synthesis of mononuclear and dinuclear (pyridyl)pyrazine carboxamide palladium(II) complexes **Pd1-Pd4**.

The new compounds were characterized using ^1H NMR, ^{13}C NMR, FT-IR spectroscopy, mass spectrometry, and single crystal x-ray analysis. The formation of the palladium(II) complexes was established by comparing the ^1H NMR of the complexes to the corresponding free ligand. For instance, the ^1H NMR spectrum of **Pd3** showed a singlet δ for the amidic proton N-H at 11.02 ppm with integral value, $I=1$, compared to the free ligand **L3** which showed the N-H signal at 10.64 ppm with $I=2$, (**Figure 3.1**). Deprotonation upon coordination has been observed in other related palladium complexes.³³ This observation could be attributed to the deprotonation of the N-H proton at one arm of the ligand before coordination with the Pd(II) atom. Similar observations were made in the ^1H NMR spectra of **Pd1** and **Pd2**. However, for complex **Pd4**, the NH signal shifted slightly upfield to 11.02 ppm in comparison to the NH peak of the respective ligand **L4** at 11.45 ppm (**Figure 3.2**). In addition, two singlets of the pyrazine protons were observed in the ^1H NMR of the palladium(II) complexes. For example, in the ^1H NMR spectrum of **Pd3**, two signals at 9.09 and 9.12 ppm assigned to $\text{H}_{\text{pyrazine}}$ were observed compared to the free ligand **L3** at 8.94 ppm. However, for complex **Pd4**, the two signals of the pyrazine protons were observed at 8.91 and 9.08 ppm compared to a singlet signal at 9.04 for **L4**. This could be the result of the coordination of the Pd(II) atom to one $\text{N}_{\text{pyrazine}}$, while the other pyrazine motif is non-coordinating. Similarly, five signals of $\text{H}_{\text{pyridine}}$ protons were observed in the ^1H NMR of the **Pd3** compared to three signals in the free ligand **L3**, which is consistent with the non-symmetrical nature of complex **Pd3**. This type of coordination has been reported for ruthenium complexes.⁴

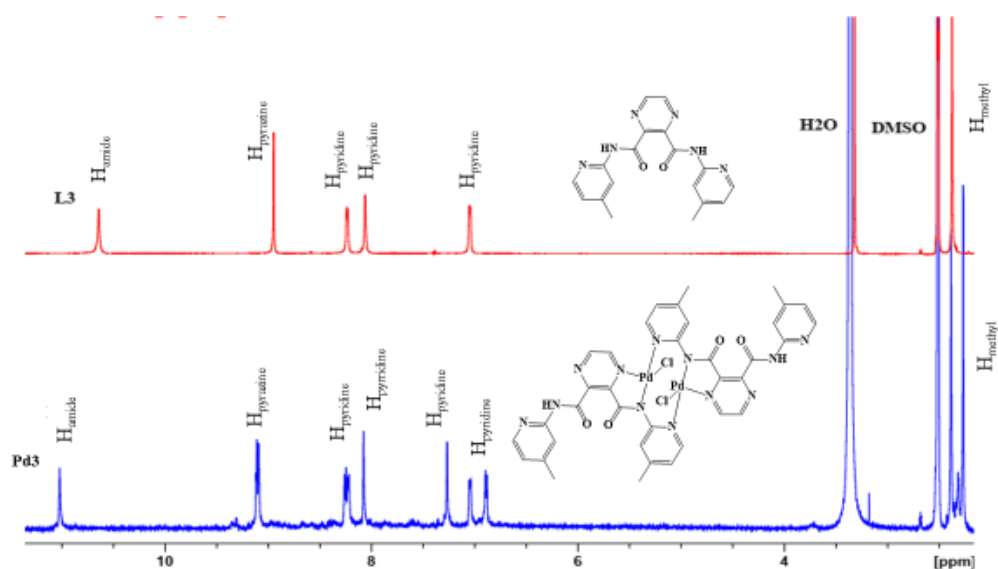


Figure 3.1: ^1H NMR spectra of ligand **L3** showing N-H singlet signal at 10.64 ppm with $I=2$ and three pyridine signals; and the corresponding complex **Pd3** showing singlet N-H signal at 11.02 ppm with $I=1$, and five pyridine signals upon coordination. The unsymmetrical nature of the complex **Pd3** confirmed the formation of the complex.

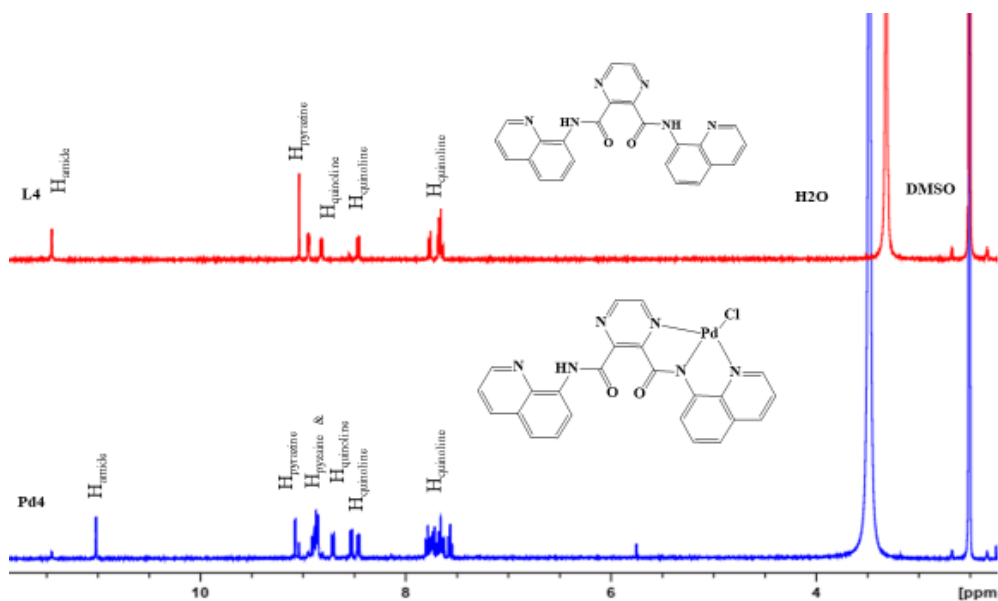


Figure 3.2: ^1H NMR spectra of ligand **L4** showing N-H signal at 11.45 ppm with $I=2$ and the corresponding complex **Pd4** showing singlet N-H signal at 11.02 ppm with $I=1$ upon coordination. This confirms the formation of the unsymmetrical complex **Pd4**.

Table 3.1: Signature ¹H NMR signals of the ligands and their palladium(II) complexes

Entry	Complex	δ (H _{Pzy}) ^a	δ (H _{Pyr}) ^a	δ (H _{amide}) ^a
1	Pd1	9.11, 9.12 (8.73)	7.45, 8.21 (8.21)	11.09 (10.73)
2	Pd2	9.07 (8.93)	7.30, 8.04 (8.01)	10.97 (10.61)
3	Pd3	9.09, 9.12, (8.94)	7.27, 8.08 (8.06)	11.02 (10.64)
4	Pd4	8.91, 9.08 (9.04)	-	11.02 (11.45)

^a ¹H NMR of ligands in the bracket

¹³C NMR data supported the trends and structures deduced from the ¹H NMR spectra of compounds **L3**, **L4**, **Pd3** (**Figure 3.3**), and **Pd4** (**Figure 3.4**). For example, upon coordination, two C=O peaks were observed at 163.3 and 166.92 ppm due to one arm coordinating in **Pd3**. The ¹³C NMR signals for the coordinated arm shifted downfield. This is ascribed to the ligand donating electrons to palladium causing electron deficiency in C=O.³⁴ Similar signals were observed in ¹³C NMR spectrum of **Pd4**. These findings have been observed in other related complexes.³⁰

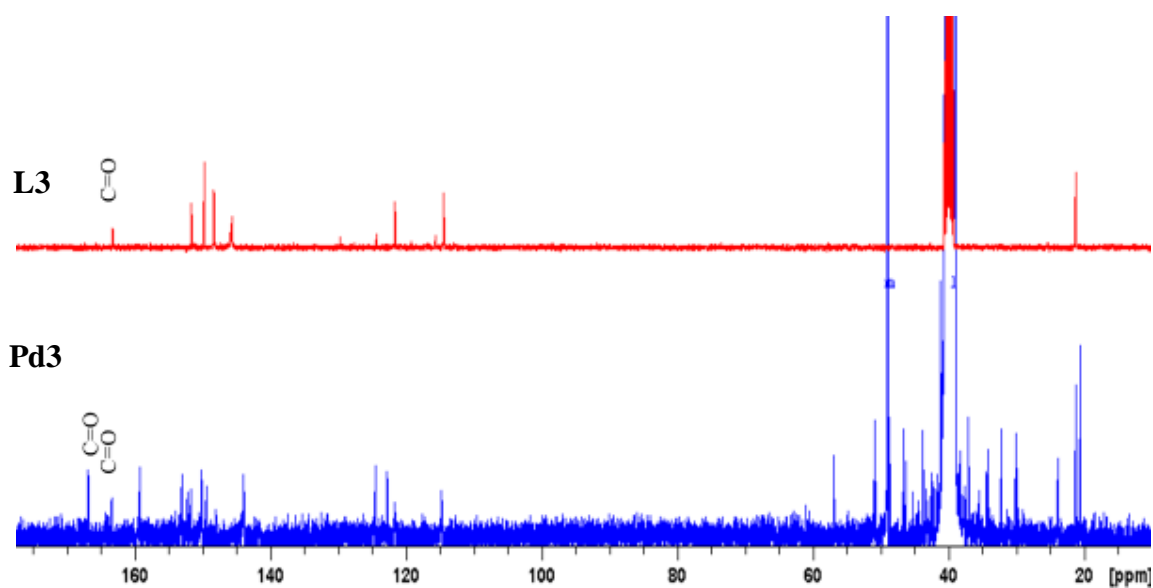


Figure 3.3: ¹³C NMR spectrum of ligand **L3** showing carbonyl signal at 163.3 ppm and the ¹³C NMR spectrum of complex **Pd3** showing two carbonyl signals at 163.4 and 166.9 ppm. This confirms the unsymmetrical nature of the dinuclear complex **Pd3** due to the non-coordination of one arm of ligand **L3**.

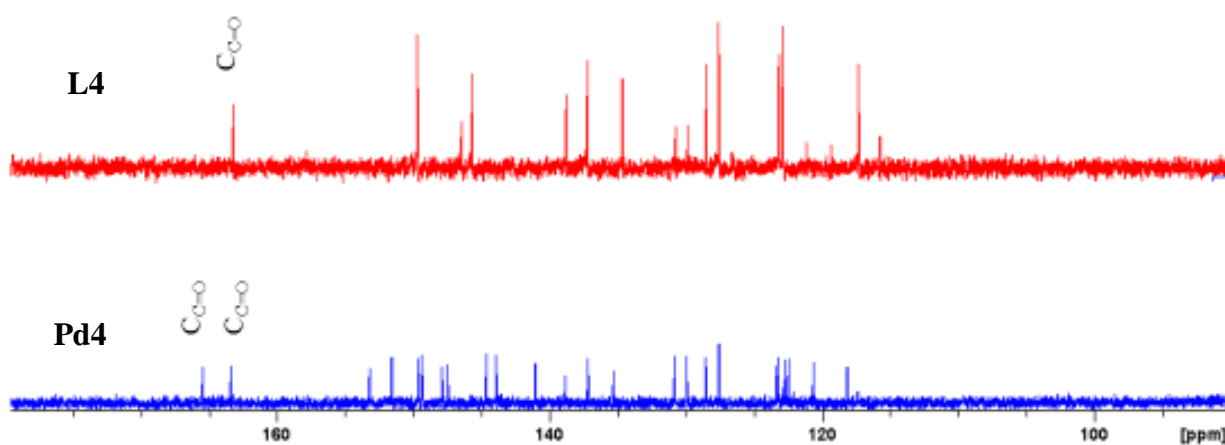


Figure 3.4: ¹³C NMR spectrum of ligand **L4** showing carbonyl signal at 163.17 ppm and the ¹³C NMR spectrum of complex **Pd4** showing two carbonyl signals at 163.34 and 165.42 ppm. This confirms the unsymmetrical nature of the mononuclear complex **Pd4** due to the non-coordination of one arm of ligand **L4**.

The FT-IR spectral data was further employed in confirming the formation of the palladium(II) complexes **Pd1-Pd4** and by making comparisons to the spectra of their respective ligands **L1-L4**. For example, two C=O signals at 1632 cm⁻¹ and 1705 cm⁻¹ were observed in the spectrum of complex **Pd3**, whereas the same absorption band of the C=O group in **L3** was recorded at 1682 cm⁻¹. A shift of one of the C=O absorption bands to a lower frequency value of 1632 cm⁻¹ was observed (**Figure 3.4**). This could be attributed to the coordination of the deprotonated arm of the ligands to palladium(II) which is in accordance with FT-IR of C=O bands (1638 and 1616 cm⁻¹) reported for carboxamide palladium, copper, and nickel complexes in literature.³⁵⁻³⁷ Moreover, the visible absorption band at 1705 cm⁻¹ was ascribed to the uncoordinated arm of the complex. This hypothesis is also supported by the presence of an absorption band of NH peak at 3495 cm⁻¹. This trend was observed in all palladium(II) complexes **Pd1-Pd4** (**Figure 3.4** and **3.5**). FT-IR spectrum of **Pd4** is in good agreement with ¹³C NMR spectral data.

Table 3.2: Selected FT-IR and ¹³C NMR data of ligands and palladium(II) complexes

Entry	Complex	$\nu(\text{C=O})^a$	$\nu(\text{N-H})^a$	¹³ C $\delta(\text{C=O})$
1	Pd1	1705, 1642 (1680)	3271 (3331)	- (162.1)
2	Pd2	1635, (1701)	3444 (3322)	166.9, 163.2 (162.0)
3	Pd3	1705, 1632 (1682)	3495 (3347)	166.9, 163.4 (163.3)
4	Pd4	1686, 1636 (1674)	3390 (3349)	165.4, 163.3 (163.1)

^a FT-IR of ligands in the bracket

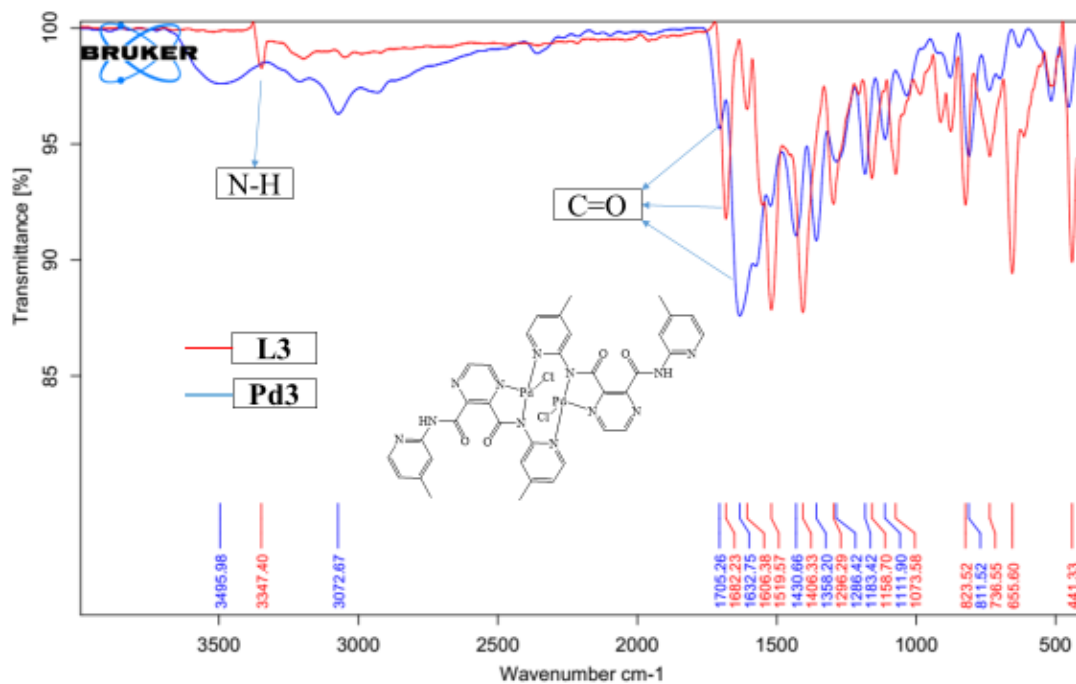


Figure 3.5: FT-IR spectra of **L3** showing single $\nu(\text{C}=\text{O})$ peak at 1682 cm^{-1} complex and **Pd3** showing the appearance of two carbonyl carbon $\nu(\text{C}=\text{O})$ at 1632 and 1705 cm^{-1} confirming the unsymmetrical nature of the dinuclear complex **Pd3** due the coordination of one arm of the ligand **L3** to palladium(II).

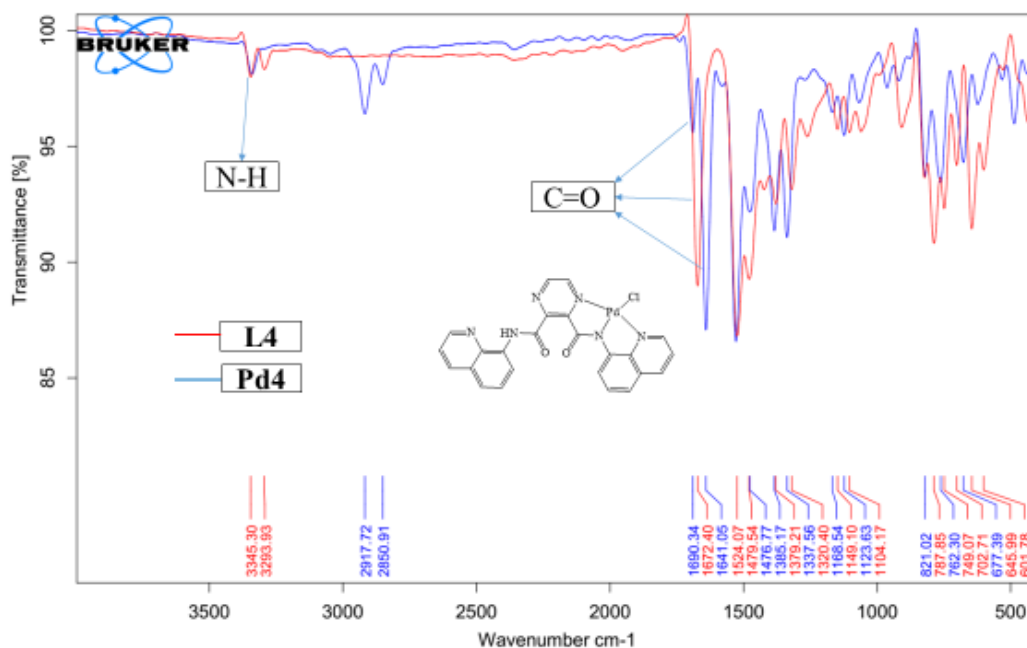


Figure 3.6: FT-IR spectra of ligand **L4** showing one $\nu(\text{C}=\text{O})$ peak at 1674 cm^{-1} and its corresponding complex **Pd4**, showing the two $\nu(\text{C}=\text{O})$ signals at 1636 and 1686 cm^{-1} confirming the unsymmetrical nature of the mononuclear complex **Pd4** due the coordination of one arm of the ligand **L4** to palladium(II).

Mass spectrometry (ESI-MS) proved to be useful in establishing the identity of the ligands and their respective palladium(II) complexes. All palladium(II) complexes and their corresponding ligands showed m/z signals that correspond to their respective molecular ion. For example, the m/z peaks at 922.96 [$\text{M}^+ + \text{H}$] (**Pd1**), 1000.2 [$\text{M}^+ + \text{Na}$] (**Pd2**), 979.10 [$\text{M}^+ + \text{H}$] (**Pd3**), and 561 [$\text{M}^+ + \text{H}$] (**Pd4**) (**Figure 3.7** and **3.8**) corresponding to their molecular ion. These m/z values were in good agreement with the calculated isotopic mass distribution of the complexes.

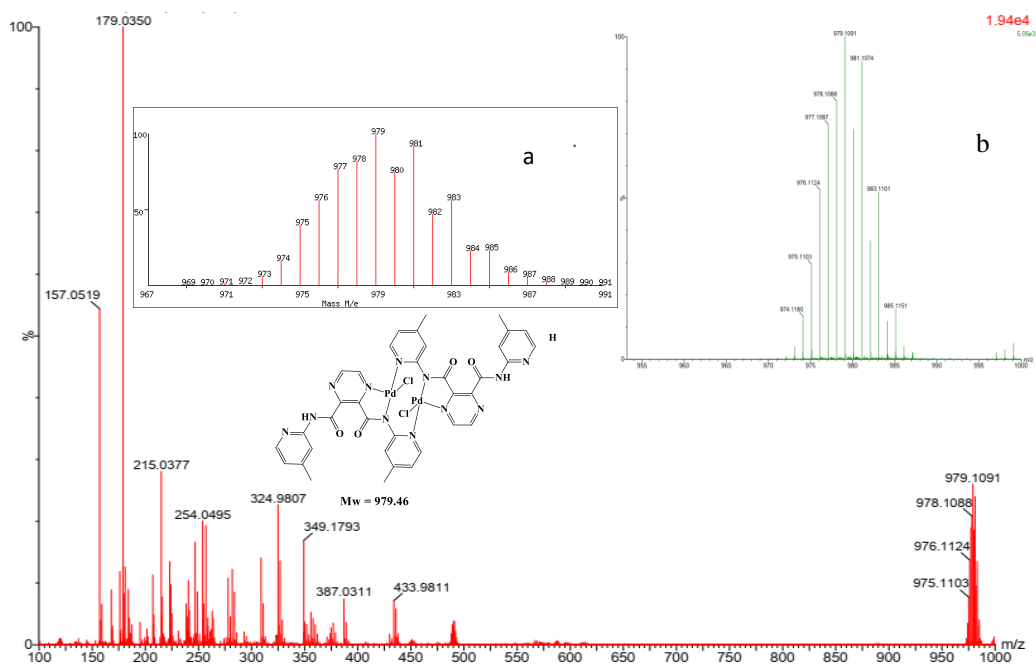


Figure 3.7: TOF-MS spectrum of complex **Pd3** showing m/z at 979 [$M^+ + H$]. Inset: theoretical (a) and experimental (b) isotopic mass distribution spectra complex **Pd3** with m/z at 979.

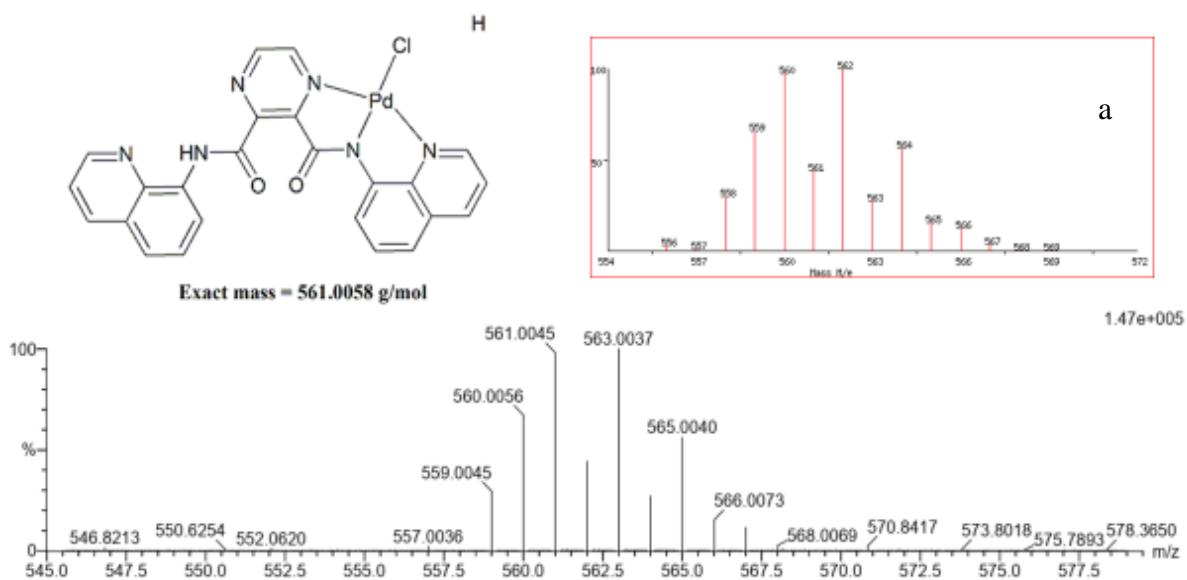


Figure 3.8: HR-MS spectrum of complex **Pd4** showing m/z at 561 [$M^+ + H$]. Inset: theoretical (a) isotopic mass distribution spectra complex **Pd4** with m/z at 560.

3.3.2. Molecular structures of compounds **L1**, **Pd1**, and **Pd3**

The solid-state structures of compounds **L3**, **Pd1**, and **Pd3** were confirmed using single-crystal X-ray crystallography. Single crystals for **L3** suitable for X-ray analyses were obtained from slow diffusion of dichloromethane and diethyl ether whereas **Pd1** and **Pd3** were obtained from slow evaporation of DMSO solution at room temperature. **Table 3.3** show crystallographic data and structure refinement parameters, while selected bond lengths and bond angles are shown in **Table 3.4**. The compounds **L3**, **Pd1**, and **Pd3** crystallize in triclinic, orthorhombic, and monoclinic systems with P-1, P2₁2₁2, and C2/c space groups respectively. **Pd1** crystallizes with two molecules of DMSO solvents in the lattice. Both **Pd1** and **Pd3** molecular structures exist as dimers with both ligands involved in the coordination around the palladium atom.

Table 3.3: Crystal data and structure refinement for compounds **L3**, **Pd1** and **Pd3**

Parameters	L3	Pd1	Pd3
Empirical formula	C ₁₈ H ₁₆ N ₆ O ₂	C ₃₂ H ₂₂ Cl ₂ N ₁₂ O ₇ Pd ₂ .3(CH ₃) ₂ SO	C ₃₆ H ₃₂ Cl ₂ N ₁₂ O ₄ Pd ₂
Formula weight	348.37	1155.48	980.44
Temperature/K	104.53	105.65	100.22
Crystal system	triclinic	orthorhombic	monoclinic
Space group	P-1	P2 ₁ 2 ₁ 2	C2/c
Unit cell dimension;			
a/Å	7.95960(10)	12.6065(6)	15.6007(5)
b/Å	9.72210(10)	22.0758(11)	17.9417(5)
c/Å	11.33312(2)	8.2272(5)	20.2484(6)
α/°	73.0790(10)	90	90
β/°	78.7580(10)	90	103.4520(10)
γ/°	79.8930(10)	90	90
Volume/Å ³	816.18(2)	2289.6(2)	5512.1(3)
Z	2	2	8
ρ _{calc} /cm ³	1.418	1.676	1.181
μ/mm ⁻¹	0.802	9.221	6.490
F(000)	364.0	1161.0	1960.0
Crystal size mm ³	0.11 x 0.105x 0.08	0.175 x 0.17 x 0.145	0.3 x 0.06 x 0.055
Theta range for data collection	8.252 to 136.756	8.01 to 139.94	7.63 to 144.198
Reflection collected	21649	4327	73551
Goodness-of-fit on F ²	1.039	1.114	1.169
Final R indices [I>2σ(I)]	R ₁ =0.0327, wR ₂ =0.0837	R ₁ =0.0296, wR ₂ =0.0700	R ₁ =0.0508, wR ₂ = 0.1417
R indices (all data)	R ₁ =0.0366, wR ₂ = 0.0865	R ₁ =0.0322, wR ₂ = 0.0712	R ₁ =0.0521, wR ₂ = 0.1424
Largest diff. peak and holes/eÅ ⁻³	0.26/-0.23	0.61/-0.48	0.82/-0.63

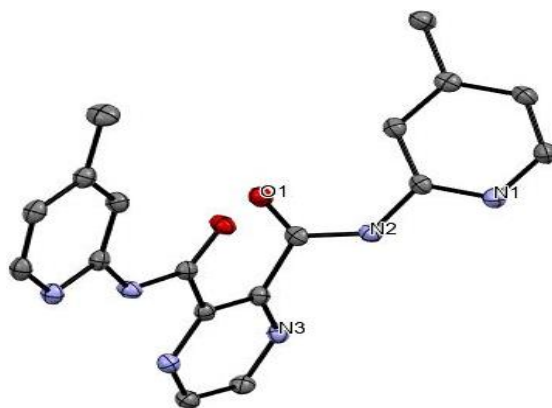


Figure 3.9: Solid state structure of **L3**, drawn with 50% probability ellipsoids. Hydrogen atoms were omitted for clarity.

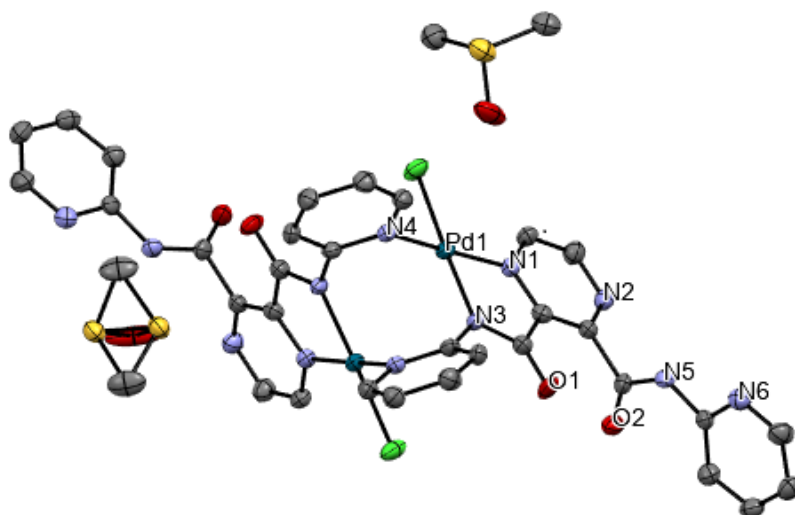


Figure 3.10: Solid state structure of complex **Pd1**, drawn with 50% probability ellipsoids. Hydrogen atoms were omitted for clarity.

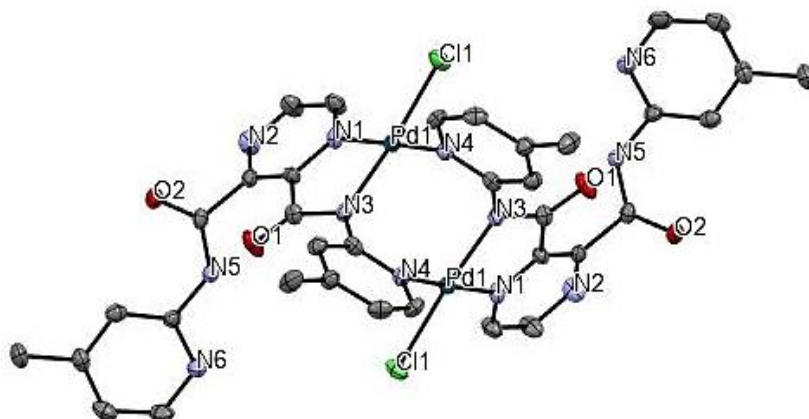


Figure 3.11: Solid-state structure of **Pd3**, drawn with 50% probability ellipsoids. Hydrogen atoms are omitted for clarity.

In the palladium complexes (**Pd1** and **Pd3**), each ligand coordinates to the palladium center with two nitrogens of N_{pyrazine} , and N_{amide} , and one N_{pyridine} of another ligand which forms a bridge between the two ligands. Chloride atoms coordinate with palladium atoms to stabilize the complex. Similar coordination of palladium and zinc complexes has been reported.^{38, 39} In **L3**, the amide group N2-O1-C7 connects the plane of methyl pyridyl moiety to the pyrazine ring with a $126.14^\circ(11)$ angle between them. The dihedral angle, N1-Pd1-N3 of $80.68^\circ(17)$ **Pd3** is larger than the N1-Pd1-N3 of $80.29^\circ(18)$ **Pd1** due to steric constraints induced by the methyl group in **Pd3** and these angles depart from 90° respectively. The bite angles $173.29^\circ(19)$ for **Pd1** and $176.23^\circ(17)$ for **Pd3** deviate from 180° . Hence, the **Pd1** and **Pd3** geometry of the palladium(II) atom is a square planar geometry. These angles are comparable to the bite angles ($80.30^\circ(13)$ and $80.47^\circ(12)$) as well as ($173.3^\circ(10)$ and $176.63^\circ(17)$) reported for similar palladium carboxamide complexes.^{33, 40, 41}

Both molecular structures of **Pd1** and **Pd3** exhibit comparable bond lengths. For instance, the Pd-N_{amide} bond length for **Pd1** of 2.004(4) Å and **Pd3** of 2.007(4) Å are comparable. The average bond length Pd-N_{amide} for **Pd1** and **Pd3** 2.005 Å is within the maximum bond length of 2.001 Å Pd-N_{amide} reported for 16 related palladium(II) complexes containing similar Pd-N_{amide} bonds.³⁶ The Pd-N_{pyz} bond length for **Pd1** of 2.013(5) Å is shorter than that of **Pd3** (2.029(4) Å). The average bond length of Pd-N_{pyz} in complexes **Pd1** and **Pd3** is 2.011 Å is within the average bond length of 2.029 ± 12 Å obtained for 29 with similar bonds.³⁰ Additionally, the average Pd-N_{pyr} of **Pd1** and **Pd3** of 2.033 Å is comparable to the average bond distance of 2.032 ± 10 Å reported for 16 related compounds bearing similar Pd-N_{pyr} bonds.⁴² The longer Pd-Cl bond length of 2.3154(13) Å for **Pd3** compared to Pd(1)-Cl(1) 2.2915(13) Å for complex **Pd1** is ascribed to the better *trans*-effect due to the presence of electron donating group CH₃ in **L3**. Moreover, the average Pd-Cl bond distances of 2.304 Å for compound complexes **Pd1** and **Pd3** are within the average Pd-Cl bond of 2.326 ± 15 Å in 42 related palladium complexes deposited in CDCC.⁴³ Notably, a difference in bond length of the C=O of the coordinated and non-coordinated arm in amide moiety O1-C6; 1.238(6) Å and O2-C11; 1.222(7) Å (**Pd1**) as well as O1-C5; 1.234(7) Å and O2-C12; 1.240(7) Å (**Pd3**), indicate that upon complexation the (pyridyl) pyrazine carboxamide ligands lose its symmetrical nature. The intratomic distance **Pd(1)-Pd(3)** in **Pd3** (3.506 Å) is longer compared to **Pd1** (3.387 Å), this could be attributed to the structural distortion of square planar in **Pd3** compared to **Pd1**.⁴⁴ The bond length of N1-C6; 1.3376(17), N2-C7; 1.3524(17), N3-C8; 1.3436(10) and O1-C7; 1.2240(15) are comparable to the N-C and O-C bond distances averaging 1.338 ± 0.028 Å, 1.350 ± 0.042 Å, and 1.3460 ± 0.015 Å reported for 192, 2467, and 225 similar molecular structure.⁴⁵

Table 3.4: Selected bond lengths and bond angles for molecular structures of **L3**, **Pd1**, and **Pd3**

Bond lengths [Å]	L3	Pd1	Pd3
Pd(1)-N(1)	-	2.013(5)	2.010(4)
Pd(1)-N(3)	-	2.004(4)	2.007(4)
Pd(1)-N(4)	-	2.036(5)	2.029(4)
Pd(1)-Cl(1)	-	2.2915(13)	2.3154(13)
N(1)-C(6)	1.3376(17)	-	1.335(7)
N(1)-C(5)	-	1.348(7)	-
N(2)-C(7)	1.3524(17)	-	1.347(7)
N(2)-C(6)	-	1.355(7)	-
N(3)-C(8)	1.3436(16)	-	1.354(6)
N(3)-C(7)	-	1.357(7)	-
O(1)-C(7)	1.2240(15)	-	1.234(7)
O(1)-C(6)	-	1.238(6)	-
O(1)-C(12)	1.2225(15)	-	1.240(7)
O(2)-C(11)	-	1.222(7)	-
Bond angles [°]			
N(1)-Pd(1)-N(4)	-	173.29(19)	176.23(17)
N(3)-Pd(1)-N(1)	-	80.29(18)	80.68(17)
N(3)-Pd(1)-N(4)	-	95.88(18)	96.38(17)
N(1)-Pd(1)-Cl(1)	-	95.58(13)	94.65(13)
N(3)-Pd(1)-Cl(1)	-	175.83(14)	174.65(13)
N(4)-Pd(1)-Cl(1)	-	88.28(13)	88.18(12)
N(1)-C(6)-N(2)	113.14(10)	-	115.5(4)
N(1)-C(5)-N(2)	-	115.5(5)	-
O(1)-C(7)-N(2)	126.14(11)	-	128.1(5)
O(1)-C(6)-N(2)	-	126.4(5)	-

3.4. Conclusions

(Pyridyl)pyrazine carboxamide based ligands (**L1-L4**) and their corresponding palladium(II) complexes(**Pd1-Pd4**) have been successfully synthesized in low to good yields. The compounds were characterized using NMR, FT-IR spectroscopy, mass spectrometry, and single X-ray crystallography. ^1H NMR reveals the appearance of the N-H signal with $I=1$ for the complexes compared to the N-H signal with $I=2$ for the ligands. ^{13}C NMR and FT-IR of the complexes showed two carbonyl peaks upon complexation which was indicative of one-arm coordination of the ligands to palladium (II). The solid-state structure of **L3** showed the formation of the expected dicarboxamide-based ligand. Coordination chemistry and geometry of complexes **Pd1** and **Pd3** showed that (pyridyl) pyrazine carboxamide-based ligands (**L1-L3**) coordinate to the palladium atom via nitrogen donor atom. The two dicarboxamide ligands coordinate with the palladium atom with one arm. The ligands are bridged by two palladium atoms to form stable complexes. Both structures adopt a distorted tetrahedral geometry. **L4** coordinate to the palladium atom via $\text{N}^{\wedge}\text{N}^{\wedge}\text{N}$ in a tridentate form in one arm of the ligand. This coordination in **Pd4** is confirmed by NMR, FT-IR, mass spectrometry, and elemental analysis.

3.5. References

1. Sigel, H.; Martin, R. B., *Chem. Rev.*, **1982**, 82 (4), 385-426.
2. Panda, C.; Sarkar, A.; Gupta, S. S., *Coord. Chem. Rev.*, **2020**, 417, 213314.
3. Rajput, A.; Mukherjee, R., *Coord. Chem. Rev.*, **2013**, 257 (2), 350-368.
4. Aradhyula, B. P. R.; Kaminsky, W.; Kollipara, M. R., *J. Mol. Struct.*, **2017**, 1149, 162-170.
5. Jacob, W.; Mukherjee, R., *Inorg. Chim. Acta.*, **2006**, 359 (14), 4565-4573.
6. van Rijt, S. H.; Hebden, A. J.; Amaresekera, T.; Deeth, R. J.; Clarkson, G. J.; Parsons, S.; McGowan, P. C.; Sadler, P. J., *Med. Chem.*, **2009**, 52 (23), 7753-7764.
7. Zhao, G.; Lin, H., *Curr. Med. Chem. Anticancer Agents.*, **2005**, 5 (2), 137-147.
8. Juribašić, M.; Molčanov, K.; Kojić-Prodić, B.; Bellotto, L.; Kralj, M.; Zani, F.; Tušek-Božić, L., *J. Inorg. Biochem.*, **2011**, 105 (6), 867-879.
9. Majeed, S. R.; Amin, M. A.; Attaby, F. A.; Soliman, A. A., *Biointerface Res. Appl. Chem.*, **2021**, 11, 14316-14335.
10. Dorairaj, D. P.; Haribabu, J.; Shashankh, P. V.; Chang, Y.-L.; Echeverria, C.; Hsu, S. C.; Karvembu, R., *J. Inorg. Biochem.*, **2022**, 233, 111843.
11. Bjelogrić, S. K.; Todorović, T. R.; Kojić, M.; Senčanski, M.; Nikolić, M.; Višnjevac, A.; Araškov, J.; Miljković, M.; Muller, C. D.; Filipović, N. R., *J. Inorg. Biochem.*, **2019**, 199, 110758.
12. Jana, S.; Naskar, R.; Manna, C. K.; Mondal, T. K., *J. Chem. Sci.*, **2020**, 132 (1), 1-9.
13. Bangde, P. S.; Prajapati, D. S.; Dandekar, P. P.; Kapdi, A. R., *ChemSelect.*, **2018**, 3 (21), 5709-5716.
14. Haribabu, J.; Balachandran, C.; Tamizh, M. M.; Arun, Y.; Bhuvanesh, N. S.; Aoki, S.; Karvembu, R., *J. Inorg. Biochem.*, **2020**, 205, 110988.

15. Naskar, R.; Ghosh, P.; Manna, C. K.; Murmu, N.; Mondal, T. K., *Inorg. Chim. Acta.*, **2022**, *534*, 120802.
16. Majeed, S. R.; Amin, M. A.; Attaby, F. A.; Alberto, M. E.; Soliman, A. A., *Molecules.*, **2022**, *27* (3), 964.
17. Balakrishnan, N.; Haribabu, J.; Malekshah, R. E.; Swaminathan, S.; Balachandran, C.; Bhuvanesh, N.; Aoki, S.; Karvembu, R., *Inorg. Chim. Acta.*, **2022**, *534*, 120805.
18. Ćočić, D.; Jovanović-Stević, S.; Jelić, R.; Matic, S.; Popović, S.; Djurdjević, P.; Baskić, D.; Petrović, B., *Dalton Trans.*, **2020**, *49* (41), 14411-14431.
19. Karami, K.; Jamshidian, N.; Zakariazadeh, M., *Appl. Organomet. Chem.*, **2019**, *33* (3), e4728.
20. Zafar, M. N.; Butt, A. M.; Perveen, F.; Nazar, M. F.; Masood, S.; Dalebrook, A. F.; Mughal, E. U.; Sumrra, S. H.; Sung, Y. Y.; Muhammad, T. S. T., *J. Inorg. Biochem.*, **2021**, *224*, 111590.
21. Gabr, I. M.; El-Asmy, H. A.; Emmam, M. S.; Mostafa, S. I., *Trans. Met. Chem.*, **2009**, *34* (4), 409-418.
22. R Solomon, V.; Lee, H., *Curr. Chem. Med.*, **2011**, *18* (10), 1488-1508.
23. Byler, K. G.; Wang, C.; Setzer, W. N., *J. Mol. Model.*, **2009**, *15* (12), 1417-1426.
24. Mjwara, P. N.; Papo, T. R.; Sithebe, S., *Molbank.*, **2022**, *2022* (4), M1496.
25. Mukherjee, T.; Sen, B.; Zangrando, E.; Hundal, G.; Chattopadhyay, B.; Chattopadhyay, P., *Inorg. Chim. Acta.*, **2013**, *406*, 176-183.
26. Rulke, R. E.; Ernsting, J. M.; Spek, A. L.; Elsevier, C. J.; van Leeuwen, P. W.; Vrieze, K., *Inorg. Chem.*, **1993**, *32* (25), 5769-5778.
27. Sheldrick, G. M., *Acta Cryst.*, **2015**, *71* (1), 3-8.
28. Dolomanov, O. V.; Bourhis, L. J.; Gildea, R. J.; Howard, J. A.; Puschmann, H. J., *Appl. Cryst.*, **2009**, *42* (2), 339-341.

29. Sheldrick, G. M., *Acta Cryst.*, **2008**, *64* (1), 112-122.
30. Omondi, R. O.; Sibuyi, N. R.; Fadaka, A. O.; Meyer, M.; Jaganyi, D.; Ojwach, S. O., *Dalton Trans.*, **2021**, *50* (23), 8127-8143.
31. Bansal, D.; Kumar, G.; Hundal, G.; Gupta, R., *Dalton Trans.*, **2014**, *43* (39), 14865-14875.
32. Thorat, R. A.; Mandhar, Y.; Parganiha, D.; Patil, K. B.; Singh, V.; Shakir, B.; Raju, S.; Kumar, S., *ChemSelect.*, **2023**, *8* (1), e202203945.
33. Shinde, V. N.; Bhuvanesh, N.; Kumar, A.; Joshi, H., *Organometallics.*, **2020**, *39* (2), 324-333.
34. Kumah, R. T.; Vijayan, P.; Ojwach, S. O., *New J. Chem.*, **2022**, *46* (7), 3146-3155.
35. Kiani, M.; Bagherzadeh, M.; Meghdadi, S.; Fadaei-Tirani, F.; Schenk-Joß, K.; Rabiee, N., *Appl. Organomet. Chem.*, **2020**, *34* (4), e5531.
36. Meghdadi, S.; Langer, V.; Farrokhpour, H.; Massoud, A. A.; Amirnasr, M., *J. Iran. Chem. Soc.*, **2012**, *9* (1), 85-92.
37. Meghdadi, S.; Amirnasr, M.; Amiri, A.; Mobarakeh, Z. M.; Azarkamanzad, Z. C. R. *Chim.*, **2014**, *17* (5), 477-483.
38. Kletskov, A. V.; Bumagin, N. A.; Petkevich, S. K.; Dikusar, E. A.; Lyakhov, A. S.; Ivashkevich, L. S.; Kolesnik, I. A.; Potkin, V. I., *Inorg. Chem.*, **2020**, *59* (15), 10384-10388.
39. Li, S.; Wen, H.; Yuan, N.; Xie, P.; Qin, J.; Wang, Z., *RSC Adv.*, **2020**, *10* (54), 32490-32496.
40. Meghdadi, S.; Amirnasr, M.; Kiani, M.; Fadaei Tirani, F.; Bagheri, M.; Schenk, K., *Coord. Chem.*, **2017**, *70* (14), 2409-2424.
41. Sudharsan, M.; Nethaji, M.; Bhuvanesh, N. S.; Suresh, D., *Asian J. Org. Chem.*, **2021**, *10* (11), 2982-2992.

42. Donzello, M. P.; Ercolani, C.; Fang, Y.; Osterloh, W. R.; Rizzoli, C.; Viola, E.; Stuzhin, P. A.; Kadish, K. M., *Inorg. Chim. Acta.*, **2022**, *534*, 120773.
43. Shit, M., *J. Indian. Chem. Soc.*, **2021**, *98* (11), 100186.
44. Sakaguchi, S.; Yoo, K. S.; O'Neill, J.; Lee, J. H.; Stewart, T.; Jung, K. W., *Angew. Chem. Int. Ed.*, **2008**, *47* (48), 9326-9329.
45. Cati, D. S.; Stoeckli-Evans, H., *Acta. Cryst.*, **2020**, *76* (3), 332-338.

Chapter 4

Investigations of DNA/BSA binding interactions, and cytotoxicity of (pyridyl)pyrazine carboxamide palladium(II) complexes

4.1. Introduction

Palladium(II) complexes have gained interest as promising anticancer agents due to their chemical resemblance with platinum-based complexes.^{1,2} With the first palladium(II) complex lacking stability to target DNA, complexes with suitable chelating ligands that can regulate the stability are being designed and developed to overcome this challenge.³ Numerous palladium(II) complexes with chelating ligands have become promising alternatives by showing good selectivity of normal cells, better anticancer activity, and lower toxicity against a wide range of normal cells.⁴⁻⁷ Additionally, palladium(II) complexes bearing chelating ligands play a major role in lowering kidney toxicity than cisplatin since the proteins are unable to displace the chelating palladium(II) complex with the sulfhydryl group.⁸ The presence of the N-H group improves cytotoxicity as the hydrogen atoms are capable of forming hydrogen bonds in DNA. Consequently, palladium complexes supported on ligands with electron-donor nitrogen atoms can coordinate with nucleic acids effectively.⁹

DNA interaction with metal complexes is the primary step in the design and development of curative cancer agents because it is the main cellular target.^{10, 11} Metal complexes bind covalently or noncovalently to the DNA to prevent cell division of cancer cells. Modes of interaction are dependent on the nature of ligand moiety, metal centre, and coordination geometry.¹² Generally, π -stacking of aromatic heterocyclic metal complexes within the DNA base pairs, hydrogen bonding, and van de Waals interactions found in groove binding as well

as the electrostatic interaction stabilize the interaction of the DNA and respective drugs.³ Hence, it is vital to investigate the binding affinity of metal complexes to DNA.

Furthermore, understanding the transportation and distribution of the developed drugs to the main target biomolecules is significant. Serum albumin proteins are known to perform this function in the bloodstream.¹³⁻¹⁵ Specifically, the interaction of metal complexes with serum albumin proteins is probed to determine the binding strength and mechanism of metal complexes to bovine serum albumin proteins due to homological similarities with human serum albumin, inexpensive, and stable.¹⁶⁻¹⁹ Thus, studying the interaction of DNA/BSA biomolecules and bioactive metal complexes is necessary to comprehend the mechanism of action to cell death.²⁰ Cisplatin and its analogues are currently being used as therapeutic agents for cancer cells and their mechanism of action is understood.^{6, 21}

Numerous dinuclear palladium(II) complexes bearing nitrogen donor ligands have been reported and display enhanced efficacy in cancer cells compared to mononuclear palladium(II) complexes. For example, Alisuf *et al.*,²² reported DNA, bovine serum albumin interactions as well as the anticancer activity of dinuclear palladium(II) complex with the general formula μ -1,4-phenylenediamine-bis-(chloroethylenediaminepalladium(II)) nitrate. The study established that the dinuclear palladium(II) complex can be transported by bovine serum albumin protein to the target DNA and then allow coordination to occur in it. Additionally, this dinuclear palladium complex exhibit enhanced anticancer cytotoxic activity compared to mononuclear complexes. Furthermore, aromaticity plays a major role in the anticancer activity, since there is a noticeable increase in the cytotoxic activity of the reported dinuclear complex than chained palladium(II) complexes.²³ This chapter reports the effect of the electron donating group such as the methyl group and increased palladium(II) metal center on the interaction of

biomolecules DNA /BSA with mononuclear and dinuclear palladium(II) complexes bearing carboxamide moiety isolated in Chapter 3 (**Figure 4.1**).

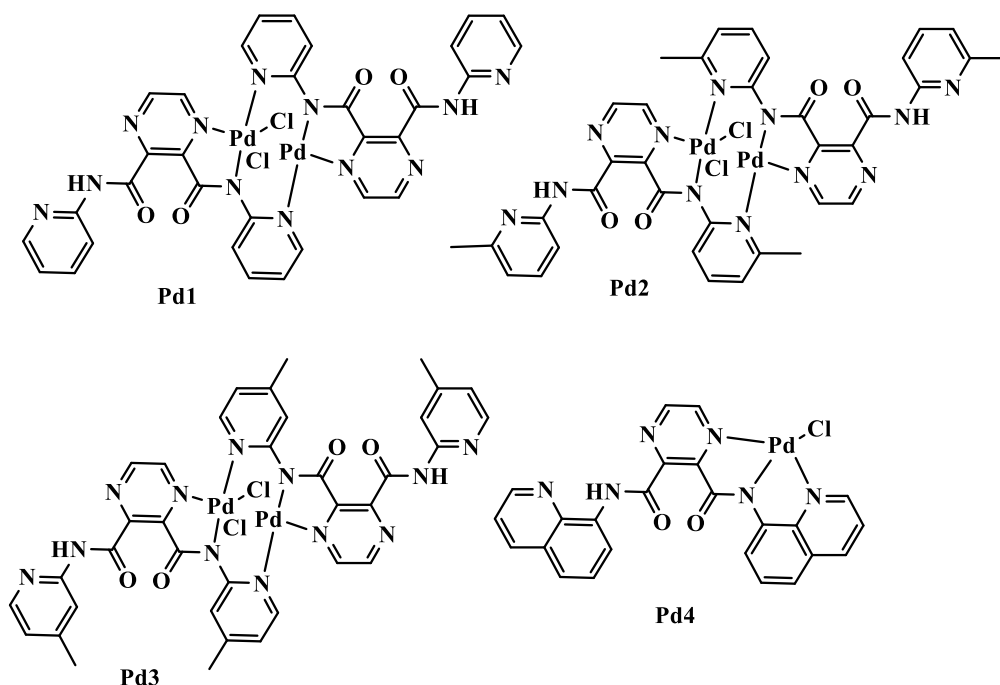


Figure 4.1: (Pyridyl)pyrazine carboxamide palladium(II) complexes used in the biological studies in this chapter.

4.2. Experimental section

4.2.1. General instrumentations and materials

Calf-thymus DNA, ethidium bromide, and bovine serum albumin were purchased from Merck and used without any further purification. Ultrapure water was used in the experiments. CT-DNA titrations were performed from a Cary 100 Series UV-vis spectrophotometer with temperature controller (± 0.05 °C). Fluorescence quenching experiments were performed from

a Perkin Elmer LS 45 Fluorescence Spectrometer using 1 cm path length cuvettes at room temperature.

4.2.2. Experimental procedure of CT-DNA and BSA binding studies

4.2.2.1. CT-DNA absorption spectral studies

CT-DNA interactions with synthesized palladium(II) complexes were performed at room temperature in 0.01 M phosphate-buffered saline(PBS) at pH = 7.4, stored at 4 ° C, and used within 4 days. When evaluated at 260 nm and 280 nm (A_{260}/A_{280}) ratio, the CT-DNA stock solution absorption ratio was in the range of 1.8 to 1.9, demonstrating that CT-DNA was sufficiently free of protein.²⁴ The concentration of CT-DNA per nucleotide was calculated using the maximum absorbance measured at 260 nm and the molar absorption coefficient, 6600 M⁻¹. A fixed concentration of the metal complex 1.0 mM in DMSO solution was titrated with increasing CT-DNA solution and in between titrations, the complex-CT-DNA solution was incubated in a cuvette for 5 min before absorption spectra measurements. The binding constant of the complexes was determined from the Wolfe-Shimer equation (Eq. 4.1).²⁵

$$[\text{DNA}]/(\varepsilon_a - \varepsilon_f) = [\text{DNA}]/(\varepsilon_b - \varepsilon_f) + 1/(K_b(\varepsilon_b - \varepsilon_f)) \quad (\text{Eq. 4.1})$$

Where [DNA] represents the concentration of CT-DNA, ε_a is the apparent extinction coefficient, ε_b is the molar extinction coefficient of the free complex, and ε_f is the extinction coefficient for the [complex-DNA]. K_b was calculated using the slope to intercept ratio of [DNA]/(a-f) vs [DNA]. Using the van't Hoff equation (Eq. 4.2), the standard Gibb's free (G) of metal complexes bound to DNA was determined.²⁶

$$\Delta G = -RT \ln K_b. \quad (\text{Eq. 4.2})$$

4.2.2.2. CT-DNA ethidium displacement studies

The displacement of ethidium bromide with metal complexes in CT-DNA was examined by performing fluorescence quenching experiments. CT-DNA- ethidium bromide was prepared by mixing equal concentrations of CT-DNA and ethidium bromide (10 μ M each) in 0.01 M phosphate-buffered saline solution, pH= 7.4.²⁷ The interaction of metal complexes with CT-DNA to displace ethidium bromide were probe by stepwise addition of increasing concentration of metal complexes, **Pd1-Pd4** to a solution of CT-DNA-EB. Fluorescence quenching emissions were measured within the wavelength of 520 to 700 nm and the excitation wavelength was set at 500 nm. Before each fluorescence measurement, the solutions were thoroughly mixed and incubated for 5 min at room temperature.²⁸

$$I_0/I = 1 + K_{sv}[Q] = 1 + k_q\tau_0[Q] \quad (\text{Eq. 4.3})$$

where I_0 and I are the emission intensities of the CT-DNA-EtBr complex before and after each addition of the complex. $[Q]$ is the concentration of the quencher palladium(II) complex. The Stern-Volmer quenching constant, K_{sv} , was obtained from the slope of the linear plot of I_0/I versus $[Q]$. The bimolecular quenching rate constant, k_q was also calculated using the Stern-Volmer equation, where τ_0 is the average fluorescence lifetime of the CT-DNA+EB complex before the addition of a quencher. The apparent binding constant, K_{app} was determined from the equation Eq. 4.4.²⁵

$$K_{EtBr}[EtBr] = K_{app}[Q] \quad (\text{Eq. 4.4})$$

where $[Q]$ is the concentration of quencher causing a 50% reduction in fluorescence intensity of CT-DNA+ EtBr complex, $K_{EB} = 1.0 \times 10^7 \text{ M}^{-1}$. Scatchard plots also gave the binding constant, K_F as determined from the fluorescence titration using the Scatchard equation Eq. 4.5.²⁹

$$\log(I_0 - I) / I = \log K_F + n \log[Q] \quad (\text{Eq. 4.5})$$

where n is the number of binding sites per nucleotide.

4.2.2.3. Bovine serum albumin quenching studies

Fluorescence quenching of the bovine serum albumin and palladium(II) complexes was investigated to ascertain the binding propensities of the complexes to the BSA. The stock solution of bovine serum albumin was made in 0.01 M PBS with a pH of 7.4 at room temperature. The absorbance at the maximum wavelength, 280 nm, was divided by the molar extinction coefficient to determine the concentration of bovine serum albumin used in the fluorescence titration. A fixed stock solution of BSA in the buffer was titrated with increasing concentration of the palladium(II) complex. The fluorescence emission spectra were recorded in the range of 300 nm to 410 nm with an excitation of 278 nm. Before the measurement of each spectral data, the solution was incubated for 5 min at room temperature.³⁰ Similar to CT-DNA- ethidium bromide, the fluorescence quenching of the compounds is explained by Stern-Volmer and Scatchard equation.

4.2.2.4. Filter effects

The inner filter effects was diminished by correcting the data obtained in spectrophotometric titrations using the following described literature procedure.³¹ The following equation 4.6³² was used.

$$F_{\text{corr}} = F_{\text{obs}} 10^{(A_{\text{ex}} + A_{\text{em}})/2} \quad \text{Eq. 4.6}$$

in which the quencher/fluorophore addition-induced corrected and observed fluorescence intensities are F_{corr} and F_{obs} . They are caused by the addition of quencher/fluorophore in a

cuvette with a 1 cm path length, respectively. The aforementioned equation is used because it is valid and appropriate in the case of typical fluorophores where scattering is negligible and absorption predominates extinction.²⁶

4.2.3. *In vitro* cytotoxicity

The human breast cancer cell line (MCF-7) was used to examine the inhibitory effects of the palladium(II) complexes (**Pd1-Pd4**) and their respective (pyridyl)pyrazine carboxamide ligands (**L1-L3**). The studies were carried out using a method that was previously reported in literature.^{25, 33} Using the MTT (3-(4,5-Dimethyl-2-thiazyl)-2,5-diphenyl-2H-tetrazolium bromide) test, the viability of the treatment was assessed after 48 hours of incubation. MCF-7 human breast cancer cell was developed in 75 cm² tissue culture flask using DMEM supplemented with 10 % Foetal Calf Serum, 2 mM L-glutamine, and 1% antibiotic-antimycotic solution (containing penicillin, streptomycin, and amphotericin B), and incubated at 37 °C in a humidified atmosphere of 5 % CO₂. Additionally, tissue cultures were rinsed with phosphate-buffered saline (PBS), trypsinised, and then the cells were suspended in a growth medium (compound stocks were prepared in DMSO but the final DMSO concentration that cells were exposed to was less than 0.1 % v/v) before being placed on culture plates. Haemocytometer was set to 5 x 10⁴ cells/ml, and 100 µl of the suspension was seeded into each well of micro-clear, flat-bottom 96-well plates. Before the treatment of culture for up to 48 h with varying concentrations of each compound prepared in a growth medium, the seeded plates were incubated for 24 h. To determine viability after treatment, 10 µl of a 5 mg/ml solution of MTT was added to each well, and the plates were incubated for 3 h. Then, the contents of each were aspirated, and 100 µl of DMSO was added to dissolve the insoluble formazan. Following that, a CLARIO star plate reader was used to read the absorbance at 570 nm (BMG LABTECH, Germany). The mean duplicate values for each treatment were calculated and expressed

relative to the mean of the duplicate negative control wells that were set to 100%. An Olympus CKX41 microscope fitted with an Olympus DP71 UTVIX-2 camera was used to assess and image treatment-induced changes to the morphology of cells. The images were captured with the Olympus cells entry software.

4.3. Result and discussion

4.3.1 CT-DNA absorption spectral studies

DNA is known to be the main biological target in the treatment of cancer using metal-based drugs.³⁴ Small complexes can bind to the DNA molecule using different binding modes. Most aromatic heterocyclic complexes destroy cancer cell growth by interfering with the hydrogen bonds of the nucleobases that are within DNA.³⁵ Therefore, it is crucial to study the drug-DNA interactions to comprehend the mechanism of action. These studies can be performed using UV-Vis spectroscopy which is an important technique in studying the interactions between DNA and metal complexes. From this technique, it is possible to establish various modes of binding between DNA and metal complexes, such as intercalation within DNA base pairs, minor and major groove binding, and sugar-phosphate backbone.³⁶ Binding of palladium(II) complexes **Pd1-Pd4** to CT-DNA duplex was monitored using electronic absorption spectroscopic titrations. Increment addition of CT-DNA concentration to a fixed concentration of palladium(II) complex resulted in a change in absorbance intensity as shown in **Figure 4.2**. The spectral changes depicted hypochromic and bathochromic shifts upon increasing CT-DNA concentration, which could be assigned to the π - π stacking of the palladium(II) complexes within the CT-DNA base pairs indicating the existence of intercalation binding mode.²⁵ Similar trends of spectral changes were observed in the absorption spectra of the complexes **Pd1-Pd4**. The intrinsic binding constant(K_b) values, 4.28 - $13.12 \times 10^6 \text{ M}^{-1}$ for palladium (II)

complexes **Pd1-Pd4** indicate a strong interaction between CT-DNA and complexes. The binding strength of the complexes to CT-DNA follows this order **Pd3** > **Pd2** > **Pd1** > **Pd4**. Additionally, the observed high binding constants for **Pd1-Pd4** are due to planarity which facilitates CT-DNA binding.^{26, 37} Among the complexes, **Pd2** and **Pd3** exhibited greatest binding constants due to the presence of a methyl group which induce hydrophobicity when the complexes interact with CT-DNA leading to enhanced CT-DNA binding affinity.³⁸ The obtained binding constants are comparable to other related palladium(II) complexes in literature with the same magnitude ($(0.53-5.53) \times 10^6 \text{ M}^{-1}$) and $((1.921-3.975) \times 10^6 \text{ M}^{-1})$.^{25, 39} Gibbs free energy(ΔG) of the complex-DNA was calculated and the results are presented in **Table 4.1**. Negative values of Gibbs energy obtained suggest that the complexes interact with CT-DNA spontaneously.^{40, 41} Free energy values of **Pd2** and **Pd3** are more negative compared to the other complexes, undoubtedly due to the presence of a methyl group.⁴²

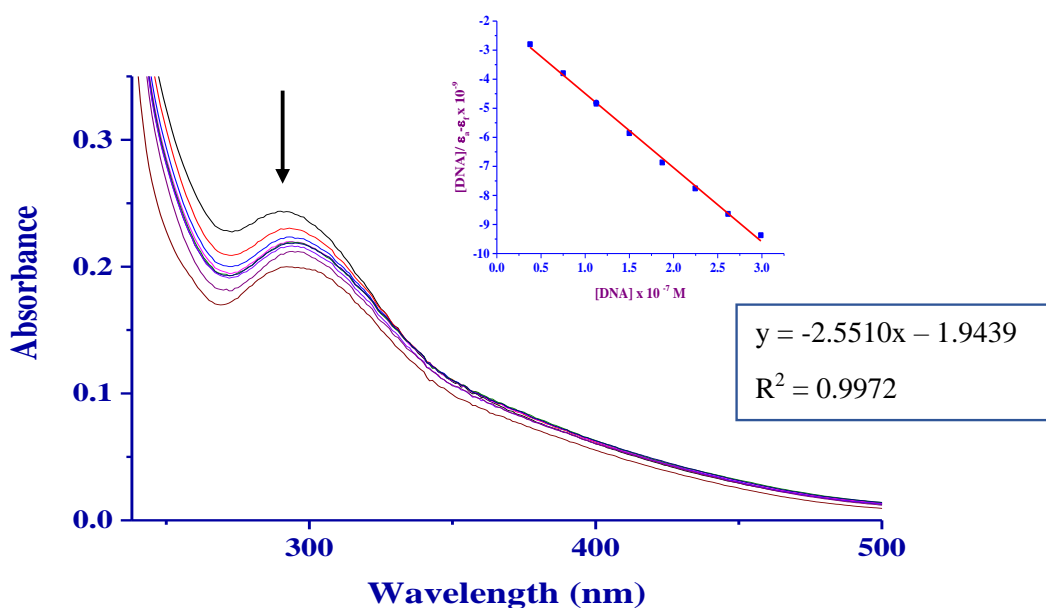


Figure 4.2: Electronic absorption spectra of **Pd3** (25 μM) in 0.01 M PBS buffer at pH=7.4 upon addition of CT-DNA (0 - 16 μM). The arrow shows the decrease in absorbance upon the addition of increasing concentration of CT-DNA. Inserted is the linear plot of $[\text{CT-DNA}]$ vs $[\text{DNA}]/(\epsilon_a - \epsilon_f)$.

4.3.2. Competitive CT-DNA ethidium fluorescence quenching studies

Ethidium bromide is a strong DNA intercalating agent that is used to probe the interactions of compounds with DNA since it could afford intense fluorescence emission when intercalating to the DNA.^{35, 43} During the interaction, ethidium bromine is displaced by intercalating complexes from DNA resulting to quenched fluorescence intensity.⁴⁴ Competitive binding experiments are conducted to assess if complexes can displace ethidium bromide in the EB-DNA complex. Thus, in this study, the interaction of palladium(II) complexes with CT-DNA was investigated by evaluating the fluorescence quenching experiments of the CT-DNA-EB complex in the presence of palladium(II) complexes. Upon the addition of increasing concentration of the complex to a constant concentration of EB-CT-DNA, fluorescence emission intensity could be reduced due to the strong interaction formed between CT-DNA and the complex when replacing ethidium bromide.³⁶ This was observed after the addition of an increasing concentration of **Pd1-Pd4** to a fixed concentration of CT-DNA-EB. The spectral data, see **Figure 4.3**, depicted a hypochromic shift in fluorescence emission at 592 nm, which indicate that the complexes intercalate within CT-DNA base pairs to displace ethidium bromide. In addition, emission intensity was quenched with a notable red shift in all spectra of complexes which points to the existence of strong interaction between palladium(II) complex and CT-DNA.²⁹

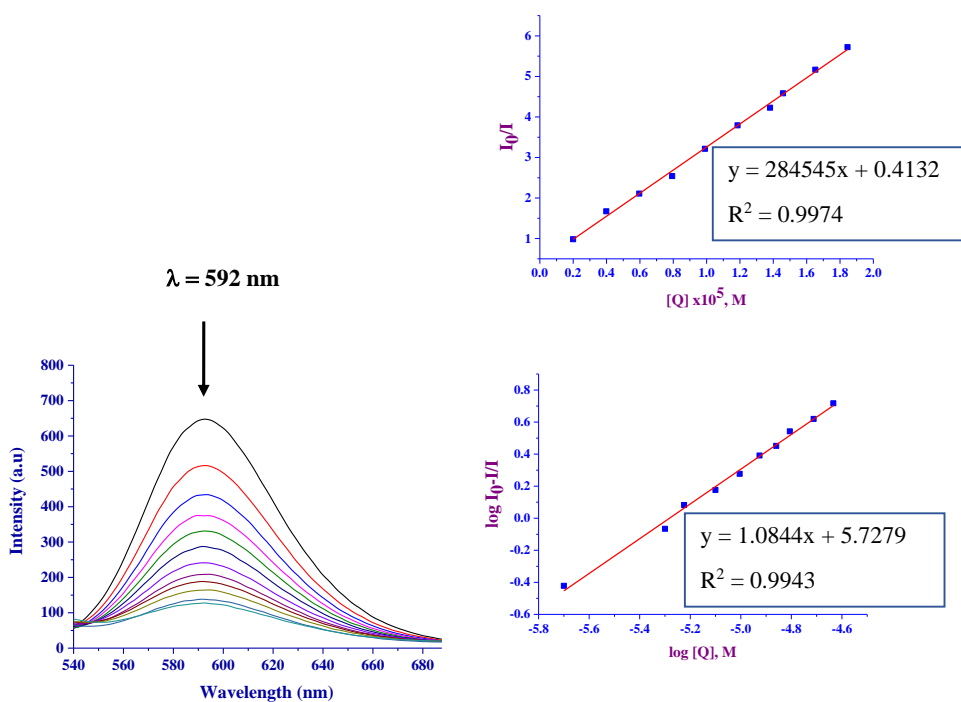


Figure 4.3: Fluorescence emission spectra depicting the quenching upon addition of an increasing amount of **Pd3** to CT-DNA-EB: [EB] = 10 μ M, [CT-DNA] = 10 μ M. The arrow shows the intensity changes upon increasing the **Pd3** complex concentration. Inserted is the Stern-Volmer plot of I_0/I vs [Q] and Scatchard plot of $\log[(I_0-I)/I]$ vs $\log[Q]$.

The Stern-Volmer quenching and biomolecular quenching rate constants were calculated by fitting the data to the Stern-Volmer equation (Eq.3). K_{sv} values of palladium(II) complexes (1.82-28.41) $\times 10^5 \text{ M}^{-1}$ signify that the complexes intercalate to the DNA to replace ethidium bromide dye. The observed K_{app} magnitudes (3.93-25.02) $\times 10^6 \text{ M}^{-1}$ for **Pd1- Pd4** are lower than the binding constants (10^7 M^{-1}) for classical intercalators and metallointercalators, which implies that the complexes intercalate strongly to the DNA base pairs.^{45, 46} In general, the dynamic quenching mechanism is signified by values lower than those of strong biopolymer fluorescence quenchers ($2 \times 10^{10} \text{ M}^{-1}\text{s}^{-1}$). In this study, the high bimolecular quenching rate constants k_q values (1.00-12.33) $\times 10^{12} \text{ M}^{-1}\text{s}^{-1}$ reported for these complexes **Pd1-Pd4** (Table

4.1) point to the displacement of ethidium bromide *via* the static mechanism.⁴⁷ The binding constants (K_F) and the number of binding sites (n) obtained from the linear plot of the Scatchard equation (Eq.5) (**Figure 4.3**) are given in **Table 4.1**. The n -values (0.75-1.08) obtained were approximately equal to one, suggesting that palladium complexes bind to a single site in CT-DNA. It is important to note that the binding constant K_F (1.01 - 53.44) $\times 10^4$ M^{-1} values support intercalative binding mode between palladium(II) complexes and CT-DNA-EB, which is consistent with the biomolecular quenching rate constant (k_q). High binding and quenching rate constants obtained are due to the planarity of the complexes that allow the complexes to effortlessly reach the active site in CT-DNA.²⁶ In addition, the binding constants of the complexes follow the order **Pd3** > **Pd2** > **Pd1** > **Pd4**, with **Pd3** exhibiting higher binding (K_F) and quenching constant (k_q) whereas complex **Pd1** showed low binding (K_F) and quenching constant (k_q) for dinuclear palladium(II) complexes. This could be due to the presence of a hydrophobic group such as methyl group in **Pd2** and **Pd3**, which increase the DNA binding affinity since complexes are more inserted and stacked with DNA than other complexes.⁴⁸ In addition, dinuclear complexes **Pd1-Pd3** showed high binding constants compared to a mononuclear **Pd4** which is a result of increased palladium center in dinuclear complexes due to favourable electrostatic interactions.⁴⁹

Table 4.1: CT-DNA binding constants, quenching constants, and Gibbs energy values for **Pd1-Pd4**

Complex	UV titration		EB fluorescence exchange titration				
	$K_b \times 10^6$ (M ⁻¹)	$K_{sv} \times 10^5$ (M ⁻¹)	$K_{app} \times 10^6$ (M ⁻¹)	$k_q \times 10^{12}$ (M ⁻¹ s ⁻¹)	$K_F \times 10^4$ (M ⁻¹)	n	$\Delta G_{25^\circ C}/kJmol^{-1}$
Pd1	4.78 ± 0.27	9.71 ± 0.48	8.07 ± 0.34	2.61 ± 0.61	1.11 ± 0.170	0.84	-38.1
Pd2	10.80 ± 0.98	23.14 ± 1.56	14.52 ± 1.41	1.02 ± 1.12	1.42 ± 0.14	0.75	-401.3
Pd3	13.12 ± 0.91	28.41 ± 2.43	25.02 ± 2.74	12.33 ± 1.91	53.44 ± 2.74	1.08	-406.1
Pd4	4.28 ± 0.41	1.82 ± 0.14	3.93 ± 0.11	1.00 ± 0.02	1.01 ± 0.17	0.94	-36.0

4.3.3. BSA fluorescence quenching

Albumin proteins are known for their transportation and distribution of drugs to the bloodstream. Their interaction with metal drugs may alter the biological properties of the drug. It is thus imperative to probe the binding mode and quenching mechanism of biologically active compounds with bovine serum albumin proteins.⁵⁰ These binding interactions can be simulated using effective methods such as fluorescence spectroscopic titrations. Interactions of palladium complexes **Pd1-Pd4** with bovine serum albumin protein were studied to get an insight into the binding mode and quenching mechanism of the synthesized metal complexes. Reductions in the fluorescence emission intensity at 348 nm upon the addition of increasing concentration of **Pd1-Pd4** to a fixed concentration of bovine serum albumin were observed indicating the change in the conformation of bovine serum albumin.⁵¹ The Stern-Volmer (K_{sv}) and bimolecular constants (K_q) were determined from the Stern-Volmer equation (Eq.3) and were used to describe the quenching mechanism of the complexes. The number of binding sites (n) and Scatchard constant (K_F) were determined from the Scatchard equation (Eq.5) and the linear plot **Figure 4.3**, (**Table. 4.2**). The high magnitudes of the dynamic collision quenching constant K_{sv} ($1.48-29.67$) $\times 10^6 \text{ M}^{-1}$ for compounds **Pd1-Pd4** was indicative of strong protein binding.⁵² Furthermore, the bimolecular constants, k_q ($0.66-13.99$) $\times 10^{14} \text{ M}^{-1}\text{s}^{-1}$ are higher than the scattered collision quenching constants ($2.0 \times 10^{10} \text{ M}^{-1}\text{s}^{-1}$) for biomolecules, which supports the existence of a static quenching mechanism for the palladium(II) complexes.²⁶ In addition, the higher values of K_{sv} and k_q indicate that the binding process is not entirely controlled by diffusion, but it appears some specific drug proteins also take part in the process resulting in enhanced k_q constant.⁵³ These constants are of the same order of the magnitude of (10^{14}) obtained for copper(II) and zinc(II) complexes of 4-acylpyrazolone ligands.⁵⁴ The computed K_F values ($0.10-16.10$) $\times 10^5 \text{ M}^{-1}$ of complexes **Pd1-Pd4** (**Table 4.2**) are within the optimum range which is high enough to promote strong binding of the complexes to the BSA and be

transported to target DNA. In addition, the binding constants are sufficiently low to be released and transported to the cancer cell targets.⁵⁵ These binding constants are below the association constant ($K_F = 10^{15}$) considered for strong protein-ligand interactions confirming that the complexes can be released to cancer cells.^{53, 56} Further, high magnitudes of K_F values (10^5) for **Pd1-Pd3**, suggest that the interactions of complexes with BSA are mainly due to hydrophobic interactions within subdomain IIA of BSA.⁵⁷ The number of binding sites n values (0.70-0.89) of **Pd1-Pd4** is closer to one, demonstrating that the compounds bind to a single site of BSA. The binding strength of the complexes to BSA follows a different order from the DNA trend **Pd2 > Pd1 > Pd3 > Pd4**.

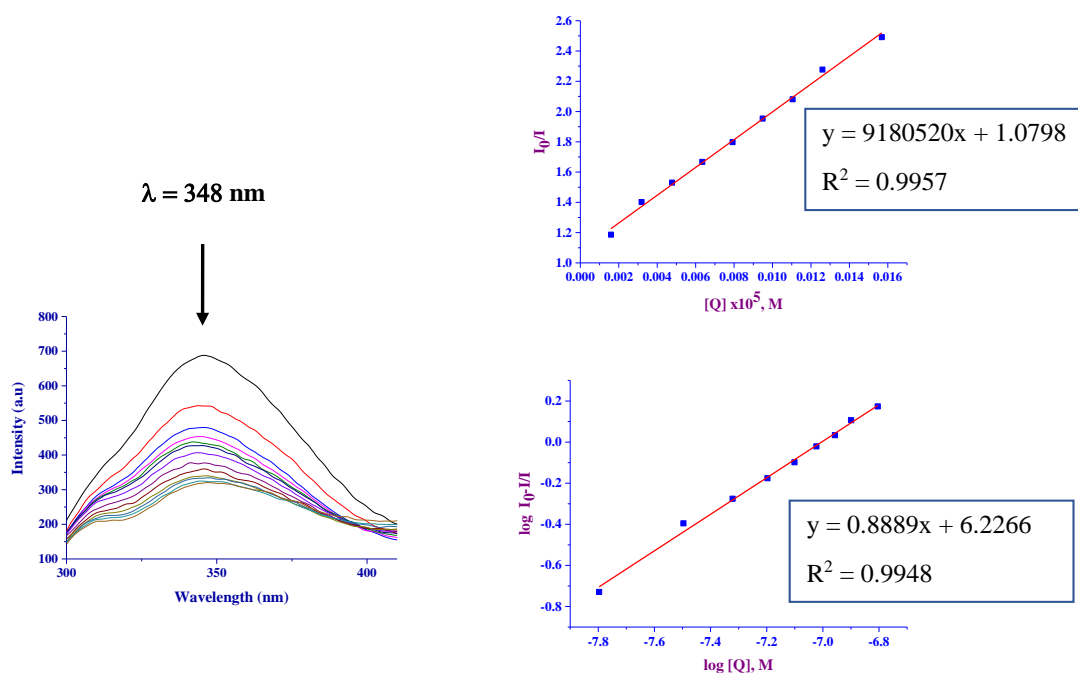


Figure 4.4: Quenching in fluorescence emission spectra of BSA in the presence of an increasing concentration of Pd3 = 0-40 μ M and [BSA] = 14 μ M. The arrow shows the decrease in fluorescence intensity upon increasing the Pd3 concentration. Inserted is the Stern-Volmer plot of I_0/I vs $[Q]$ and Scatchard plot of $\log[(I_0 - I)/I]$ vs $\log[Q]$.

Table 4.2: BSA binding constant, quenching constants, and number of binding sites for **Pd1-Pd4**

Complex	$K_{sv} \times 10^6$ (M^{-1})	$k_q \times 10^{14}$ ($M^{-1} s^{-1}$)	$K_F \times 10^5$ (M^{-1})	n
Pd1	9.18 ± 0.76	4.14 ± 0.21	8.43 ± 0.23	0.89
Pd2	29.67 ± 2.87	13.99 ± 0.97	16.10 ± 0.82	0.71
Pd3	7.95 ± 0.89	3.55 ± 0.18	0.15 ± 0.01	0.80
Pd4	1.48 ± 0.15	0.66 ± 0.05	0.10 ± 0.01	0.70

4.3.4. *In vitro* cytotoxicity studies of ligands L1-L3 and palladium complexes Pd1-Pd4

The cytotoxic activity of the (pyridyl)pyrazine ligands **L1-L3** and their palladium(II) complexes **Pd1-Pd4** was examined on a human breast cancer cell line (MCF-7) using MTT assay. The activity of the compounds was measured after the cells were exposed to variable concentrations of the compounds for 48 h. As shown in **Figure 4.5**, the percentage cell viability of the compounds was reduced upon increasing the concentration of the compounds, suggesting concentration-dependent toxicities against the MCF-7 cancer cell line. For example, complex **Pd2** showed cell viabilities of 95 % and 75 % at concentrations of 12.5 μ M and 100 μ M respectively (**Figure 4.5B**). The *in vitro* cytotoxicity data for the compounds is represented as half inhibition concentration (IC_{50}) in **Table 4.3**. In general, the (pyridyl)pyrazine ligands showed lower cytotoxic activities compared to their respective palladium(II) complexes (**Table 4.3**). For example, both ligands **L1** and **L2** can be said to be inactive ($IC_{50} > 100 \mu$ M), whereas ligand **L3** displayed low cytotoxicity with an IC_{50} of 80 μ M, in comparison to the cytotoxicity of the respective palladium(II) complexes **Pd1** ($IC_{50} = 11.4 \mu$ M), **Pd2** ($IC_{50} = 154.9 \mu$ M) and

Pd3 ($IC_{50} = 230 \mu\text{M}$) respectively. The higher cytotoxicity of the palladium(II) complex **Pd1** relative to the ligands can be attributed to the more facile binding of the complexes to the DNA nucleobases resulting in limited cell growth.^{58, 59}

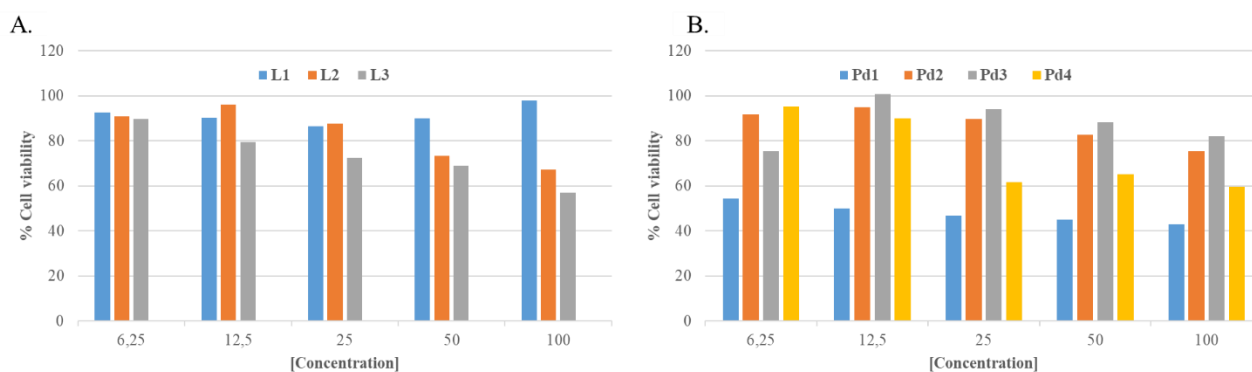


Figure 4.5: Effect of ligands L1-L3 and palladium (II) complexes Pd1-Pd4 on the human breast cancer cell line (MCF-7) after 48 h treatment. Each bar represents the percentage cell viability value for the effect of the concentration of each compound.

Within the palladium(II) complexes, **Pd1** and **Pd4** displayed good and moderate cytotoxic effects against the human breast cancer cell line (MCF-7) with IC_{50} values of $11.4 \mu\text{M}$ and $61.5 \mu\text{M}$ respectively. The higher cytotoxic activity of complex **Pd1** ($IC_{50} = 11.4 \mu\text{M}$) in comparison to the corresponding complex **Pd4** ($IC_{50} = 61.5 \mu\text{M}$) could be associated with the dinuclear nature of complex **Pd1** relative to the mono-nuclear complex **Pd4**. This trend correlates well with the observed higher cytotoxicity values of complexes (**Pd1-Pd3**) relative to the ligands (**L1-L3**). Interestingly, complexes **Pd2** and **Pd3** were inactive displaying IC_{50} values of $154.9 \mu\text{M}$ and $230.1 \mu\text{M}$ respectively. In terms of structural comparisons, complexes **Pd2** and **Pd3** bear the methyl substituents on the ligand motif. The methyl groups in complexes **Pd2** and **Pd3** are likely to reduce low solubility in water which may reduce their bioavailability and

absorption, impose some steric hindrance and loss of planarity, resulting in possible disruption complex-DNA interactions, consistent with the poor cytotoxicity observed.^{26,60, 61} Thus, the anticancer activity of the palladium(II) complexes against the MCF-7 cancer cell line follow the order **Pd1 > Pd4 > Pd2 > Pd3**.

Table 4.3: Cytotoxic activity of the ligands (**L1-L3**) and palladium(II) complexes (**Pd1-Pd4**) against the human breast cancer cell line (MCF-7)^a

Complex	IC ₅₀ (μM)
	MCF-7
L1	>400
L2	182.4
L3	80.2
Pd1	11.2
Pd2	154.9
Pd3	230.1
Pd4	61.5

^aThe IC₅₀ values were determined using MTT assay after 48 h treatment with the compounds at various concentrations. Results are expressed as mean ± SD of the duplicate experiments.

Attempts were made to correlate the relative cytotoxicity of the palladium complexes to their respective DNA & BSA binding affinities to establish if there is any dependency or trend (**Table 4.4**). From the summarised data shown in **Table 4.4**, the palladium(II) complexes **Pd2** showed the highest BSA binding interactions ($K_F = 16.10 \pm 0.82 \times 10^5 \text{ M}^{-1}$) while complex

Pd3 displayed the highest DNA binding constants of $K_F = 53.44 \pm 2.74 \times 10^4 \text{ M}^{-1}$. Interestingly, these compounds (**Pd2** and **Pd3**) were inactive against the MCF-7 cell line, while compounds **Pd1** ($1.11 \pm 0.17 \times 10^4 \text{ M}^{-1}$) and **Pd4** ($1.01 \pm 0.17 \times 10^4 \text{ M}^{-1}$) with lower DNA interactions were active displaying IC_{50} values of 11.2 μM and 61.5 μM (**Table 4.4**). One would thus expect complexes **Pd2** and **Pd3** to display higher cytotoxicity in comparison to complexes **Pd1** and **Pd4**.⁶² The opposite results observed in this study thus highlights that the cytotoxicity of these complexes is not entirely dependent on the respective DNA/BSA interactions, but could be a result of other factors such as solubility, permeability among, and lability.⁶³

Table 4.4: Summarized values of biological activity palladium(II) complexes

Complex	DNA/ $K_F \times 10^4 \text{ (M}^{-1}\text{)}$	BSA/ $K_F \times 10^5 \text{ (M}^{-1}\text{)}$	$\text{IC}_{50} \text{ (}\mu\text{M)}$
			MCF-7
Pd1	1.11 ± 0.17	8.43 ± 0.23	11.2
Pd2	1.42 ± 0.14	16.10 ± 0.82	154.9
Pd3	53.44 ± 2.74	0.15 ± 0.01	230.1
Pd4	1.01 ± 0.17	0.10 ± 0.01	61.5

4.4. Conclusions

In this study, the interactions of CT-DNA and BSA with mononuclear and dinuclear palladium(II) carboxamide complexes **Pd1-Pd4** were evaluated using different spectroscopic measurements. CT-DNA interaction results obtained from electronic absorption titration and fluorescence quenching experiments demonstrate that palladium(II) complexes interact with

DNA via intercalation mode. Dinuclear complexes **Pd1-Pd3** bind strongly to the DNA molecule in comparison to the mononuclear palladium (II) complex **Pd4** as a result of the increased metal centre due to favorable electrostatic interactions. Additionally, **Pd3** and **Pd2** exhibited high CT-DNA binding constants when compared to **Pd1**. Furthermore, examination of the interaction of bovine serum albumin (BSA) complexes with the palladium(II) complexes using fluorescence quenching experiments reveals that **Pd1-Pd4** interacts with BSA *via* a static mechanism in a single site. Complex **Pd2** showed a higher binding constant while **Pd4** exhibited a low binding constant which is inconsistent with CT-DNA binding constants. Hence, the results showed that the dinuclear complexes and the presence of alkyl groups increase the binding strength of palladium(II) carboxamide complexes to DNA/BSA respectively. The (pyridyl)pyrazine carboxamide ligands (**L1-L3**) and the palladium(II) complexes (**Pd1-Pd4**) were investigated for their cytotoxic activity against the MCF-7 cancer cell lines. The ligands and complexes **Pd2** and **Pd3** were generally inactive, while complexes **Pd1** and **Pd4** displayed high and moderate cytotoxic. Thus, the palladium atom, nuclearity and coordination nature of the compounds appear to control the cytotoxicity of these compounds. There was no clear correlation between the cytotoxicity and DNA/BSA interactions of the complexes, pointing to complex mechanisms of the anti-cancer activities of these compounds.

4.5 References

1. Ayyannan, G.; Mohanraj, M.; Gopiraman, M.; Uthayamalar, R.; Raja, G.; Bhuvanesh, N.; Nandhakumar, R.; Jayabalakrishnan, C., *Inorg. Chim. Acta.*, **2020**, *512*, 119868.
2. Dorairaj, D. P.; Haribabu, J.; Chang, Y. L.; Echeverria, C.; Hsu, S. C.; Karvembu, R., *Appl. Organomet. Chem.*, **2022**, *36* (8), e6765.
3. Karami, K.; Jamshidian, N.; Zakariazadeh, M., *Appl. Organomet. Chem.*, **2019**, *33* (3), e4728.
4. Bhaduri, R.; Pan, A.; Tarai, S. K.; Mandal, S.; Bagchi, A.; Biswas, A.; Moi, S. C., *J. Mol. Liq.*, **2022**, *367*, 120540.
5. Dorafshan Tabatabai, A. S.; Dehghanian, E.; Mansouri-Torshizi, H., *Biometals.*, **2022**, *35* (2), 245-266.
6. Aminzadeh, M.; Mansouri-Torshizi, H.; Aleeshah, R.; Abdi, K.; Saeidifar, M., *Biometals.*, **2021**, *34* (5), 1173-1189.
7. Naskar, R.; Ghosh, P.; Mandal, S.; Jana, S.; Murmu, N.; Mondal, T. K., *J. Chem. Sci.*, **2022**, *134* (4), 103.
8. Jahromi, E. Z.; Divsalar, A.; Saboury, A. A.; Khaleghizadeh, S.; Mansouri-Torshizi, H.; Kostova, I., *J. Iran. Chem. Soc.*, **2016**, *13*, 967-989.
9. Rajković, S.; Franich, A. A.; Čupurdija, V.; Živković, M. D., *EABR*, 10.2478/sjecr-2021-0030
10. Karami, K.; Alinaghi, M.; Amirghofran, Z.; Lipkowski, J., *Inorg. Chim. Acta.*, **2018**, *471*, 797-807.
11. Ramachandran, E.; Kalaivani, P.; Prabhakaran, R.; Zeller, M.; Bartlett, J. H.; Adero, P. O.; Wagner, T. R.; Natarajan, K., *Inorg. Chim. Acta.*, **2012**, *385*, 94-99.

12. Franich, A. A.; Živković, M. D.; Milovanović, J.; Arsenijević, D.; Arsenijević, A.; Milovanović, M.; Djuran, M. I.; Rajković, S., *J. Inorg. Biochem.*, **2020**, *210*, 111158.
13. Gayathri, S.; Viswanathamurthi, P.; Thuslim, V.; Sathya, M.; Ranjani, M.; Prabhakaran, R.; Haribabu, J.; Echeverria, C., *Inorg. Chim. Acta.*, **2022**, *533*, 120780.
14. Zhao, C.; Huang, L.; Wang, Q., *J. Appl. Spectr.*, **2022**, *88* (6), 1247-1256.
15. Shao, J.; Zhang, Q.; Wei, J.; Yuchi, Z.; Cao, P.; Li, S.-Q.; Wang, S.; Xu, J.-Y.; Yang, S.; Zhang, Y., *Dalton Trans.*, **2021**, *50* (38), 13387-13398.
16. Kalantari, R.; Asadi, Z., *J. Mol. Struct.*, **2020**, *1219*, 128664.
17. Zarei, L.; Asadi, Z.; Samolova, E.; Dusek, M.; Amirghofran, Z., *Inorg. Chim. Acta.*, **2020**, *509*, 119674.
18. Feizi-Dehmayebi, M.; Dehghanian, E.; Mansouri-Torshizi, H., *J. Spectrosc. Acta A. Biomol Spectrosc.*, **2022**, *281*, 121543.
19. Konovalov, B.; Franich, A. A.; Jovanović, M.; Jurisević, M.; Gajović, N.; Jovanović, M.; Arsenijević, N.; Maric, V.; Jovanović, I.; Živković, M. D., *Appl. Organomet. Chem.*, **2021**, *35* (3), e6112.
20. Yang, J.; Liao, G.; Liu, X.; Zhao, S.; Yang, Z., *J. Inorg. Biochem.*, **2022**, *236*, 111941.
21. Balakrishnan, N.; Haribabu, J.; Malekshah, R. E.; Swaminathan, S.; Balachandran, C.; Bhuvanesh, N.; Aoki, S.; Karvembu, R., *Inorg. Chim. Acta.*, **2022**, *534*, 120805.
22. Alisufi, N.; Mansouri-Torshizi, H., *J. Iran. Chem. Soc.*, **2021**, *18* (5), 1147-1166.
23. Mohammadlou, F.; Mansouri-Torshizi, H.; Abdi, K., *J. Biomol. Struct. Dyn.*, **2021**, *39* (4), 1354-1372.
24. Adeleke, A. A.; Islam, M. S.; Olofinisan, K.; Salau, V. F.; Mocktar, C.; Omondi, B., *New J. Chem.*, **2021**, *45* (38), 17827-17846.
25. Omondi, R. O.; Bellam, R.; Ojwach, S. O.; Jaganyi, D.; Fatokun, A. A., *J. Inorg. Biochem.*, **2020**, *210*, 111156.

26. Omondi, R. O.; Sibuyi, N. R.; Fadaka, A. O.; Meyer, M.; Jaganyi, D.; Ojwach, S. O., *Dalton Trans.*, **2021**, 50 (23), 8127-8143.
27. Milić, S. S. J.; Jevtić, V. V.; Avdović, E. H.; Petrović, B.; Međedović, M.; Petrović, Đ. S.; Milovanović, M.; Milovanović, J.; Arsenijević, N.; Stojković, D. L., *Monatsh. Chem.*, **2021**, 152 (8), 951-958.
28. Franich, A. A.; Živković, M. D.; Čočić, D.; Petrović, B.; Milovanović, M.; Arsenijević, A.; Milovanović, J.; Arsenijević, D.; Stojanović, B.; Djuran, M. I., *J. Inorg. Biochem.*, **2019**, 24 (7), 1009-1022.
29. Bellam, R.; Jaganyi, D.; Robinson, R. S., *ACS Omega*, **2022**, 7 (30), 26226-26245.
30. Maikoo, S.; Xulu, B.; Mambanda, A.; Mkhwanazi, N.; Davison, C.; de la Mare, J. A.; Booysen, I. N., *ChemMedChem*, **2022**, 17 (20), e202200444.
31. Parker, C.; Rees, W., *Analyst*, **1962**, 87 (1031), 83-111.
32. Puchalski, M.; Morra, M.; Von Wandruszka, R., *Fresenius J. Anal. Chem.*, **1991**, 340, 341-344.
33. Omondi, R. O.; Jaganyi, D.; Ojwach, S. O.; Fatokun, A. A., *Inorg. Chim. Acta.*, **2018**, 482, 213-220.
34. Čočić, D.; Jovanović, S.; Radisavljević, S.; Korzekwa, J.; Scheurer, A.; Puchta, R.; Baskić, D.; Todorović, D.; Popović, S.; Matić, S., *J. Inorg. Biochem.*, **2018**, 189, 91-102.
35. Mondal, A.; Sen, U.; Roy, N.; Muthukumar, V.; Sahoo, S. K.; Bose, B.; Paira, P., *Dalton Trans.*, **2021**, 50 (3), 979-997.
36. Čočić, D.; Jovanović, S.; Nišavić, M.; Baskić, D.; Todorović, D.; Popović, S.; Bugarčić, Ž. D.; Petrović, B., *J. Inorg. Biochem.*, **2017**, 175, 67-79.
37. Jovanović, S.; Obrenčević, K.; Bugarčić, Ž. D.; Popović, I.; Žakula, J.; Petrović, B., *Dalton Trans.*, **2016**, 45 (31), 12444-12457.
38. Şenel, P.; İnci, D.; Aydın, R.; Huriyet, H.; Zorlu, Y.; Çinkılıç, N., *Appl. Organomet. Chem.*, **2019**, 33 (10), e5122.

39. Shanmugapriya, A.; Jain, R.; Sabarinathan, D.; Kalaiarasi, G.; Dallemer, F.; Prabhakaran, R. *New J. Chem.*, **2017**, *41* (18), 10324-10338.
40. Ćočić, D.; Jovanović-Stević, S.; Jelić, R.; Matic, S.; Popović, S.; Djurdjević, P.; Baskić, D.; Petrović, B., *Dalton Trans.*, **2020**, *49* (41), 14411-14431.
41. Mandal, S.; Tarai, S. K.; Pan, A.; Bhaduri, R.; Biswas, P.; Moi, S. C., *Bioorg. Chem.*, **2022**, *128*, 106093.
42. Mudasira; Yoshiokab, N.; Inoueb, H., *Z. Naturforsch. B.*, **2008**, *63* (1), 37-46.
43. Lu, Y.; Hou, Z.; Li, M.; Wang, N.; Wang, J.; Ni, F.; Zhao, Y.; Zhang, B.; Xi, N., *Dalton Trans.*, **2022**, *51* (42), 16224-16235.
44. de Almeida, P. S.; de Arruda, H. J.; Sousa, G. L. S.; Ribeiro, F. V.; de Azevedo-França, J. A.; Ferreira, L. A.; Guedes, G. P.; Silva, H.; Kummerle, A. E.; Neves, A. P., *Dalton Trans.*, **2021**, *50* (41), 14908-14919.
45. Bera, P.; Aher, A.; Brandao, P.; Manna, S. K.; Bhattacharyya, I.; Pramanik, C.; Mandal, B.; Das, S.; Bera, P., *J. Mol. Struct.*, **2021**, *1224*, 129015.
46. Cory, M.; McKee, D. D.; Kagan, J.; Henry, D.; Miller, J. A., *J. Am. Chem. Soc.*, **1985**, *107* (8), 2528-2536.
47. Mitra, I.; Mukherjee, S.; Misini, B.; Das, P.; Dasgupta, S.; Linert, W.; Moi, S. C., *New J. Chem.*, **2018**, *42* (4), 2574-2589.
48. Pages, B. J.; Li, F.; Wormell, P.; Ang, D. L.; Clegg, J. K.; Kepert, C. J.; Spare, L. K.; Danchaiwijit, S.; Aldrich-Wright, J. R., *Dalton Trans.*, **2014**, *43* (41), 15566-15575.
49. Mutua, G. K.; Bellam, R.; Jaganyi, D.; Mambanda, A., *J. Coord. Chem.*, **2019**, *72* (17), 2931-2956.
50. Kljun, J.; Bratsos, I.; Alessio, E.; Psomas, G.; Repnik, U. k.; Butinar, M.; Turk, B.; Turel, I., *Inorg. Chem.*, **2013**, *52* (15), 9039-9052.

51. Karami, K.; Lighvan, Z. M.; Barzani, S. A.; Faal, A. Y.; Poshteh-Shirani, M.; Khayamian, T.; Eigner, V.; Dušek, M., *New J. Chem.*, **2015**, *39* (11), 8708-8719.
52. Abedi, A.; Lighvan, Z. M.; Ostad, S. N., *Monatsh. Chem.*, **2016**, *147* (9), 1651-1658.
53. Milutinović, M. M.; Rilak, A.; Bratsos, I.; Klisurić, O.; Vraneš, M.; Gligorijević, N.; Radulović, S.; Bugarčić, Ž. D., *J. Inorg. Biochem.*, **2017**, *169*, 1-12.
54. Zhang, Y. P.; Li, Y.; Xu, G. C.; Li, J. Y.; Luo, H. Y.; Li, J. Y.; Zhang, L.; Jia, D. Z., *Appl. Organomet. Chem.*, **2019**, *33* (3), e4668.
55. Jain, S.; Bhar, K.; Kumar, S.; Bandyopadhyaya, S.; Tapryal, S.; Mandal, C. C.; Sharma, A. K., *Dalton Trans.*, **2020**, *49* (13), 4100-4113.
56. Psomas, G.; Kessissoglou, D. P., *Dalton Trans.*, **2013**, *42* (18), 6252-6276.
57. Bellam, R.; Jaganyi, D.; Mambanda, A.; Robinson, R.; BalaKumaran, M. D., *RSC Adv.*, **2019**, *9* (55), 31877-31894.
58. Bera, B.; Mondal, S.; Gharami, S.; Naskar, R.; Saha, K. D.; Mondal, T. K., *New J. Chem.*, **2022**, *46* (23), 11277-11285.
59. Alizadeh, H.; Mirzaei, M.; Saljooghi, A. S.; Jodaian, V.; Bazargan, M.; Mague, J. T.; Gomila, R. M.; Frontera, A., *RSC Adv.*, **2021**, *11* (59), 37403-37412.
60. Barreiro, E. J.; Kümmerle, A. E.; Fraga, C. A., *Chem. Rev.*, **2011**, *111* (9), 5215-5246.
61. Zafar, M. N.; Butt, A. M.; Perveen, F.; Nazar, M. F.; Masood, S.; Dalebrook, A. F.; Mughal, E. U.; Sumrra, S. H.; Sung, Y. Y.; Muhammad, T. S. T., *J. Inorg. Biochem.*, **2021**, *224*, 111590.
62. Castro-Ramírez, R.; Ortiz-Pastrana, N.; Caballero, A. B.; Zimmerman, M. T.; Stadelman, B. S.; Gaertner, A. A.; Brumaghim, J. L.; Korrodi-Gregório, L.; Pérez-Tomás, R.; Gamez, P., *Dalton Trans.*, **2018**, *47* (22), 7551-7560.
63. Omondi, R. O.; Ojwach, S. O.; Jaganyi, D., *Inorg. Chim. Acta.*, **2020**, *512*, 119883.

Chapter 5

General conclusions and proposed future work

5.1 General conclusions

In conclusion, this study focused on the synthesis of mononuclear and dinuclear palladium(II) complexes supported on (pyridyl)pyrazine carboxamide complexes, their influence on the DNA/BSA interactions, and cytotoxicity investigations. The (pyridyl)pyrazine carboxamide ligands (**L1-L4**) were obtained from the synthesis of pyrazine-2,3-dicarboxylic acid and respective amines. The mononuclear and dinuclear palladium(II) complexes were obtained from the reactions of respective ligands with PdCl₂(CNMe)₂ metal precursor. Ligands **L1-L4** and their respective mononuclear and dinuclear palladium(II) complexes **Pd1-Pd4** were characterized using the ¹H NMR, ¹³C NMR, FT-IR, MS, and X-ray crystallography. The molecular structures of **Pd1** and **Pd3** showed that (pyridyl) pyrazine carboxamide-based ligands (**L1-L3**) coordinate to the palladium atom *via* nitrogen donor atoms. The two (pyridyl)pyrazine carboxamide ligands coordinate to palladium atoms with one arm, while the other arms are non-coordinated. The ligands are bridged by two palladium atoms to form dimer dinuclear complexes **Pd1-Pd3**. **L4** is a tridentate ligand, thus coordinating with the palladium atom *via* N^NN resulting in the formation of a mononuclear complex **Pd4**. Hence, ligands-controlled coordination diversity in these complexes is well illustrated by the mononuclear nature of complex **Pd4**.

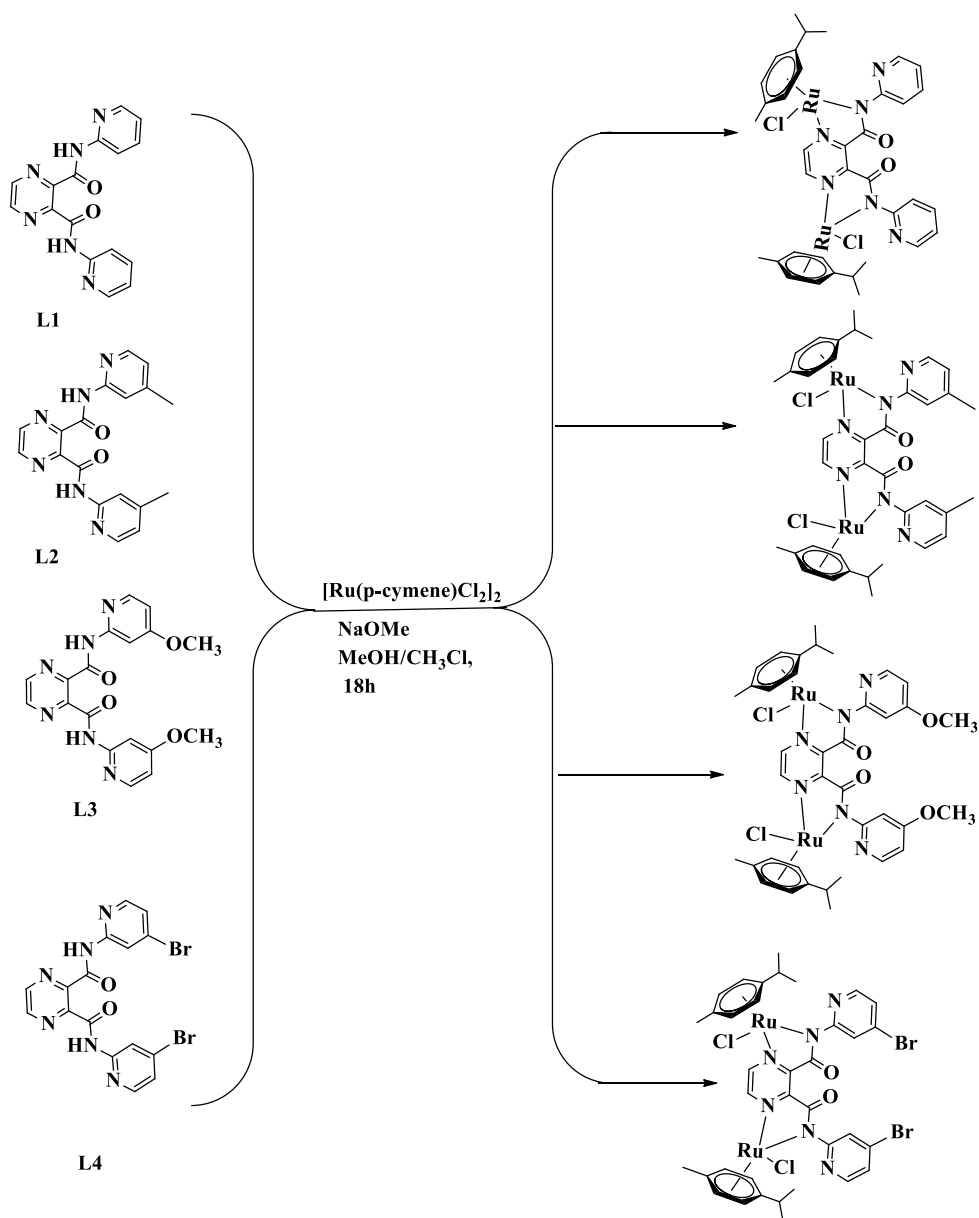
The interaction of CT-DNA and BSA with the mononuclear and dinuclear palladium(II) carboxamide complexes (**Pd1-Pd4**) was examined. All the complexes **Pd1-Pd4** interact with CT-DNA *via* intercalation mode. This was confirmed by both the electronic absorption

titration and fluorescence quenching experiments. The results reveal that increasing the metal nuclearity had a major effect on the interaction of the complexes with CT-DNA. This was observed from the binding constants of dinuclear palladium(II) complexes **Pd1-Pd3** which showed a high binding affinity in comparison to the mononuclear palladium (II) complex **Pd4**. Moreover, the DNA/BSA binding interactions displayed a dependence on the electronic parameters of the complexes of coordinated ligands. In general, the presence of the methyl group in complexes **Pd3** and **Pd2** enhanced their CT-DNA binding constants compared to **Pd1**. The interaction of bovine serum albumin with palladium(II) complexes revealed that **Pd1-Pd4** binds to the protein through a static mechanism. **Pd2** showed a higher binding constant while **Pd4** exhibited a low binding constant which is inconsistent with CT-DNA binding constants. Thus, in this study, it can be concluded that the presence of methyl group on the ligand backbone and nuclearity of the palladium(II) complexes increase the binding affinity between complexes and CT-DNA/BSA molecules.

(Pyridyl)pyrazine carboxamide ligands **L1-L3** demonstrated poor cytotoxicity due to the absence of a palladium metal centre causing more facile binding of the complexes to the DNA nucleobases resulting in restricted cell growth. Complexes **Pd2** and **Pd3** containing a methyl substituent were inactive due to low solubility in water which may reduce their bioavailability, and loss of planarity. High and moderate cytotoxic activity exhibited by **Pd1** and **Pd4** could be explained by the planarity of the free ligands. Therefore, it is clear that through careful ligand modification, the structures of the carboxamide palladium(II) complexes could be regulated, which in turn could modulate their biological behaviors and activities.

5.2. Future work

In this study, palladium(II) complexes supported on (pyridyl)pyrazine caboxamide ligands have displayed good DNA and bovine serum albumin interactions controlled by nuclearity, and the presence of methyl group complexes. Cytotoxicity of palladium(II) complexes investigated in this study highlights that the methyl substituent and the planarity of the free ligand have a major influence on the activity of complexes against cancer. Thus, it is recommended to explore the CT-DNA/BSA interaction and cytotoxicity of other metal complexes such as ruthenium complexes with the same ligands scaffold. However, the substituents on the free ligand could be manipulated to enhance cytotoxicity. Hence, ruthenium complexes are recommended due to the properties that make them appropriate for application in pharmacology. These properties include the ability of ruthenium to imitate iron properties when binding to biological molecules such as serum albumin,¹ octahedral geometry which differs from a square planar of platinum, consisting of a wide range of oxidation states; +2, +3, and +4 under biologically relevant conditions, and a well-developed preparative coordination chemistry that provides dependable routes to new compounds.² The mode of interaction of these complexes *in vivo* involves the reduction of Ru(III) to the more reactive Ru(II) species. As a result of this advantage Ru(II) arene complexes are investigated due to the ability of the arene to stabilise ruthenium in the +2 oxidation state.³ Thus, it would be of interest to investigate the biological activity of ruthenium(II) complexes *p*-cymene with the same ligand scaffold shown in Scheme 5.1. since they have previously reported to exhibit high anticancer activity.



Scheme 5.1: Role of electron-donating and electron-withdrawing groups of dicarboxamide ruthenium(II) *p*-cymene complexes in CT-DNA/BSA interactions, and cytotoxicity.⁴

5.3. References

1. Süss-Fink, G., *Dalton trans.*, **2010**, 39 (7), 1673-1688.
2. Omondi, R. O.; Jaganyi, D.; Ojwach, S. O.; Fatokun, A. A., *Inorg. Chim. Acta.*, **2018**, 482, 213-220.
3. Peacock, A. F.; Sadler, P. J., *Chem. Asian. J.*, **2008**, 3 (11), 1890-1899.
4. Kumah, R. T.; Mvelase, S. T.; Ojwach, S. O., *Inorganics.*, **2022**, 10 (11), 190.

5.4. Appendix

Supplemental Material

1. ^1H NMR spectral data of ligands and their respective complexes

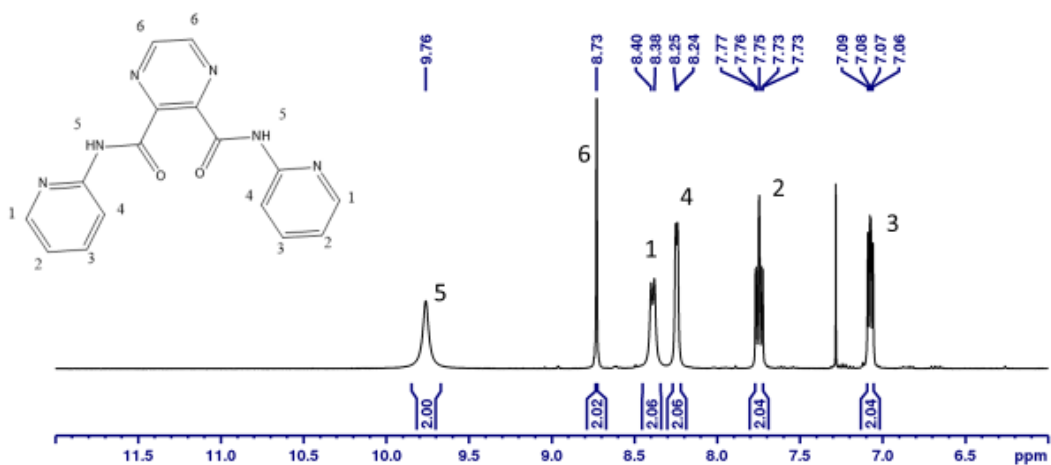


Figure S1: ^1H NMR spectrum of $[\text{N}^2, \text{N}^3\text{-bis(pyridin-2-yl)pyrazine-2,3-dicarboxamide}]$ (L1) showing N-H signal at 9.76 ppm with I=2.

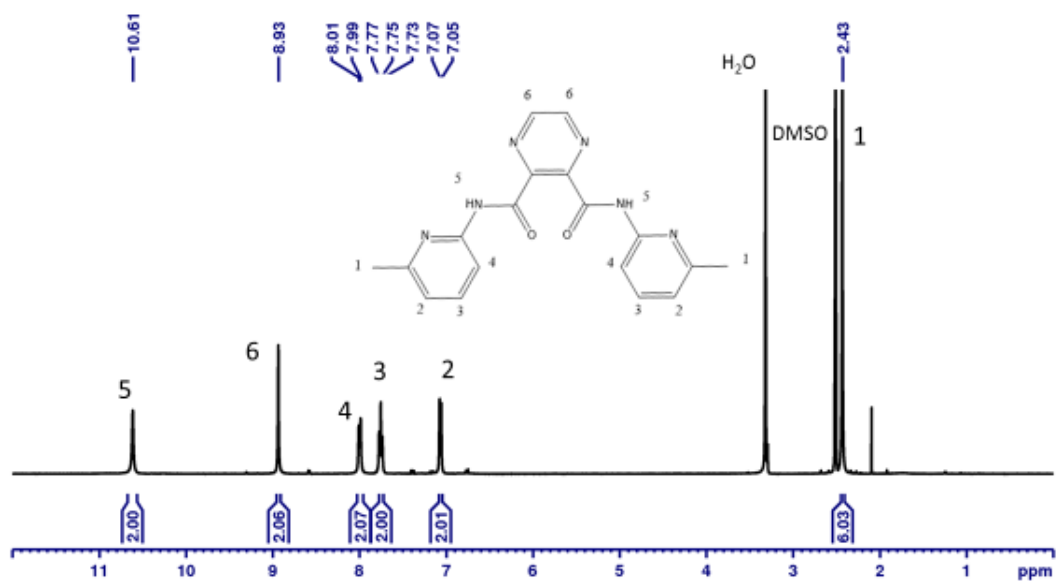


Figure S2: ^1H NMR spectrum of $[\text{N}^2, \text{N}^3\text{-bis(6-methylpyridin-2-yl)pyrazine-2,3-dicarboxamide}]$ (**L2**) showing N-H signal at 10.61 ppm with I=2.

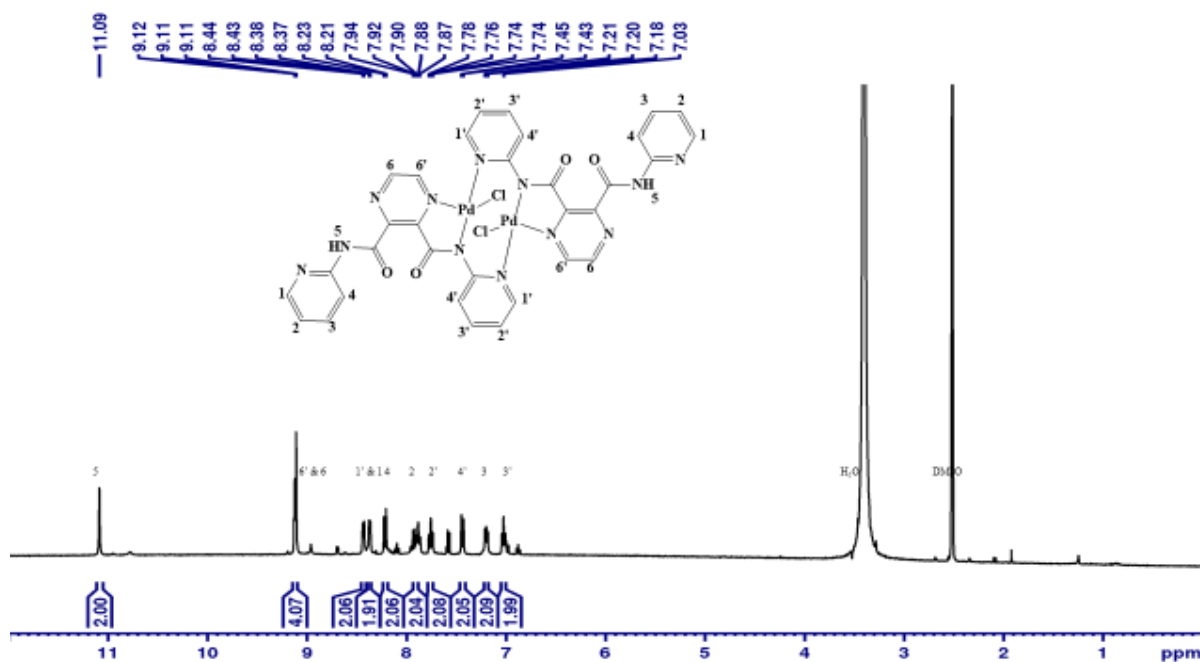


Figure S3: ^1H NMR spectra complex **Pd1** showing singlet N-H signal at 11.09 ppm with I=2, and eight pyridine signals upon coordination. The unsymmetrical nature of the complex **Pd1** confirmed the formation of the complex

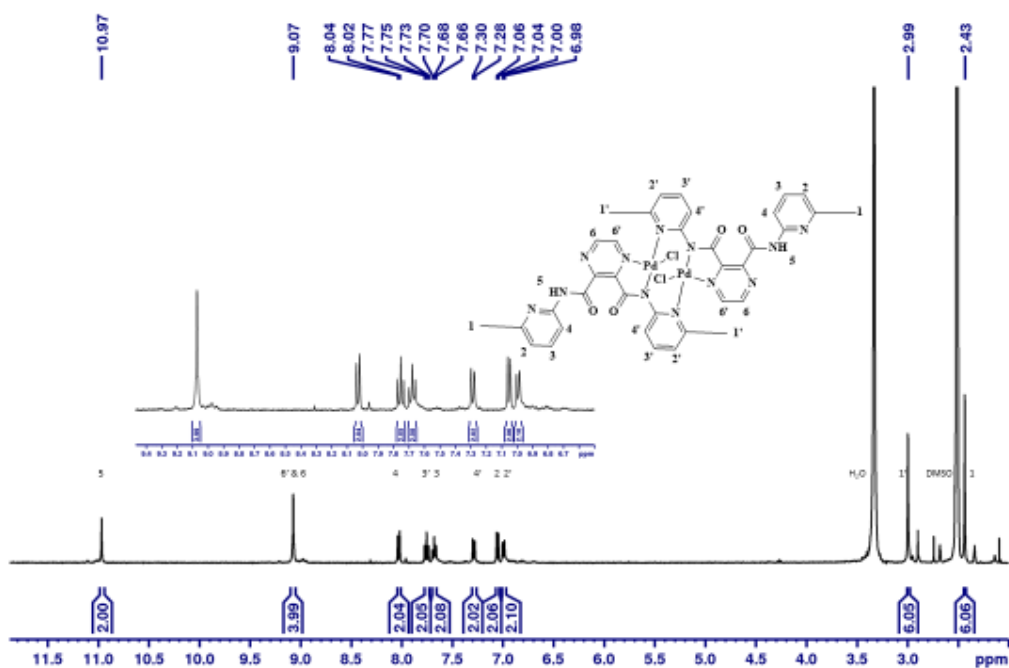


Figure S4: ^1H NMR spectra complex **Pd2** showing singlet N-H signal at 10.97 ppm with I=2, and six pyridine signals upon coordination. The unsymmetrical nature of the complex **Pd2** confirmed the formation of the complex.

2. ^{13}C NMR spectral data of ligands and their respective complexes

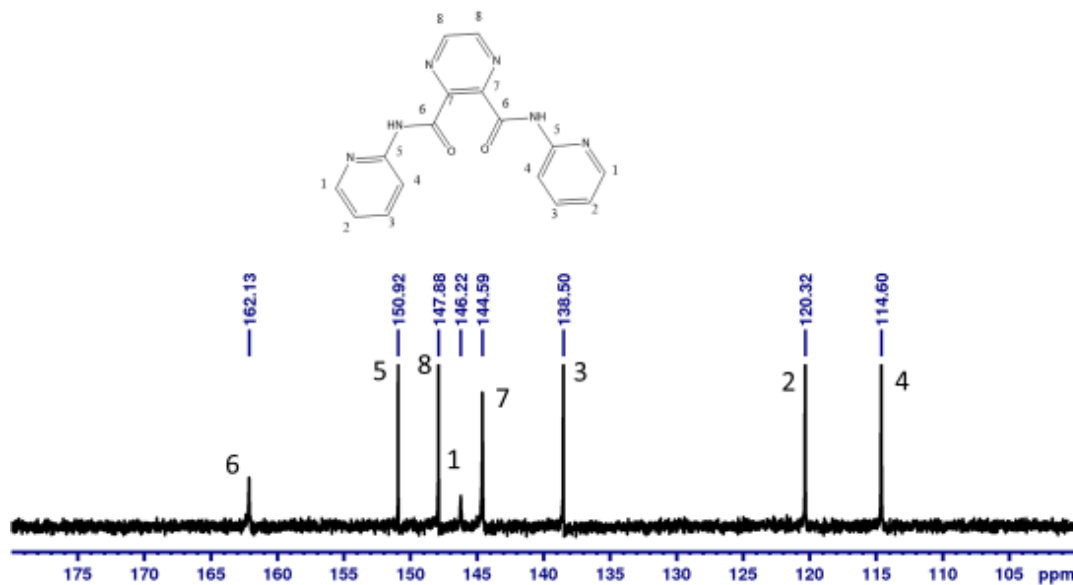


Figure S4: ¹³C NMR spectrum of [N²,N³-bis(pyridin-2-yl)pyrazine-2,3-dicarboxamide] (L1) showing carbonyl signal at 162.13 ppm

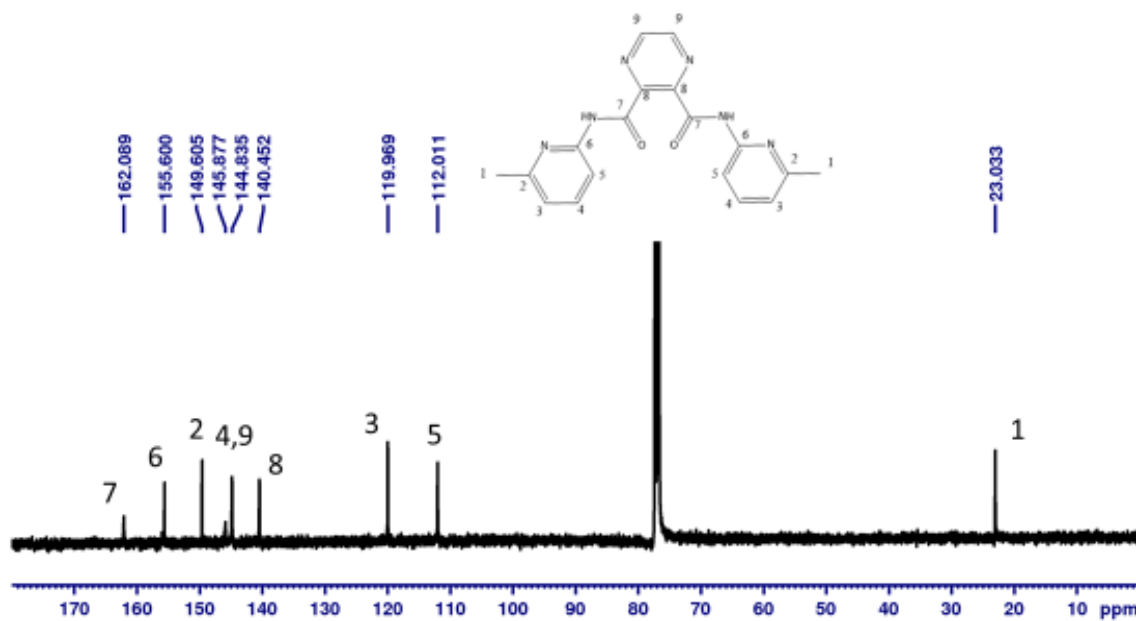


Figure S5: ¹³C NMR spectrum of [N²,N³-bis(6-methylpyridin-2-yl)pyrazine-2,3-dicarboxamide] (L2) showing carbonyl signal at 162.089 ppm.

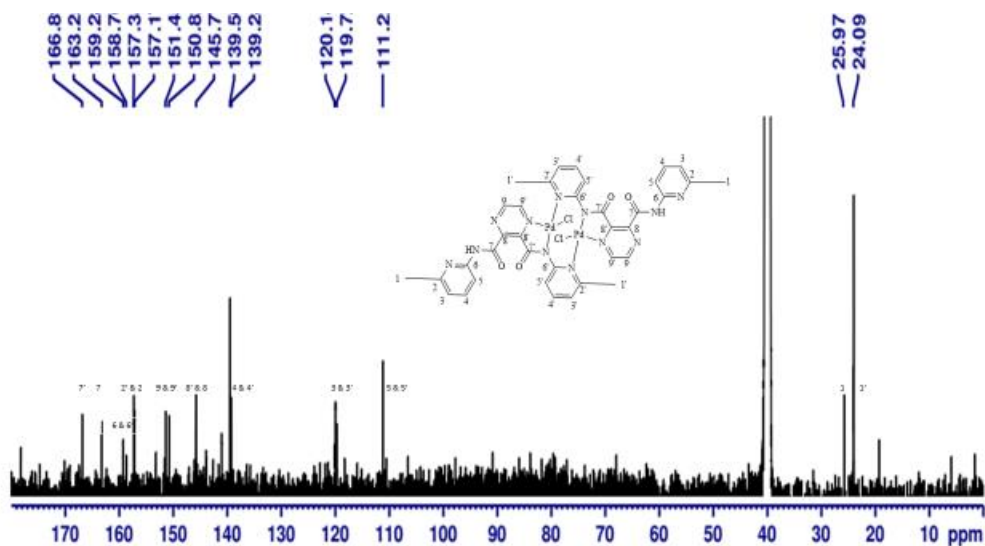


Figure S6: ^{13}C NMR spectrum of complex **Pd2** showing two carbonyl signals at 163.25 and 166.89 ppm. This confirms the unsymmetrical nature of the dinuclear complex **Pd2** due to the non-coordination of one arm of ligand **L2**.

3. FT-IR spectral data of ligands and their respective complexes

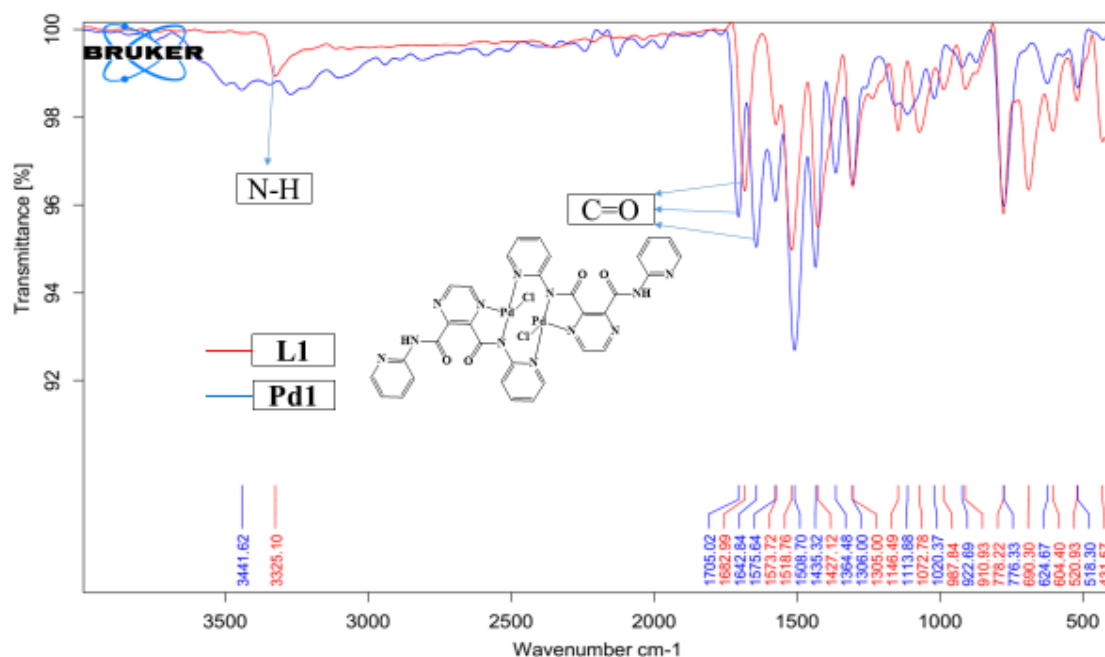


Figure S7: FT-IR spectra of **L1** showing single $\nu(\text{C}=\text{O})$ peak at 1682 cm^{-1} complex and **Pd1** showing the appearance of two carbonyl carbon $\nu(\text{C}=\text{O})$ at 1632 and 1705 cm^{-1} confirming the unsymmetrical nature of the dinuclear complex **Pd1** due the coordination of one arm of the ligand **L1** to palladium(II).

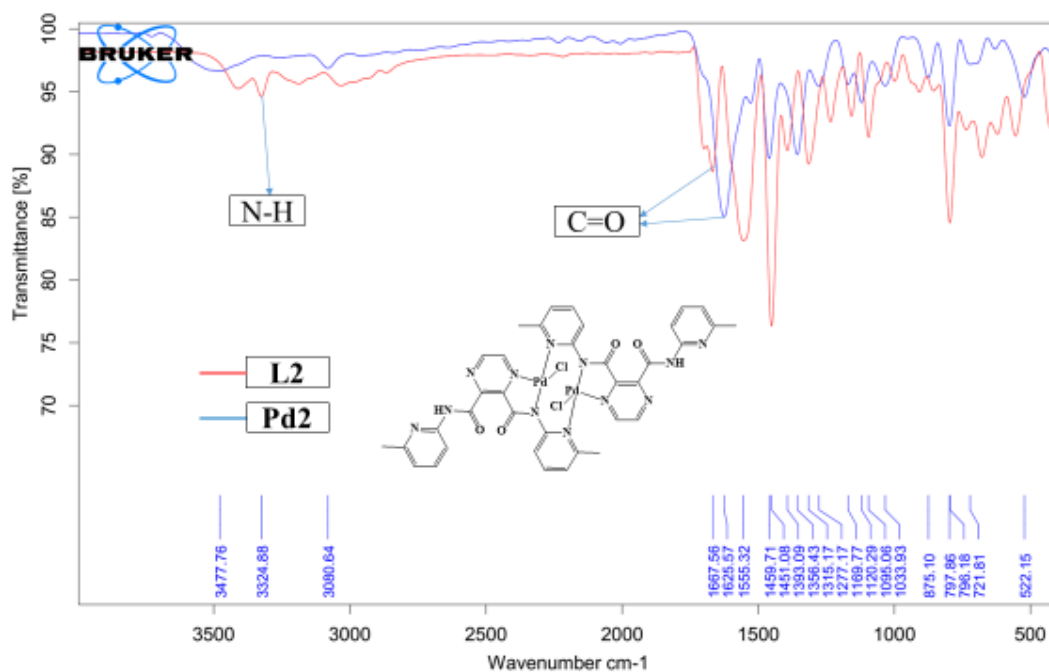


Figure S8: FT-IR spectra of **L2** showing single $\nu(\text{C}=\text{O})$ peak at 1667 cm^{-1} complex and **Pd2** showing the appearance of two carbonyl carbon $\nu(\text{C}=\text{O})$ at 1625 cm^{-1} confirming the unsymmetrical nature of the dinuclear complex **Pd2** due the coordination of one arm of the ligand **L2** to palladium(II).

4. Mass spectral data of ligands and their respective complexes

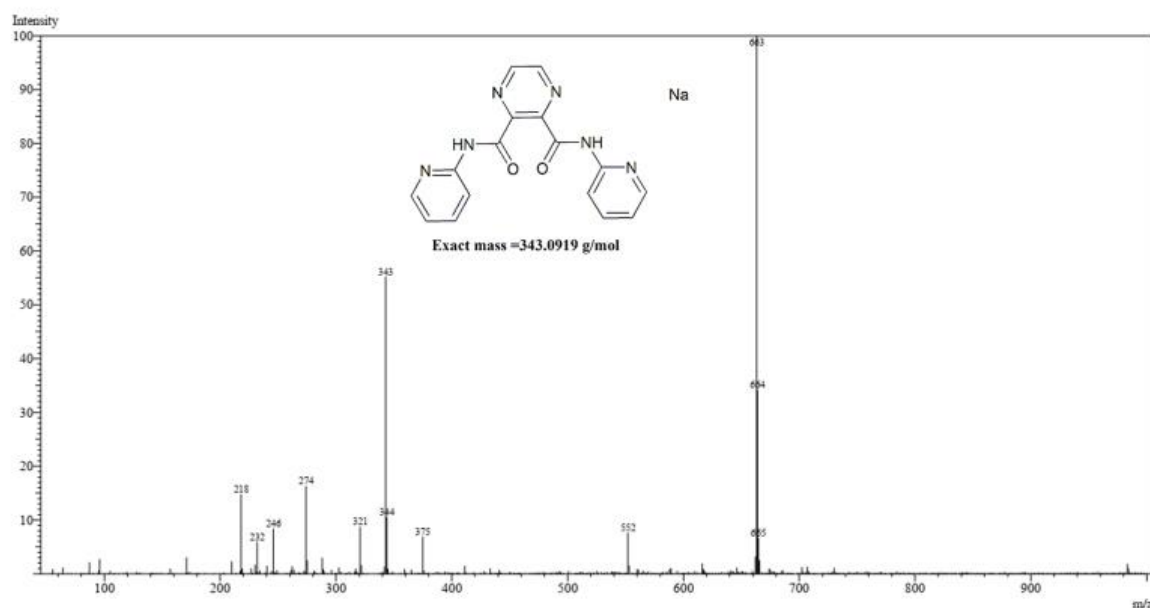


Figure S9: ESI-MS spectrum of $[N^2, N^3\text{-bis(pyridin-2-yl)pyrazine-2,3-dicarboxamide}]$ (L1) showing m/z at 343 [$M^+ + Na$, 55%].

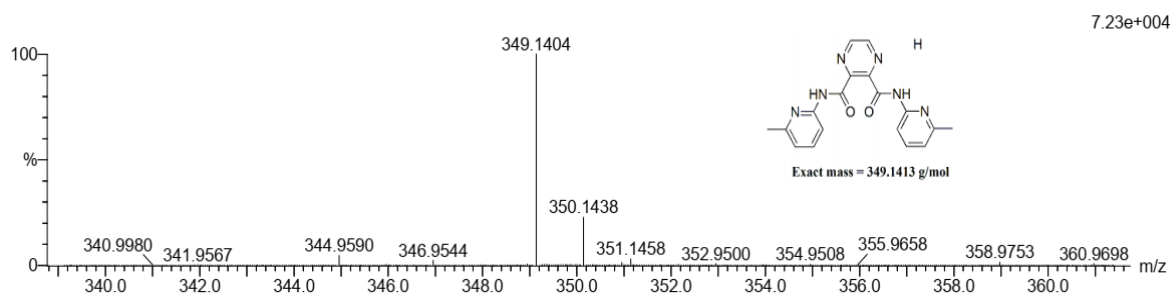


Figure S10: TOF-MS spectrum of $[N^2, N^3\text{-bis(6-methylpyridin-2-yl)pyrazine-2,3-dicarboxamide}]$ (L2) showing m/z at 349 [$M^+ + H$, 100%].

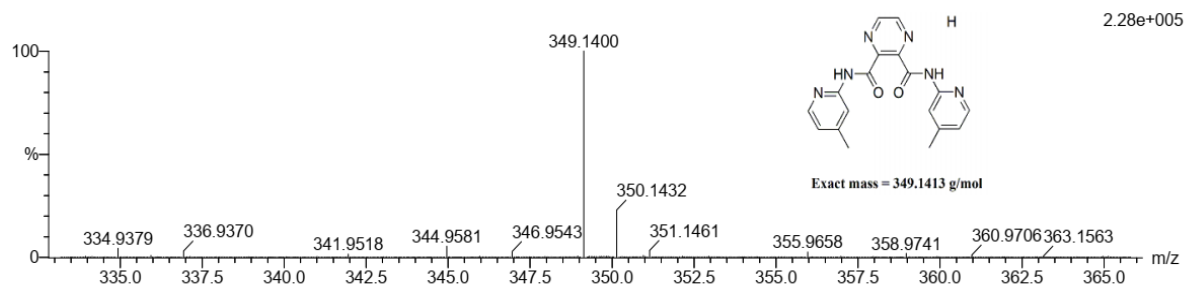


Figure S11: TOF-MS spectrum of $[N^2, N^3\text{-bis(4-methylpyridin-2-yl)pyrazine-2,3-dicarboxamide}]$ (**L3**) showing m/z at 349 [$M^+ + H$, 100%].

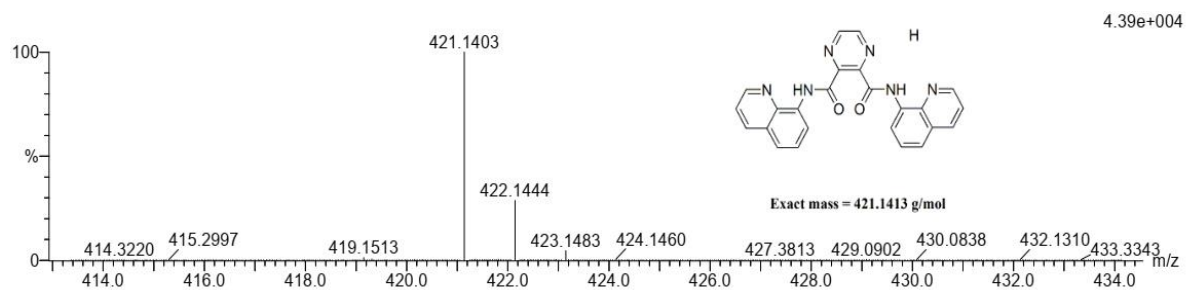


Figure S12: TOF-MS spectrum of $[N^2, N^3\text{-bis(quinoline-8-yl)pyrazine-2,3-dicarboxamide}]$ (**L4**) showing m/z at 421 [$M^+ + H$, 100%].

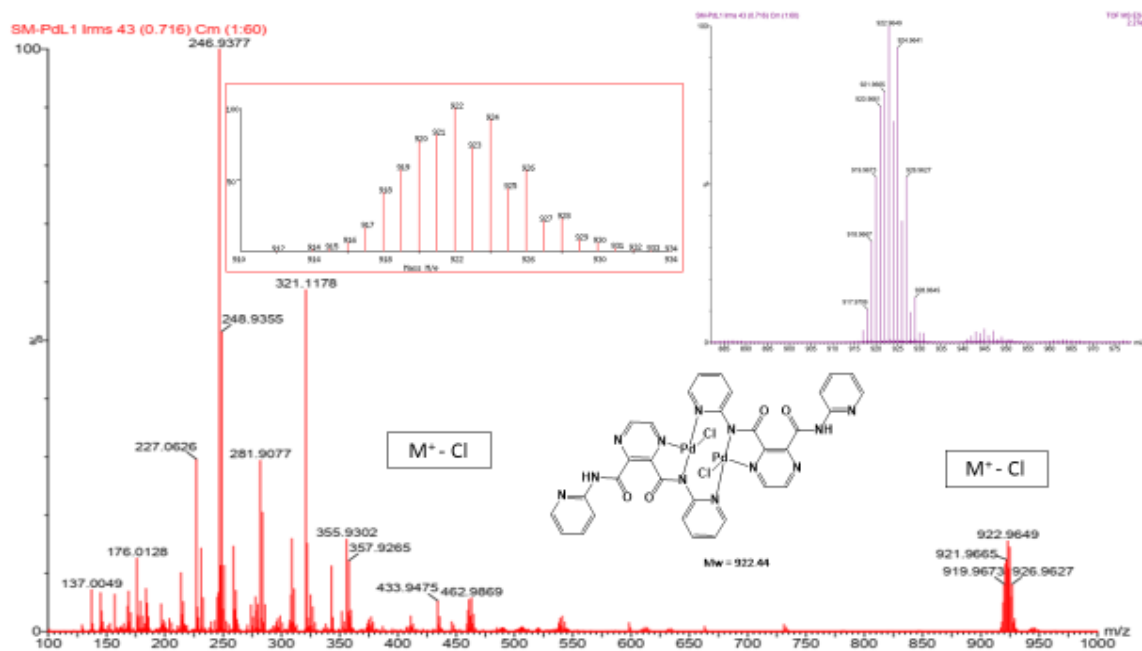


Figure S13: TOF-MS spectrum of complex **Pd1** showing m/z at 922 [$M^+ + H$]. Insert: experimental and theoretical isotopic mass distribution spectra complex **Pd1** with m/z at 922.

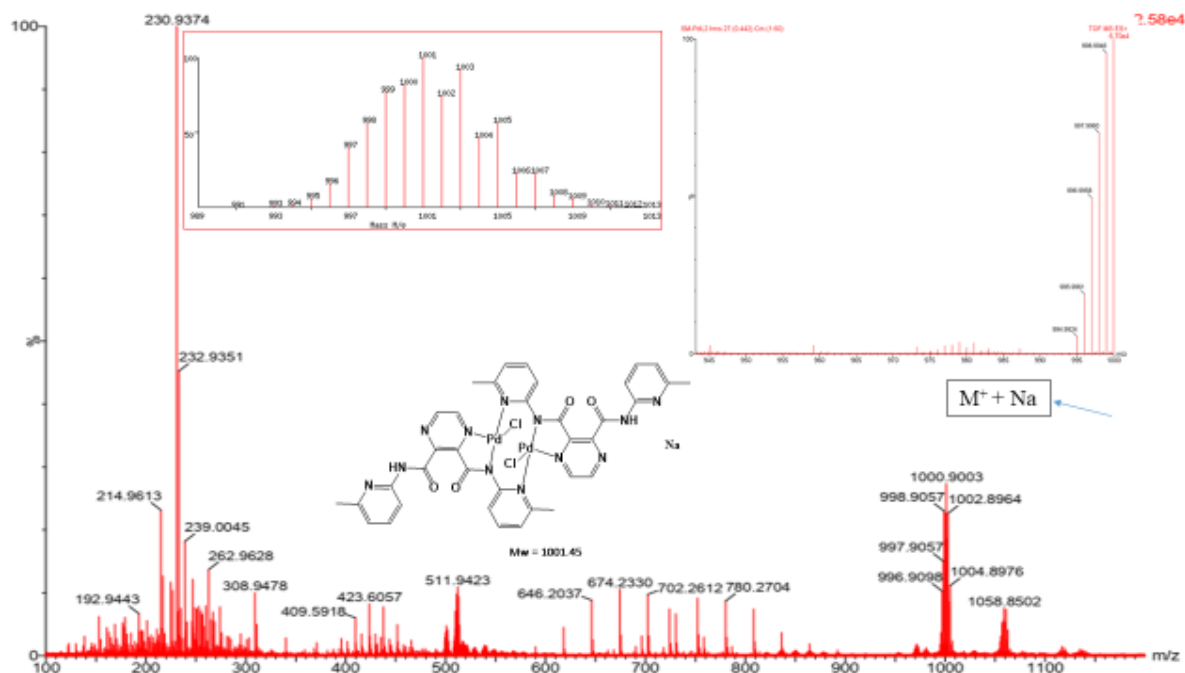


Figure S14: TOF-MS spectrum of complex **Pd2** showing m/z at 1000 [$M^+ + Na$]. Insert: experimental and theoretical isotopic mass distribution spectra complex **Pd2**.

6. CT-DNA UV-vis absorption spectral studies

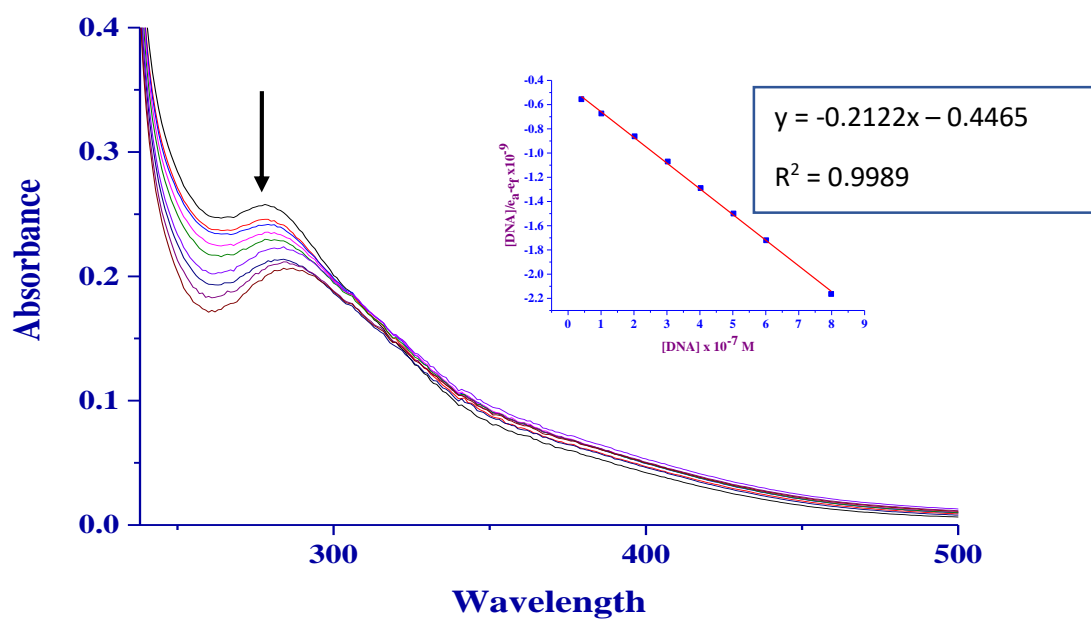


Figure S15: Electronic absorption spectra of **Pd1** (25 μM) in 0.01 M PBS buffer at pH 7.4 upon addition of CT-DNA (0 - 16 μM). The arrow shows the decrease in absorbance upon addition of increasing concentration of CT-DNA. Inserted is the linear plot of [CT-DNA] vs [DNA]/(e_a-e_f).

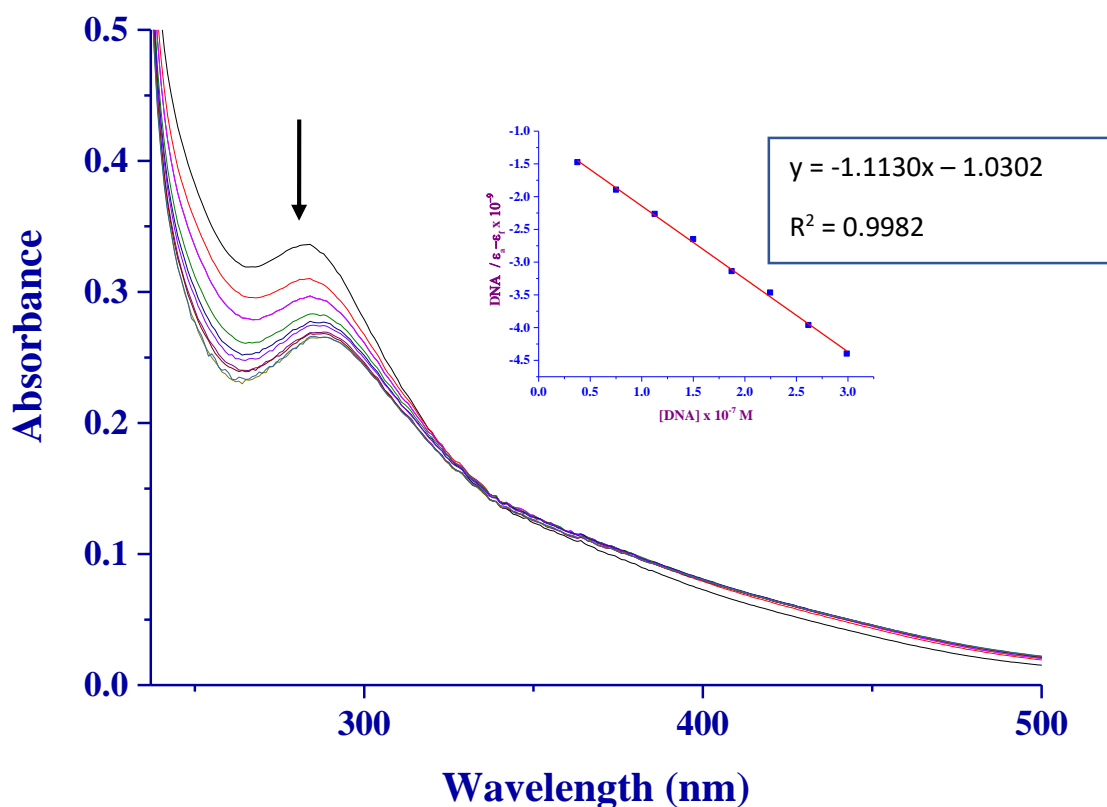


Figure S16: Electronic absorption spectra of **Pd2** (25 μM) in 0.01 M PBS buffer at pH 7.4 upon addition of CT-DNA (0 - 16 μM). The arrow shows the decrease in absorbance upon addition of increasing concentration of CT-DNA. Inserted is the linear plot of [CT-DNA] vs [DNA]/ ($\epsilon_a - \epsilon_f$).

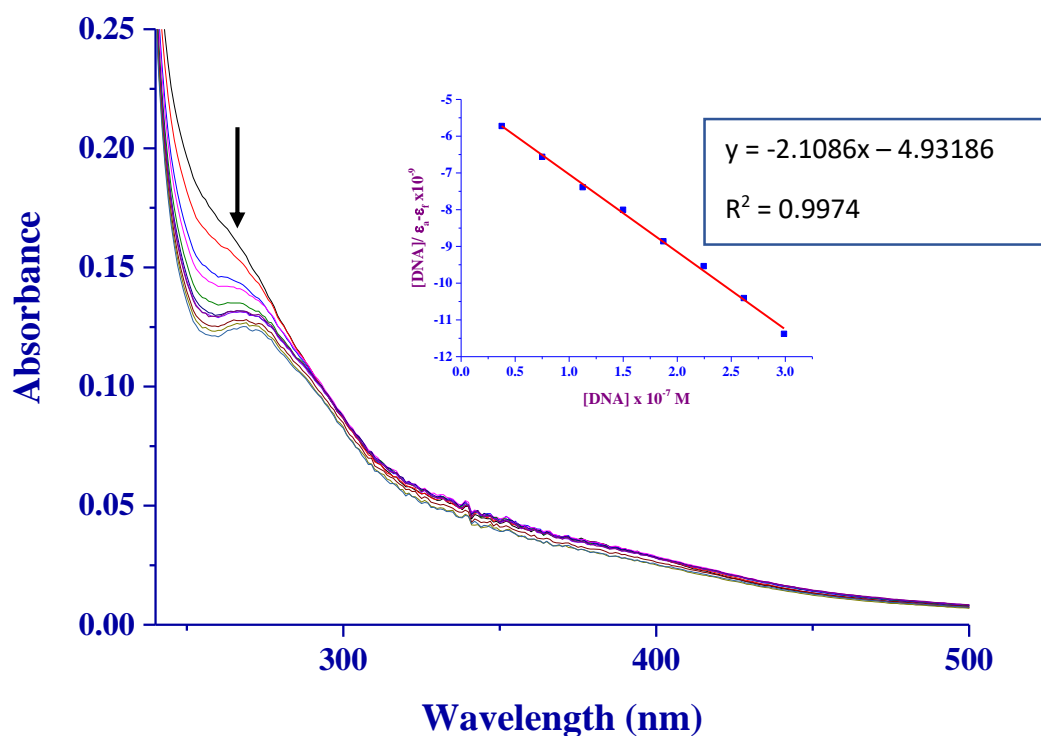


Figure S17: Electronic absorption spectra of **Pd4** (25 μM) in 0.01 M PBS buffer at pH 7.4 upon addition of CT-DNA (0 - 16 μM). The arrow shows the decrease in absorbance upon addition of increasing concentration of CT-DNA. Inserted is the linear plot of [CT-DNA] vs [DNA]/ ($\epsilon_a - \epsilon_f$).

7. Competitive binding studies (CT-DNA-EB) fluorescence spectroscopy

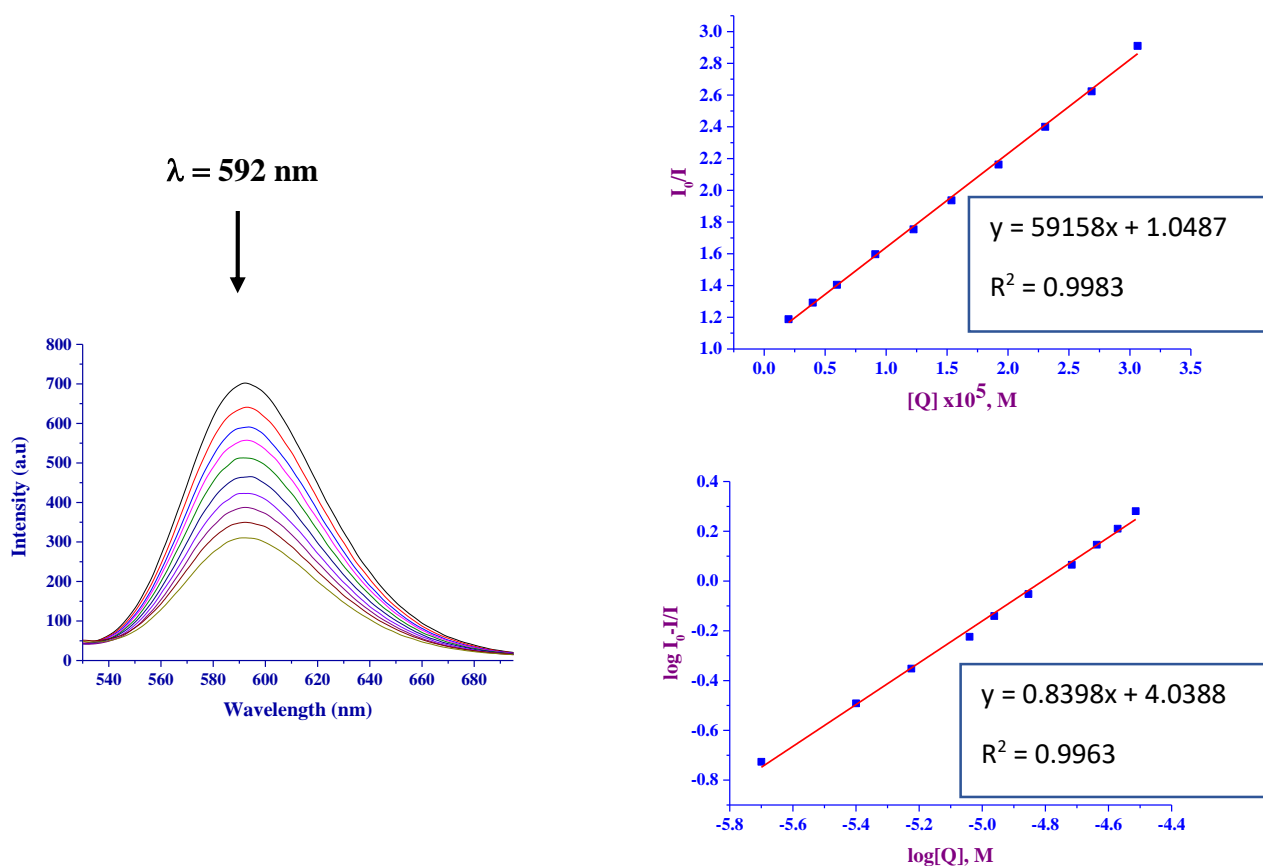


Figure S18: Fluorescence emission spectra depicting the quenching upon addition of increasing amount of **Pd1** to CT-DNA-EB: [EB] = 10 μ M, [CT-DNA] = 10 μ M and [**Pd1**] = 0-200 μ M. The arrow shows the intensity changes upon increasing the **Pd1** complex concentration. Inserted is the Stern-Volmer plot of I_0/I vs $[Q]$ and Scatchard plot of $\log[(I_0 - I)/I]$ vs $\log[Q]$.

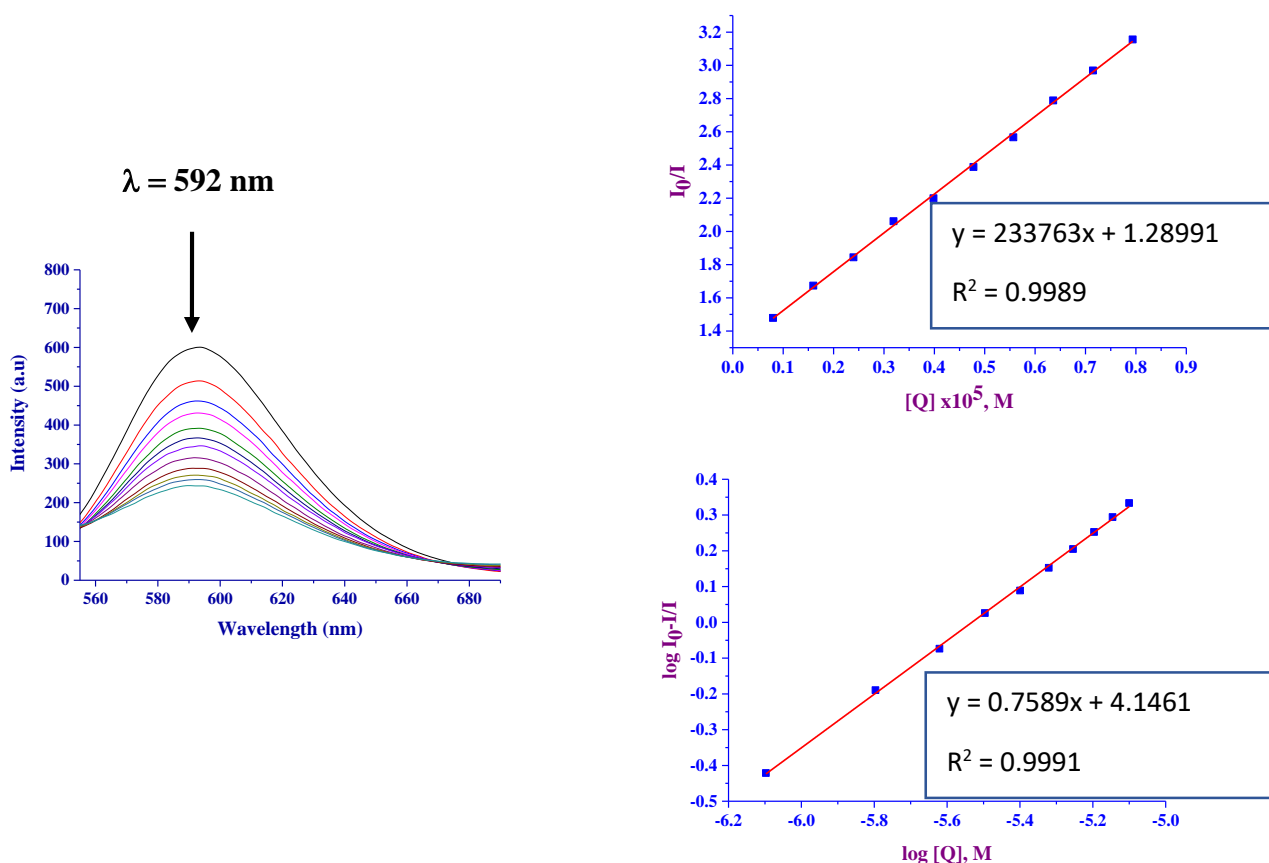


Figure S19: Fluorescence emission spectra depicting the quenching upon addition of increasing amount of **Pd2** to CT-DNA-EB: [EB] = 10 μ M, [CT-DNA] = 10 μ M, and [**Pd2**] = 0-200 μ M. The arrow shows the intensity changes upon increasing the **Pd2** complex concentration. Inserted is the Stern-Volmer plot of I_0/I vs $[Q]$ and Scatchard plot of $\log[(I_0 - I)/I]$ vs $\log[Q]$.

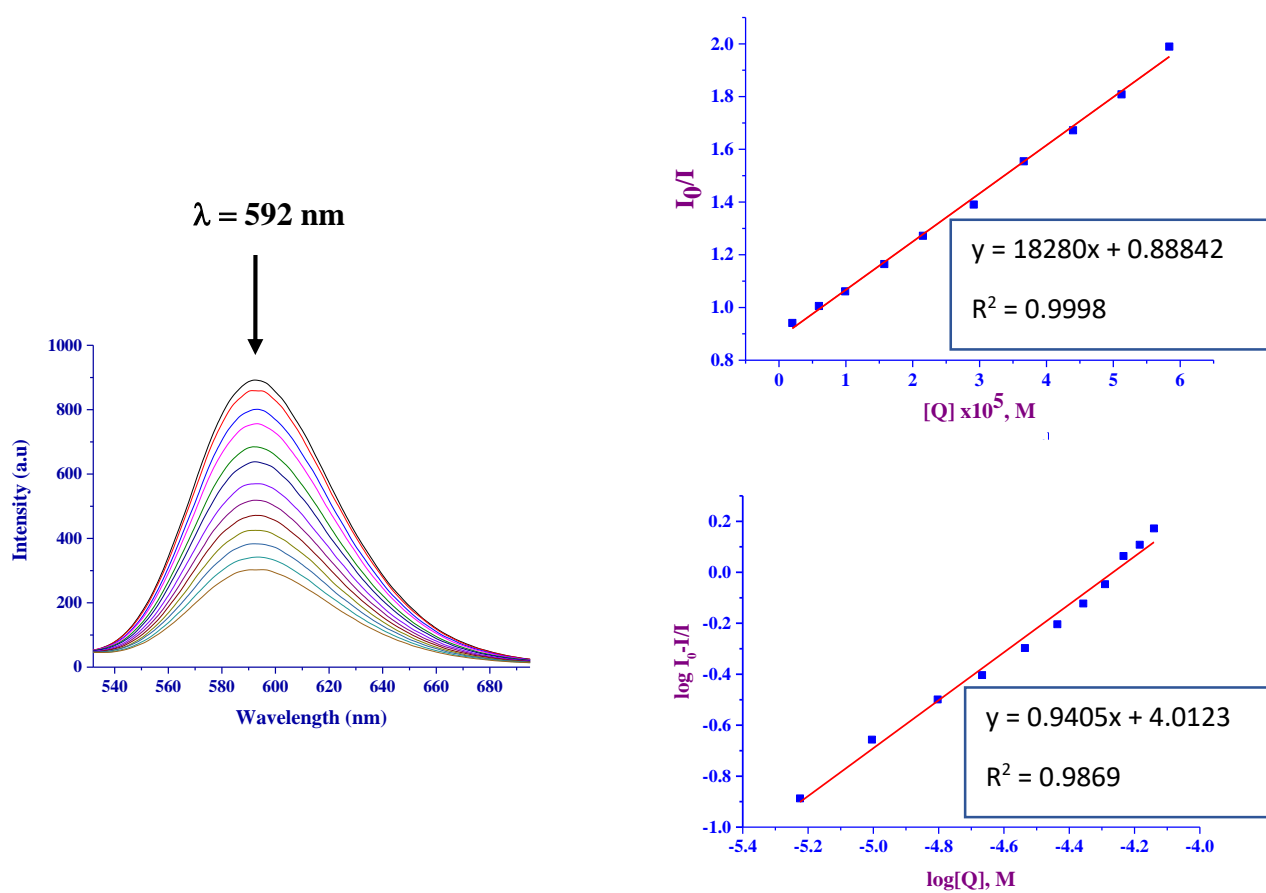


Figure S20: Fluorescence emission spectra depicting the quenching upon addition of increasing amount of **Pd4** to CT-DNA-EB: [EB] = 10 μ M, [CT-DNA] = 10 μ M, [**Pd4**] = 0-200 μ M . The arrow shows the intensity changes upon increasing the **Pd4** complex concentration. Inserted is the Stern-Volmer plot of I_0/I vs $[Q]$ and Scatchard plot of $\log[(I_0 - I)/I]$ vs \log

8. Fluorescence quenching studies bovine serum albumin.

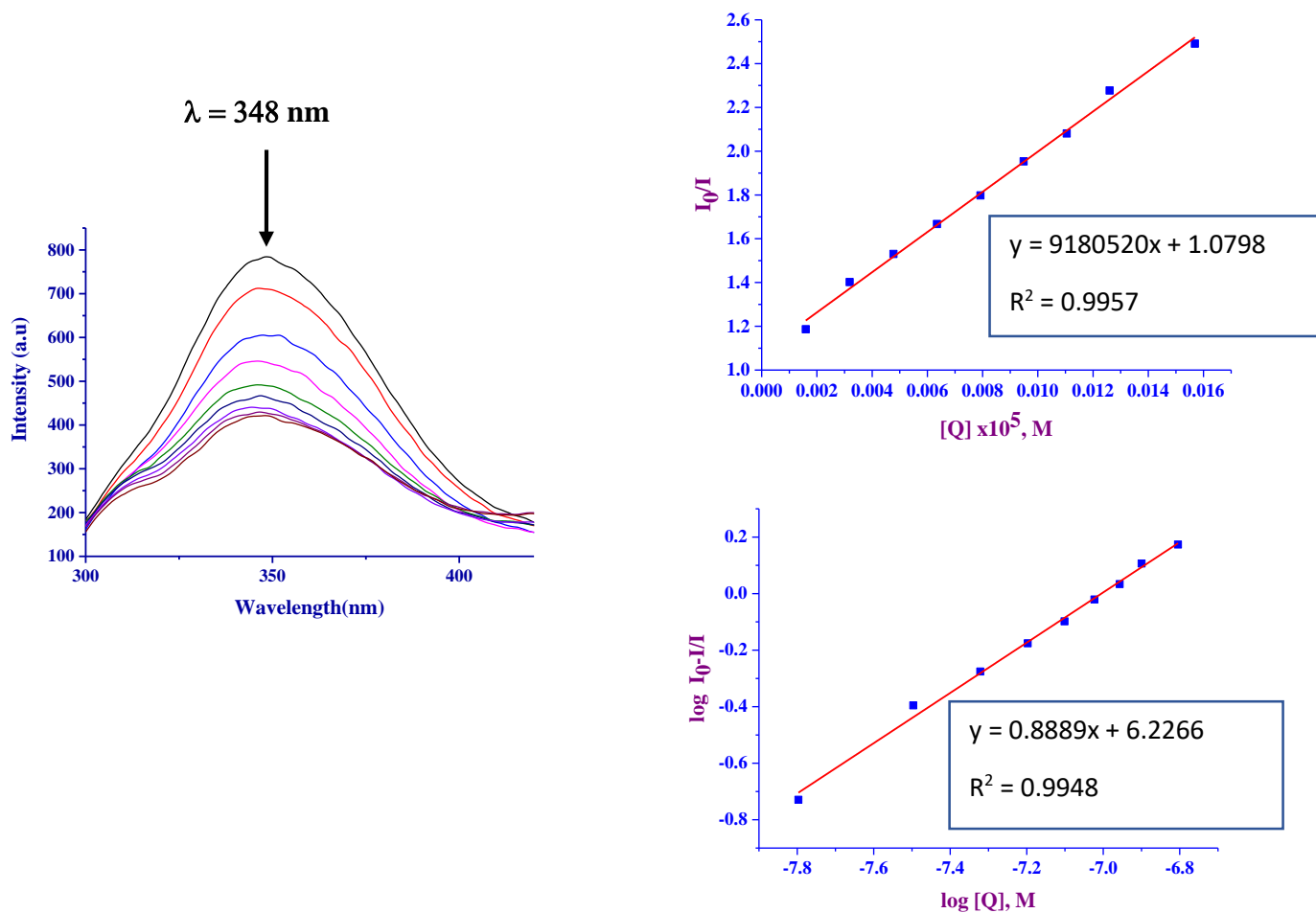


Figure S21: Quenching in fluorescence emission spectra of BSA in the presence of increasing concentration of **Pd1** = 0-40 μM and [BSA] = 14 μM. The arrow shows the decrease in fluorescence intensity upon increasing the **Pd1** concentration. Inserted is the Stern-Volmer plot of I_0/I vs $[Q]$ and Scatchard plot of $\log[(I_0 - I)/I]$ vs $\log[Q]$.

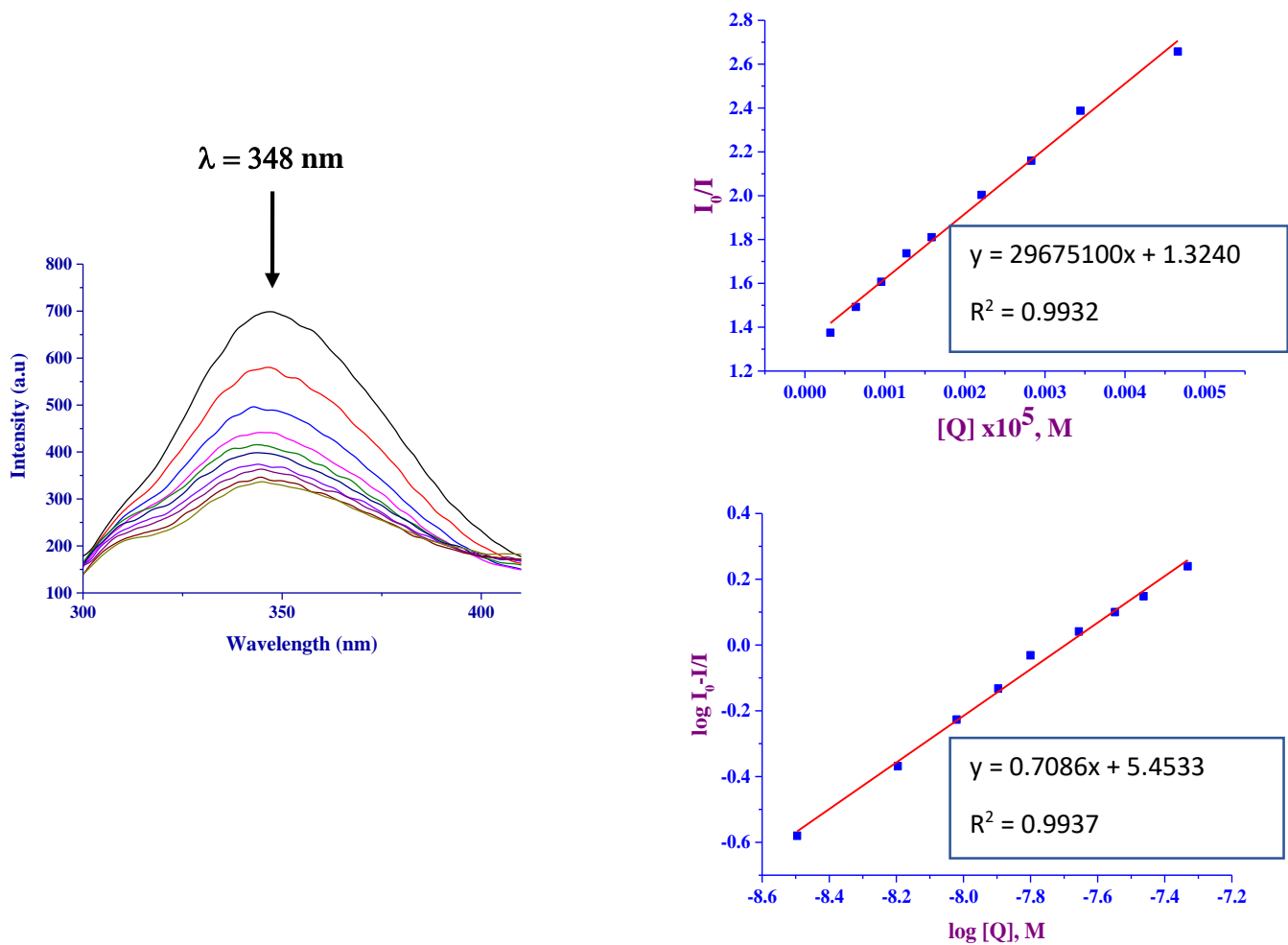


Figure S22: Quenching in fluorescence emission spectra of BSA in the presence of increasing concentration of **Pd²⁺** = 0-40 μM and $[\text{BSA}] = 14\mu\text{M}$. The arrow shows the decrease in fluorescence intensity upon increasing the **Pd²⁺** concentration. Inserted is the Stern-Volmer plot of I_0/I vs $[Q]$ and Scatchard plot of $\log[(I_0-I)/I]$ vs $\log[Q]$.

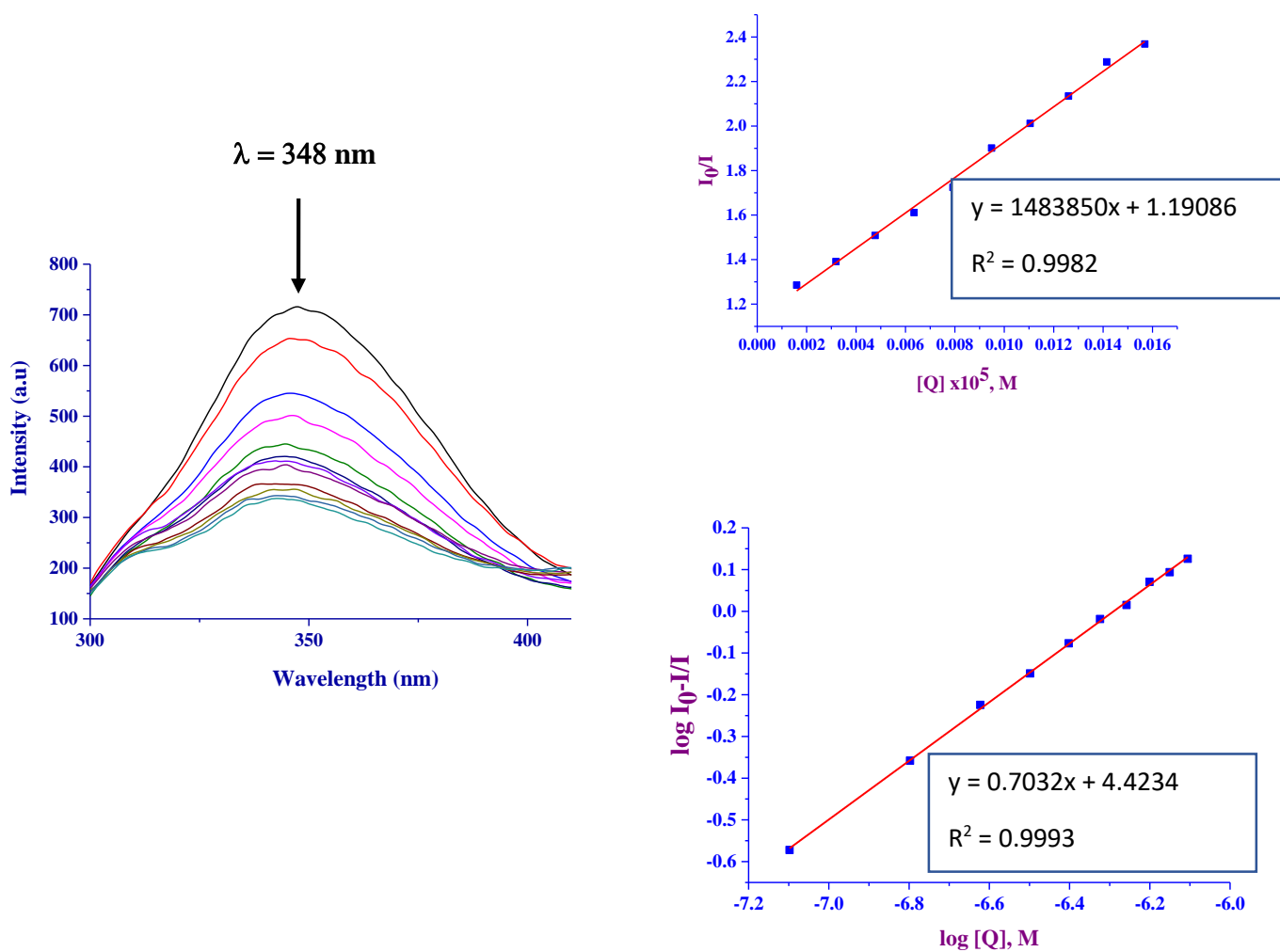


Figure S23: Quenching in fluorescence emission spectra of BSA in the presence of increasing concentration of **Pd4** = 0-40 μM and $[\text{BSA}] = 14\mu\text{M}$. The arrow shows the decrease in fluorescence intensity upon increasing the **Pd4** concentration. Inserted is the Stern-Volmer plot of I_0/I vs $[Q]$ and Scatchard plot of $\log[(I_0-I)/I]$ vs $\log[Q]$.